P-ISSN 0126-3188
E-ISSN 2443-3926

LIPI

METALURGI

MAJALAH ILMU DAN TEKNOLOGI

VOLUME 36 Nomor 2, AGUSTUS 2021
AKREDITASI JURNAL ILMIAH NO.3/E/KPT/2019

Pusat Penelitian Metalurgi dan Material
Lembaga Ilmu Pengetahuan Indonesia

LIPI

Penanggung Jawab :
Kapuslit Metalurgi dan Material – LIPI

Ketua Dewan Redaksi :
Dr. Ika Kartika, S.T, M.T, P2MM - LIPI

Dewan Editor :
Prof. Dr. F. Firdiyono (P2MM - LIPI)
Prof. Dr. Rudi Subagja (P2MM - LIPI)
Prof. Dr. Akhmad Herman Yuwono, M.Phil. Eng (Teknik Material Metalurgi-Universitas Indonesia)
Dr. I Nyoman Jujur, M.Eng (PTM-BPPT)

Mitra Bestari :
Dr. Anawati, M.Sc (Fakultas MIPA, Universitas Indonesia)
Dr. Yuliati Herbani, M.Sc (Pusat Penelitian Fisika - LIPI)
Prof. Dr. mont. Mohammad Zaki Mubarok, S.T, M.T (Teknik Metalurgi-Institut Teknologi Bandung)
Dr. Asep Ridwan S. (Teknik Mesin-Institut Teknologi Bandung)
Nofrijon Sofyan, Ph. D (Teknik Material Metalurgi-Universitas Indonesia)
Prof. Dr. Timotius Pasang (Oregon Institute of Technology, United State)

Redaksi :
Lia Andriyah, M.Si (P2MM- LIPI)
Tri Arini, M.T (P2MM- LIPI)
Nadia Natasha, M.Si (P2MM- LIPI)
Galih Senopati, M.T (P2MM- LIPI)

Disain Grafis :
Andri Agus Rahman, A.Md (LIPI Press)
Arif Nurhakim, M.A (PDDI LIPI)

Website :
Daniel Panghihutan, M.Si (P2MM- LIPI)
Adi Noer Syahid, A.Md (P2MM- LIPI)

Sekretariat dan Penerbit :
Pusat Penelitian Metalurgi dan Material – LIPI Ged. 470, Kawasan Puspiptek Serpong, Tangerang Selatan, 15314
Telp: (021) 7560911

E-mail: jurnalmetalurgi@mail.lipi.go.id

Majalah ilmu dan teknologi terbit berkala setiap tahun, satu volume terdiri atas 3 nomor

METALURGI

VOLUME 36 NOMOR 2, AGUSTUS 2021

P-ISSN 0126-3188
E-ISSN 2443-3926

AKREDITASI : SK No. 3/E/KPT/2019

PENGANTAR REDAKSI

Puji syukur Majalah Metalurgi Volume 36 Nomor 2, Agustus 2021 kali ini dapat menampilkan 6 buah tulisan.

Tulisan pertama merupakan hasil kegiatan penelitian yang disampaikan oleh Wahyu Mayangsari dan kawan-kawan mengenai *The Effect of Alkali Roasting of Ferronickel Slag Prior to the Leaching and Precipitation Processes*. Tulisan kedua disampaikan oleh Ahmad Sahid dan kawan-kawan menampilkan topik *Atmospheric Plasma Spray Coating of Ni-Al and Al-Si on Austenitic Stainless-Steel Casing with Limited Short Spray Distance*. Untuk tulisan ketiga dengan penulis Yohana Fransiska Ferawati dan kawan-kawan mengenai Peran N-Doping terhadap Karakteristik Pori Karbon Aktif yang Dihasilkan dari Limbah Destilasi Akar Wangi. Tulisan selanjutnya memiliki topik *The Effect of ECAP Processing on Hardness, Surface Morphology, and Corrosion Resistance of 6061 Alloys* yang dipaparkan oleh I Nyoman Gede Putrayasa dan kawan-kawan. Tulisan kelima, Kevin Cleary Wanta dan kawan-kawan menyampaikan topik *Increasing of Metal Recovery in Leaching Process of Spent Catalyst at Low Temperature: The Addition of Hydrogen Peroxide and Sodium Chloride*. Tulisan keenam disampaikan oleh Rizta Febian Adi Endani dan kawan-kawan dengan tema *The Effect of Variations in Electrolyte Temperature and Current on the Synthesis of Manganese Dioxide from Manganese Sulfate Precursors by Electrolysis Method*.

Semoga penerbitan Majalah Metalurgi volume ini dapat bermanfaat bagi perkembangan dunia penelitian di Indonesia.

REDAKSI

METALURGI

ISSN 0126 – 3188 Metalurgi, Vol. 36 No. 2 Agustus 2021

UDC (OXDCF) 553.4

Wahyu Mayangsari[a], Agus Budi Prasetyo[a], Eni Febriana[a], Januar Irawan[a], Rudi Subagja[a], Florentinus Firdiyono[a], Johny Wahyuadi Soedarsono[b] ([a]Pusat Penelitian Metalurgi dan Material-LIPI, [b]Departemen Teknik Metalurgi dan Material, Universitas Indonesia)

Pengaruh Pemanggangan Alkali pada Terak Feronikel sebelum Proses Pelindian dan Pengendapan

Metalurgi, Vol. 36 No. 2 Agustus 2021

Terak feronikel dihasilkan sebagai produk samping dari produksi feronikel. Terak feronikel mempunyai potensi untuk dimanfaatkan sebagai bahan baku beberapa komponen berharga karena komposisinya melalui proses bertahap. Tujuan dari penelitian ini adalah untuk mengetahui pengaruh dari proses pemanggangan campuran terak feronikel dan Na_2CO_3 sebelum pelindian dengan air panas dan presipitasi untuk menghasilkan endapan silika. Proses pemanggangan terak feronikel dengan penambahan Na_2CO_3 telah dilakukan untuk pembentukan natrium silikat. Kemudian dilarutkan melalui proses pelindian menggunakan air panas 90 °C selama 120 menit. Endapan silika didapatkan dengan proses presipitasi sodium silikat terlarut diikuti dengan pemeraman selama tiga hari. Berdasarkan hasilnya, pemanggangan menyebabkan perubahan komposisi yang mempengaruhi persen pelindian dan perolehan silika. Reaksi terjadi dari permukaan ke inti yang dibuktikan dengan pengecilan ukuran residu pelindian dari RAF (roasted of alkalinized ferronickel slag). Natrium silikat dalam bentuk Na_4SiO_4 diketahui terlarut pada tahap pelindian dengan air panas. Pengendapan dan pemeraman larutan natrium silikat telah menghasilkan endapan silika dengan ukuran partikel lebih dari 100 µm. Proses pemanggangan pada 1000 °C selama 240 menit menghasilkan perolehan silika tertinggi.

Kata Kunci: Feronikel, terak, pemanggangan, pelindian, pengendapan, silika

The Effect of Alkali Roasting of Ferronickel Slag Prior to the Leaching and Precipitation Processes

As a by-product of ferronickel production, ferronickel slag was created. Because of its composition, it has the potential to be used as a raw material for some valuable elements through a series of processing. The purpose of this research is to determine the effect of roasting ferronickel slag and Na_2CO_3 prior to hot water leaching and precipitation to obtain silica precipitate. To produce sodium silicate, ferronickel slag was roasted with Na_2CO_3 addition. It was then dissolved by leaching for 120 minutes in hot water at around 90 °C. Silica precipitate is made by precipitating dissolved sodium silicate and aging it for three days. According to the findings, roasting causes a change in composition, which influences the leaching percentage and silica recovery. Size reduction of leaching residue from its RAF (roasted alkalinized ferronickel slag) demonstrated that reactions occurred from the surface to the core. When water is leached, sodium silicate in the form of Na_4SiO_4 is observed and dissolved. The precipitation and aging of sodium silicate solution produced silica precipitate with particle sizes greater than 100 µm. The highest silica recovery is obtained by roasting at 1000 °C for 240 minutes

Keywords: Ferronickel, slag, roasting, leaching, precipitation, silica

METALURGI

ISSN 0126 – 3188 Metalurgi, Vol. 36 No. 2 Agustus 2021

UDC (OXDCF) 621.004

Ahmad Sahid[a], Ekavianty Prajatelistia[a], Ahmad Afandi[b] ([a]Material Science and Engineering Research Group Faculty of Mechanical and Aerospace Engineering, Institut Teknologi Bandung , [b]Research Center for Physics, Indonesian Institute of Sciences)

Lapisan Plasma Spray Ni-Al dan Al-Si pada Selubung Baja Tahan Karat Austenitik dengan Jarak Semprot Terbatas

Metalurgi, Vol. 36 No. 2 Agustus 2021

Proses plasma spray atmosferik merupakan proses pelapisan yang banyak digunakan dalam aplikasi industri. Densitas dan kekuatan ikatan yang tinggi merupakan ciri utama dari proses ini dan diperlukan dalam hampir semua sifat lapisan untuk aplikasi-aplikasi khusus. Keterbatasan jarak semprot antara pistol nozel dan permukaan benda kerja pada saat proses plasma spray memerlukan modifikasi parameter proses standar. Pada penelitian ini, modifikasi parameter proses plasma spray dilakukan pada lapisan Ni-Al dan Al-Si untuk mendapatkan hasil lapisan yang optimum. Lapisan diverifikasi dengan uji kekuatan ikatan tarik, uji keras, dan analisis struktur mikro. Dari modifikasi parameter yang dilakukan, penurunan kecepatan gerak pistol menunjukkan hasil yang paling optimum. Kekuatan ikatan tarik rata-rata yang diperoleh untuk lapisan Ni-Al dan Al-Si berturut-turut sebesar 9110 Psi dan 7283 Psi. Nilai kekerasan rata-rata yang diperoleh untuk lapisan Ni-Al dan Al-Si berturut-turut sebesar 77 HR_B dan 106 HR_H. Pengamatan struktur mikro lapisan Ni-Al menunjukkan struktur mikro yang lebih padat dibandingkan dengan struktur mikro lapisan dengan parameter standar. Untuk lapisan Al-Si, selain struktur mikro yang lebih padat, juga diperoleh fasa eutektik yang lebih proporsional dibandingkan dengan struktur mikro lapisan dengan parameter standar.

Kata Kunci: Plasma spray atmosferik, lapisan, Ni-Al, Al-Si, kecepatan lintas, kekuatan ikatan tarik, kekerasan

Atmospheric Plasma Spray Coating of Ni-Al and Al-Si on Austenitic Stainless-Steel Casing with Limited Short Spray Distance

The atmospheric plasma spray coating is a coating process that many used in industrial applications. High density and bond strength are the main features of this process. The limited spray distance between nozzle gun and work piece surface during the plasma spray process requires standard process parameters modification. In the present study, an effort carried out a change of process parameters on the Ni-Al and Al-Si for optimum results. Tensile bond strength, hardness, and microstructure tests were used to validate the coating. The Ni-Al and Al-Si layers had average tensile strengths of 9110 and 7283 Psi, respectively. The Ni-Al and Al-Si layers had average hardness values of 77 HR_B and 106 HR_H, respectively. When compared to the microstructure with standard parameters, the microstructure of the Ni-Al layer showed a denser microstructure. In addition to the denser microstructure of the Al-Si layer, a more proportional eutectic phase was obtained when compared to the microstructure of the layer with standard parameters.

Keywords: Atmospheric plasma spray, coating, Ni-Al, Al-Si, traverse speed, tensile bond strength, hardness

METALURGI

ISSN 0126 – 3188 Metalurgi, Vol. 36 No. 2 Agustus 2021

UDC (OXDCF) 546.7

Yohana Fransiska Ferawati dan Ratna Frida Susanti (Jurusan Teknik Kimia, Universitas Katolik Parahyangan)

Peran N-Doping terhadap Karakteristik Pori Karbon Aktif yang Dihasilkan dari Limbah Destilasi Akar Wangi

Metalurgi, Vol. 36 No. 2 Agustus 2021

Pada penelitian ini modifikasi gugus fungsi permukaan nitrogen pada karbon aktif dari limbah akar wangi diteliti pengaruhnya terhadap pengembangan pori karbon aktif. Sintesis karbon aktif dilakukan dengan cara karbonisasi hidrotermal LAW (limbah akar wangi) pada suhu 225 °C selama 18 jam dilanjutkan dengan aktivasi menggunakan tungku tabung dalam atmosfer nitrogen dengan laju 100 mL/menit pada suhu 800 °C selama 2 jam dengan bahan pengaktivasi K_2FeO_4. Urea digunakan sebagai sumber nitrogen. Variasi konsentrasi urea yang diteliti adalah 1:0 (AC-0), 1:3 (AC-3) dan 1:5 (AC-5). Hasil yang diperoleh menunjukkan bahwa ketiga karbon aktif ini memiliki karakteristik mesopori dengan luas permukaan S_{BET} (brunauer emmett teller) terbesar yaitu 552,90 m^2g^{-1} dan diameter pori rata-rata 3,43 nm. Keberadaan gugus fungsi nitrogen juga tampak pada analisa FTIR (fourier transform infrared spectrometer). Berdasarkan hasil analisa SEM-EDX (scanning electron microscopy-energy dispersive x-ray), semakin besar rasio penambahan urea maka unsur N yang terkandung pada karbon aktif semakin meningkat. Sintesis karbon aktif dari limbah akar wangi dengan penambahan urea merupakan metode terbaru untuk menghasilkan karbon aktif mesopori yang nantinya dapat digunakan dalam aplikasi elektroda dan katalis pendukung.

Kata Kunci: Doping nitrogen, urea, limbah akar wangi, karbon aktif

The Role of N-Doping to the Pore Characteristics of Activated Carbon from Vetiver Root Distillation Waste

This work studied the effect of nitrogen functional group modification on activated carbon synthesized from vetiver root waste on pores development. Synthesis of activated carbon was carried out by hydrothermal carbonization of vetiver root waste at a temperature of 225 °C for 18 hours followed by chemical activation using K_2FeO_4 as an activated agent in a tubular furnace at a temperature of 800 °C for 2 hours with nitrogen atmosphere flowed at a rate of 100 mL/minute. Urea was used as a nitrogen source. The variation of urea concentration was 1:0 (AC–0), 1:3 (AC–3), and 1:5 (AC–5). The results showed that these activated carbons have mesoporous characteristics with the largest S_{BET} (brunauer emmett teller) surface area of 552.90 m^2g^{-1} and average pore width 3.43 nm. The presence of the nitrogen functional group was observed in the FTIR (fourier transform infrared spectrometer) analysis. Based on SEM-EDX (scanning electron microscopy-energy dispersive x-ray) analysis, a higher amount of urea addition will increase the nitrogen content in activated carbon. Synthesis of activated carbon from vetiver root waste with an addition of urea is the newest method to produce mesoporous activated carbon for electrode and support catalyst purposes.

Keywords: Nitrogen doping, urea, vetiver root waste, activated carbon

METALURGI

ISSN 0126 – 3188 Metalurgi, Vol. 36 No. 2 Agustus 2021

UDC (OXDCF) 620.112

I Nyoman Gede Putrayasa Astawa, Vinda Puspasari, Efendi Mabruri, Satrio Herbirowo, Edi Priyanto Utomo (Pusat Penelitian Metalurgi dan Material-LIPI)

Pengaruh Proses ECAP terhadap Sifat Keras, Morfologi Permukaan, dan Ketahanan Korosi Paduan Aluminium 6061

Metalurgi, Vol. 36 No. 2 Agustus 2021

Paduan aluminum Al-Mg-Si (6xxx) telah banyak digunakan sebagai material struktural untuk bangunan dan kendaraan bermotor karena memiliki kekuatan mekanik dan ketahan korosi yang baik. Proses ECAP (equal channel angular pressing) merupakan metode yang paling menjanjikan dengan mengaplikasikan deformasi plastis yang memproduksi material utuh dengan butir yang halus tanpa porositas sisa. Penelitian ini mempelajari tentang pengaruh jumlah pass pada proses ECAP terhadap kekerasan, struktur mikro, dan perilaku korosi pada paduan aluminum 6061. Material paduan terlebih dahulu dilakukan proses aniling di dalam tungku dengan lingkungan gas argon pada T = 530 °C selama 4 jam kemudian dicelupkan pada nitrogen cair selama 5 menit sebelum proses ECAP. Proses ECAP dilakukan melalui rute Bc dengan cetakan yang memiliki lubang dalam bersudut 120° dan variasi pass dari 1, 2, 3, dan 4. Kekerasan optimal yang diperoleh yaitu 107,58 HB pada paduan Al 6061 dengan 3 pass ECAP. Peningkatan jumlah pass pada ECAP menyebabkan adanya pengurangan ukuran butir dari ukuran 10 µm pada paduan hasil aniling menjadi ukuran 2,5 µm pada paduan dengan 4 pass. Ketahanan korosi meningkat seiring dengan peningkatan jumlah ECAP pass.

Kata Kunci: Paduan Al-Mg-Si, ECAP, kriogenik, struktur mikro, ketahanan korosi

The Effect of ECAP Processing on Hardness, Surface Morphology, and Corrosion Resistance of 6061 Alloys

Al-Mg-Si alloys (6xxx) have been widely used as structural materials in buildings and vehicles because of their excellent strength and corrosion resistance. ECAP (equal channel angular pressing) is the most promising method to apply SPD (severe plastic deformation), producing ultra-fine grain in the bulk material without residual porosity. This study presents some experiments results on the effect of ECAP number of passes variation on the hardness, microstructure, and corrosion behavior of Al 6061 alloys. The alloy was annealed in the furnace with an argon gas environment at 530°C for 4 hours and then immersed in liquid nitrogen for 5 minutes before the ECAP process. The ECAP process was carried out via the Bc route, with dies with an internal channel angle of 120° and pass variations of 1, 2, 3, and 4. The optimum hardness was 107.58 HB in Al 6061 alloy with three passes of ECAP. The increasing ECAP number of passes leads to a significant grain size reduction from the 0-way pass; the grain size was around 10 µm, while for a 4-way pass, the grain size was around 2.5 µm. The corrosion resistance of Al 6061 alloys increased with the increasing number of passes in the ECAP process.

Keywords: Al-Mg-Si alloys, ECAP, cryogenic, hardness, microstructure, corrosion resistance

METALURGI

ISSN 0126 – 3188 Metalurgi, Vol. 36 No. 2 Agustus 2021

UDC (OXDCF) 553.4

Kevin Cleary Wanta[a], Edward Yonathan Natapraja[a], Ratna Frida Susanti[a], Gelar Panji Gemilar[b], Widi Astuti[c], Himawan Tri Bayu Murti Petrus[d] ([a]Department of Chemical Engineering, Faculty of Industrial Technology, Parahyangan Catholic University, [b]PT Petrokimia Gresik, [c]Research Unit for Mineral Technology, Indonesian Institute of Sciences, [d]Department of Chemical Engineering, Gadjah Mada University)

Peningkatan Perolehan Logam dalam Proses Leaching Spent Catalyst pada Temperatur Rendah: Penambahan Hidrogen Peroksida dan Natrium Klorida

Metalurgi, Vol. 36 No. 2 Agustus 2021

Salah satu faktor yang memengaruhi proses leaching dari suatu sumber mineral adalah karakteristik mineral dari bahan baku tersebut. Tidak semua fasa mineral dapat dilakukan proses leaching secara langsung dan sempurna. Dengan demikian, beberapa mineral memerlukan perlakuan khusus sehingga proses leaching dapat berlangsung dengan maksimal. Studi ini akan terfokus pada mempelajari pengaruh penambahan senyawa aditif, yaitu hidrogen peroksida dan natrium klorida, dalam proses leaching spent catalyst dengan menggunakan larutan asam sulfat. Proses leaching dilakukan pada konsentrasi larutan asam sulfat 1 M selama 240 menit pada suhu ruang. Konsentrasi hidrogen peroksida divariasikan pada 0–9%v/v sedangkan konsentrasi natrium klorida divariasikan pada 0–0,8 mol/L. Hasil percobaan menunjukkan bahwa kedua senyawa aditif tersebut mampu meningkatkan perolehan nikel secara signifikan. Perolehan nikel tertinggi sebesar 95,08% tercapai saat penggunaan hidrogen peroksida sebesar 9%v/v. Perolehan nikel ini lebih tinggi 3,5 kali dibandingkan dengan tanpa penambahan hidrogen peroksida. Sementara itu, konsentrasi natrium klorida sebesar 0,8 mol/L mampu memberikan perolehan nikel tertinggi sebesar 50,38% atau meningkat sebesar 1,9 kali bila dibandingkan dengan tanpa penambahan natrium klorida.

Kata Kunci: Leaching, spent catalyst, hidrogen peroksida, natrium klorida, nikel

Increasing of Metal Recovery in Leaching Process of Spent Catalyst at Low Temperature: The Addition of Hydrogen Peroxide and Sodium Chloride

One of the factors that affect the leaching process of a mineral source is the mineral characteristics of the raw materials. Not all mineral phases can be leached completely and directly. Thus, some minerals require special treatment so that the leaching process can take place optimally. The purpose of this research is to investigate the effect of adding additive compounds, such as hydrogen peroxide and sodium chloride, to the leaching process of spent catalyst using a sulfuric acid solution. The leaching process was carried out at room temperature for 240 minutes with a concentration of 1 M sulfuric acid solution. The highest nickel recovery of 95.08% was obtained when hydrogen peroxide was used at a concentration of 9% v/v. The experimental results showed that the two additive compounds were able to increase nickel recovery significantly. The highest nickel recovery of 95.08% was achieved when hydrogen peroxide was used at 9%v/v. The nickel recovery is 3.5 times higher than without the addition of hydrogen peroxide. Meanwhile, a sodium chloride concentration of 0.8 mol/L was able to provide the highest nickel recovery of 50.38 %, or a 1.9 times increase over the control.

Keywords: Leaching, spent catalyst, hydrogen peroxide, sodium chloride, nickel

METALURGI

ISSN 0126 – 3188 Metalurgi, Vol. 36 No. 2 Agustus 2021

UDC (OXDCF) 620.112

Rizta Febian Adi Endani[a], Lia Andriyah[b], Soesaptri Oediyani[a], Latifa Hanum Lalasari[b], Tri Arini[b], Nadia Chrisayu Natasha[b], Fariza Eka Yunita[b], Ariyo Suharyanto[b] ([a]Metallurgical Engineering, Sultan Ageng Tirtayasa University, [b]Research Center for Metallurgy and Materials-Indonesian Institute of Sciences)

Pengaruh Variasi Suhu dan Arus Elektrolit Terhadap Sintesis Mangan Dioksida dari Prekursor Mangan Sulfat Menggunakan Metode Elektrolisis

Metalurgi, Vol. 36 No. 2 Agustus 2021

Perkembangan ilmu dan teknologi dewasa ini dalam bidang elektronik, khususnya penyimpanan energi meningkatkan permintaan dalam penggunaan baterai sekunder litium. Pengembangan baterai litium difokuskan pada kapasitas penyimpanan energi dengan menggunakan mangan dioksida (MnO_2) sebagai bahan katoda baterai litium. Mangan dioksida dipilih sebagai bahan katoda baterai litium karena memiliki kapasitas penyimpanan yang tinggi yaitu sekitar 615 mAh/g dibandingkan dengan material lain seperti grafit yang memiliki kapasitas penyimpanan 372 mAh/g. Sintesis MnO_2 dilakukan dengan metode elektrolisis dari prekursor mangan sulfat ($MnSO_4$) yang diperoleh dari proses pelindian bijih mangan Kabupaten Trenggalek. Proses elektrolisis dilakukan selama 5 jam dengan menggunakan variasi temperatur elektrolit 30, 40, 50 dan 60 °C serta variasi arus 2, 3, 4 dan 5 A untuk mengetahui pengaruh temperatur elektrolit dan arus terhadap perolehan massa, polimorfi struktur dan morfologi MnO_2 yang terbentuk. Perolehan massa tertinggi diperoleh pada penggunaan temperatur elektrolit 60 °C dan arus 5 A yaitu sebesar 11,4 gram. Hasil karakterisasi MnO_2 dengan menggunakan XRF (x-ray fluorescence) Thermo type ARL 9900 menunjukkan kadar mangan dioksida sebesar 85,472% dan hasil analisa dengan menggunakan XRD (x-ray diffraction) Shimadzu type 7000 diperoleh polimorfi struktur senyawa MnO_2 yang terbentuk adalah polimorfi α-MnO_2. Citra SEM (scanning electron microscope) menunjukkan bahwa partikel MnO_2 memiliki bentuk bulat berduri dan cenderung beraglomerasi dengan nilai diameter partikel berkisar antara 50-70 nm.

Kata Kunci: Elektrolisis, MnO_2, $MnSO_4$, temperatur elektrolit, arus

The Effect of ECAP Processing on Hardness, Surface Morphology, and Corrosion Resistance of 6061 Alloys

The advancement of science and technology in the field of electronics, particularly in the field of energy storage, is increasing the demand for the use of lithium secondary batteries. The use of manganese dioxide (MnO_2) as a lithium battery cathode material is focusing the development of lithium batteries on energy storage capacity. Manganese dioxide was chosen as the cathode material for lithium batteries because it has a high storage capacity of about 615 mAh/g compared to other materials such as graphite which has a storage capacity of 372 mAh/g. MnO_2 was synthesized by the electrolysis method from manganese sulfate ($MnSO_4$) precursor which was obtained from the Trenggalek manganese ore leaching process. The electrolysis process was carried out for 5 hours using variations in electrolyte temperature of 30, 40, 50, and 60 °C as well as variations in a current of 2, 3, 4, and 5 A to determine the effect of electrolyte temperature and current on mass gain, structural polymorphy, and morphology of MnO_2 formed. The highest mass gain was obtained at the use of an electrolyte temperature of 60 °C and a current of 5 A, which was 11.4 grams. The characterization of MnO_2 using XRF (x-ray fluorescence) Thermo type ARL 9900 revealed manganese dioxide levels of 85.472%, and the analysis using XRD (x-ray diffraction) Shimadzu type 7000 revealed that the polymorphy structure of the MnO_2 compound formed was α-MnO_2 polymorphy. The MnO_2 particles have a spiny round shape and tend to agglomerate, as shown by the SEM (scanning electron microscope) image, with particle diameter values ranging from 50 to 170 nm.

Keywords: Electrolysis, MnO_2, $MnSO_4$, electrolyte temperature, current

METALURGI
Majalah Ilmu dan Teknologi
p-ISSN 0126-3188 | e-ISSN 2443-3926
www.ejurnalmaterialmetalurgi.com

THE EFFECT OF ALKALI ROASTING OF FERRONICKEL SLAG PRIOR TO THE LEACHING AND PRECIPITATION PROCESS

Wahyu Mayangsari[a,*], Agus Budi Prasetyo[a], Eni Febriana[a], Januar Irawan[a], Rudi Subagja[a], Florentinus Firdiyono[a] and Johny Wahyuadi Soedarsono[b]

[a]Pusat Penelitian Metalurgi dan Material - LIPI
Gedung 470, Kawasan PUSPIPTEK Serpong, Banten, Indonesia 15343
[b]Departemen Teknik Metalurgi dan Material, Universitas Indonesia
Jl. Kampus UI Depok, Depok, Jawa Barat, Indonesia 16424
*E-mail: wahy035@lipi.go.id

Masuk tanggal : 04-05-2021, revisi tanggal : 09-08-2021, diterima untuk diterbitkan tanggal 09-09-2021

Abstrak

Terak feronikel dihasilkan sebagai produk samping dari produksi feronikel. Terak feronikel mempunyai potensi untuk dimanfaatkan sebagai bahan baku beberapa komponen berharga karena komposisinya melalui proses bertahap. Tujuan dari penelitian ini adalah untuk mengetahui pengaruh dari proses pemanggangan campuran terak feronikel dan Na_2CO_3 sebelum pelindian dengan air panas dan presipitasi untuk menghasilkan endapan silika. Proses pemanggangan terak feronikel dengan penambahan Na_2CO_3 telah dilakukan untuk pembentukan natrium silikat. Kemudian dilarutkan melalui proses pelindian menggunakan air panas 90 °C selama 120 menit. Endapan silika didapatkan dengan proses presipitasi sodium silikat terlarut diikuti dengan pemeraman selama tiga hari. Berdasarkan hasilnya, pemanggangan menyebabkan perubahan komposisi yang mempengaruhi persen pelindian dan perolehan silika. Reaksi terjadi dari permukaan ke inti yang dibuktikan dengan pengecilan ukuran residu pelindian dari RAF (*roasted of alkalinized ferronickel slag*). Natrium silikat dalam bentuk Na_4SiO_4 diketahui terlarut pada tahap pelindian dengan air panas. Pengendapan dan pemeraman larutan natrium silikat telah menghasilkan endapan silika dengan ukuran partikel lebih dari 100 µm. Proses pemanggangan pada 1000 °C selama 240 menit menghasilkan perolehan silika tertinggi.

Kata Kunci: Feronikel, terak, pemanggangan, pelindian, pengendapan, silika

Abstract

As a by-product of ferronickel production, ferronickel slag was created. Because of its composition, it has the potential to be used as a raw material for some valuable elements through a series of processing. The purpose of this research is to determine the effect of roasting ferronickel slag and Na_2CO_3 prior to hot water leaching and precipitation to obtain silica precipitate. To produce sodium silicate, ferronickel slag was roasted with Na_2CO_3 addition. It was then dissolved by leaching for 120 minutes in hot water at around 90 °C. Silica precipitate is made by precipitating dissolved sodium silicate and aging it for three days. According to the findings, roasting causes a change in composition, which influences the leaching percentage and silica recovery. Size reduction of leaching residue from its RAF (roasted alkalinized ferronickel slag) demonstrated that reactions occurred from the surface to the core. When water is leached, sodium silicate in the form of Na_4SiO_4 is observed and dissolved. The precipitation and aging of sodium silicate solution produced silica precipitate with particle sizes greater than 100 µm. The highest silica recovery is obtained by roasting at 1000 °C for 240 minutes.

Keywords: *Ferronickel, slag, roasting, leaching, precipitation, silica*

1. INTRODUCTION

The smelting process of lateritic nickel ore produces ferronickel or nickel matte as the main product and ferronickel slag as a by-product. Ferronickel has been used mostly as material for stainless steel. Meanwhile, nickel matte is commonly used for producing pure nickel as well as nickel sulfate for cathode materials in battery which has been developed recently. However, mostly ferronickel slag is just used as reclamation materials [1] without further processing,

DOI : http://dx.doi.org/10.14203/metalurgi.v36i2.588

Metalurgi is Sinta 2 Journal (https://sinta.ristekbrin.go.id/journals/detail?id=3708) accredited by Ministry of Research & Technology, Republic Indonesia

therefore it does not own the added value. Ferronickel slag contains various valuable elements such as Al, Cr, Fe, Mg, Si [2]-[4] as well as rare earth elements [5] that potentially recover. However, presently research for ferronickel slag mostly tends to make it as construction materials [6]–[10] due to its properties. The methodology to recover its valuable elements is still rare and challenging, therefore study about the recovery of valuable materials from ferronickel slag is essential to be carried out.

Fang et. al., [11] tried to recycle Si and Al from ferronickel slag with sodium hydroxide addition through alkali roasting and water leaching processes. The extraction percentage of Si increases as roasting temperature and time increase. About 80% Si can be recovered from the water leaching process of roasted mixture of ferronickel slag and sodium hydroxide at 550 °C. Gu et. al., [12] obtained 92.33% of chromium from the selective recovery of ferronickel slag with Na_2O_2 addition. The optimum result is obtained from roasting at 600 °C for one hour with the ratio of ferronickel slag and Na_2O_2 is 1:1, leaching temperature of 50 °C for one hour, and liquid/ solid ratio 10 ml/g. Prasetyo et. al., [5] carried out roasting processes to the mixture of ferronickel slag and Na_2CO_3. Sodium silicate is observed in the XRD (x-ray diffraction) analysis of the roasted products. Moreover, magnesium was also recovered by the calcination process followed by leaching using NaOH solution to dissolve silica and recover magnesium, in which 73.10% of magnesium can be obtained from this process [13].

In the previous study [14], alkali fusion of ferronickel slag using Na_2CO_3 through the roasting process was carried out. Weight loss percentage due to the roasting process, reaction mechanism proposed as well as quantitative analysis of Al, Fe, and Mg in the roasted ferronickel slag are discussed. In this study, hot water leaching of RAF and precipitation were carried out. Na_2CO_3 was added as an additive to lower the melting point of the mixture [5],[14] since the melting point of ferronickel slag is high, at about 1400 °C, depends on the compositions [2]. Moreover, it provides better separation of Ca to the leaching residue instead of to the leachate due to $CaCO_3$ formation [15]. Meanwhile, the sodium ion is expected to react with SiO_2 to form sodium silicate which is dissolved in the water when the leaching process is carried out, and then it can be separated and precipitated by acid to produce silica precipitate. This study aims to determine the effect of roasting processing of ferronickel slag with Na_2CO_3 addition prior to hot water leaching and precipitation to obtain silica precipitate.

2. MATERIALS AND METHODS

Ferronickel slag used is from a smelting plant at Morowali, Centre of Sulawesi, Indonesia. Size reduction was conducted to the ferronickel slag to obtain 0.15 mm fine grain. It was then physically mixed with the analytical grade of sodium carbonate (Na_2CO_3) from Merck with a 50: 50 by weight. Roasting processes at specific temperatures and times were conducted to the weighted ferronickel slag and Na_2CO_3 mixture in the CWF 1300 muffle furnace to produce RAF. Roasting temperature and time used for this study are 800 - 1000 °C and for 60, 120, and 240 minutes. Roasted slag resulted from the roasting process at a temperature of 800, 900, and 1000 °C is then referred to as RAF 800, RAF 900, and RAF 1000 respectively.

Leaching processes using hot water accompanied by heating at about 90 °C and stirring, were carried out to 10 g of the RAF and 100 ml hot water for 120 minutes in the beaker glass which was heated in a hot plate. The process was then continued with filtration to separate leachate and leaching residue. The mass differences of RAF weight for leaching and residue leaching were used to calculate the leaching percentage. The leaching residues were dried in the oven at 110 °C for characterization. Meanwhile, silica precipitation using 20 ml of HCl was performed on the leachates. HCl has added drops-wisely together to obtain a homogeneous mixture, which was then aged for three days for precipitations subsequently. The precipitates formed were then filtered to separate it with the solution and dried in the oven at 110 °C for 6 hours. The precipitates resulted were then weighted to calculate the recovery and characterize.

To determine the effect of roasting processes before the leaching, SEM-EDS (scanning electron microscope-energy dispersive spectroscopy) analysis was performed on the raw ferronickel slag, RAF, residue leaching, and silica precipitate to determine the microstructure of ferronickel slag and its transformations due to roasting and leaching processes. Furthermore, XRD (x-ray diffraction) analysis was performed to determined phases transformations of roasted product and leaching residue. Figure 1 shows the process flow diagram of this research.

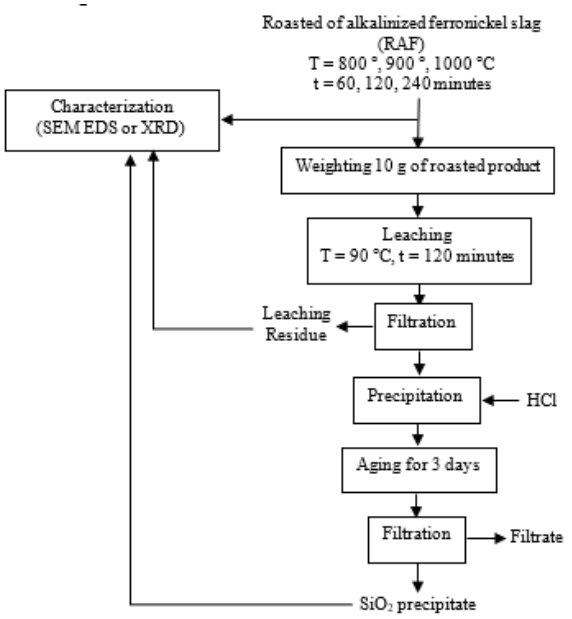

Figure 1. Process flow diagram

3. RESULTS AND DISCUSSIONS

A characterization of the raw ferronickel slag was carried out by SEM-EDS (scanning electron microscope-energy dispersive spectroscopy) analysis to determine the morphology and the compositions. Figure 2 shows the morphology of the ferronickel slag and its EDS analysis in the captured area summarized in Table 1. The morphology is rough and has various particle sizes, while the EDS shows that Si and O are the main components followed by Mg and Fe.

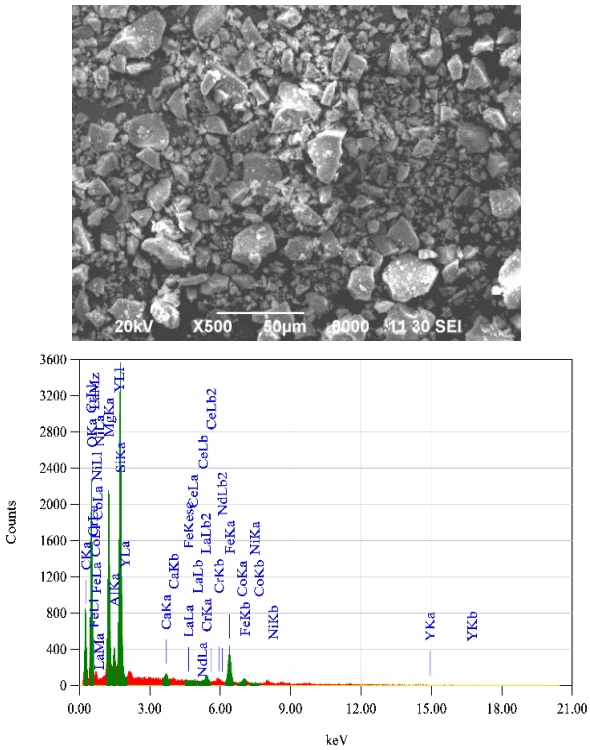

Figure 2. SEM-EDS of ferronickel slag

Table 1. Compositions of ferronickel slag

Element	Wt.%
O	45.96
Mg	14.59
Al	3.08
Si	20.84
Ca	1.60
Cr	1.60
Fe	11.84
Co	0.39
Ni	0.058
Cu	0.97

The leaching process was conducted at 90 °C for 120 minutes to the RAF which was previously roasted at various temperatures and times. The leaching percentage was then calculated to determine the ratio of dissolved materials to the initial mass of the roasted slag which is used in the leaching process. The effect of alkali roasting prior to the leaching process toward the leaching percentage, microstructure transformations, and its compositions as well as phase transformations is discussed here.

3.1 The Effect of Alkali Roasting Prior to Leaching Process toward Leaching Percentage

The leaching processes were carried out to the RAF 800, RAF 900, and RAF 1000 which were roasted previously for 60-240 minutes by using hot water. The leaching was performed at a temperature of 90 °C for 120 minutes with a solid/ liquid ratio of 1 g/ 10 ml.

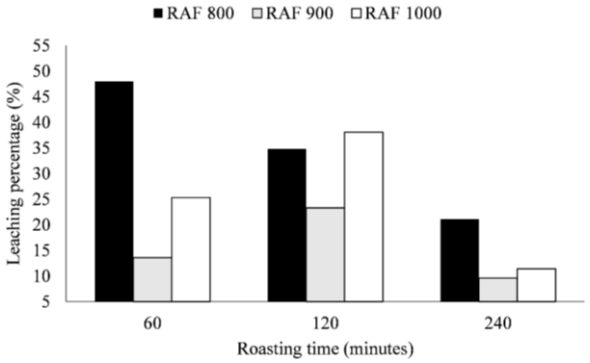

Figure 3. The effect of alkali roasting process at various temperature and time prior to leaching process toward leaching percentage

Figure 3 shows the effect of the alkali roasting process at various temperatures and times before the leaching process toward the leaching percentage. The higher leaching percentage means more RAF dissolved in the hot water during leaching. The trend of leaching percentage resulted from the leaching process of RAF 800 is different, the longer leaching time,

the lower leaching percentage resulted. Meanwhile, RAF 900 and RAF 1000 have a similar tendency, showing the highest leaching percentage at 120 minutes.

The melting point of Na_2CO_3 is 851 °C, roasting at a temperature of 800 °C might be affecting the lower decomposition of the mixture of ferronickel slag and Na_2CO_3 in the roasting process due to solid-solid reactions. Moreover, most of Na_2CO_3 remains in the initial form, the previous study shows that the mapping of the roasted product of the mixture of ferronickel slag and Na_2CO_3 at a similar process condition demonstrating sodium distributes on the specific area [5]. The presence of Na_2CO_3 in the initial form contributes to the rise in the leaching percentage of the RAF due to the initial characteristic of Na_2CO_3 that easily dissolves in the water, it is not caused by a good decomposition that resulted from the desired compositions. Furthermore, as the contact of the mixtures was longer by increasing leaching time, the reaction might be better, resulting product that is more difficult to dissolved in the hot water such as sodium magnesium silicate as illustrates in Fig. 5. Therefore, the leaching percentage was higher in the first 60 minutes and constantly decrease as longer leaching time was performed.

When the roasting process was carried out at the temperature 900 and 1000 °C, higher than the melting point of Na_2CO_3, the solid-liquid reactions might have occurred and better decomposition has resulted. Based on the previous study, the sharp peak of an endothermic reaction is observed on the TG-DTA analysis of ferronickel slag and Na_2CO_3 at 900 °C [5]. RAF 900 and RAF 1000 have a similar tendency, showing the highest leaching percentage at 120 minutes. RAF at 900 °C has a lower leaching percentage, about 15%, than the leaching percentage of RAF 1000. It is in good agreement with the previous study that the leaching percentage increases as the roasting temperature rises. Moreover, the leaching percentage decreased as roasting time escalates more than 3 hours [12].

3.2 The Effect of Alkali Roasting Prior to Leaching Process toward Microstructure Transformation and Composition

In order to determine the effect of alkali roasting prior to the leaching process toward microstructure transformation and its composition, SEM-EDS was performed to the RAF 800, RAF 900, RAF 1000 (resulted from the roasting process for 60 minutes) and its leaching residue. Figure 4 shows the SEM analysis of the roasted products (RAF 800, RAF 900, RAF 1000) and their leaching residue. The differences between the three are obvious. RAF 800, RAF 900, RAF 1000 are shown in Figs. 4(a), 4(c), 4(e) have the greater particle size, white and porous microstructure on the surface. Moreover, Figs. 4(b), 4(d), 4(f) show the microstructure of leaching residue. It can be seen that the particle size is reduced to the smaller size, the white and porous sharp is also reduced, the dark and compact form leftover, which indicated some elements or compounds dissolved into hot water even though just on the surfaces, therefore affect the microstructure itself. Figures 4(a) and 4(b) change slightly. Figures 4(c) and 4(d) show the greater particle size. It is caused by elements content escalation (Table 2) at these process conditions, reducing the solubility to the hot water [16]. On the other hand, Fig. 4(e) shows the greatest melting component than the others and the greatest dissolved components into the hot water. It can be shown by the greater differences in particle size in Fig. 4(f) compared to the others.

Table 2. Composition of RAF (*roasted alkalinized ferronickel)* and leaching residue

Elements	RAF 800	Leaching residue RAF 800	RAF 900	Leaching residue RAF 900	RAF 1000	Leaching residue RAF 1000
O	32.30	28.79	51.18	32.29	41.96	30.20
Na	8.08	7.87	21.92	11.75	20.04	16.04
Mg	18.41	18.36	9.04	13.38	7.71	13.61
Al	3.47	2.63	2.15	2.95	1.63	2.63
Si	21.00	15.11	13.00	15.31	12.37	19.34
Ca	0.87	1.27	-	-	-	-
Cr	1.20	1.95	2.12	3.91	1.67	1.19
Fe	13.19	18.69	13.78	16.43	10.77	12.21
Co	-	-	0.39	-	0.13	-
Ni	-	-	0.12	-	-	-
Cu	-	2.77	3.98	2.44	-	2.23
Zn	1.49	1.56	1.65	1.56	2.38	1.37
Mn	-	0.99	-	-	1.33	1.18

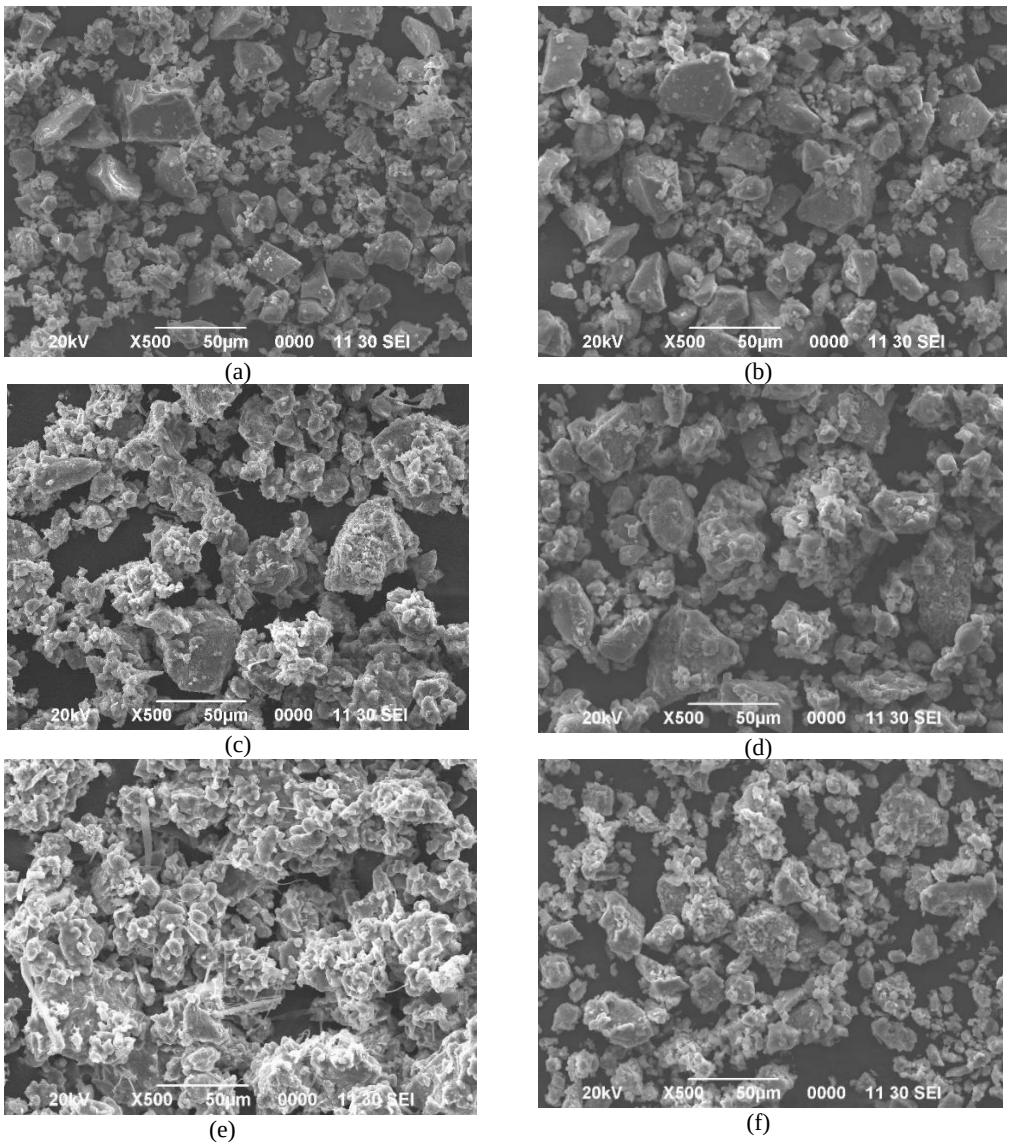

Figure 3. SEM analysis of (a) RAF 800 (b) leaching residue 800 (c) RAF 900 (d) leaching residue 900 (e) RAF 1000 (f) leaching residue 1000

AS the EDS analysis of RAF 800, RAF 900, and RAF 1000 which were roasted for 60 minutes, and their leaching residue is shown in Table 2.

RAF 800 was slightly changed in the content compared of the element to the raw ferronickel slag. It might be caused by reactions that occurred to the spinel phases that bearing Al and Mg [14]. Moreover, Fe as Fe_2SiO_4 from olivine also reacted with Na_2CO_3 at about 610 °C [14]. Therefore, the content of Al, Mg, and Fe slightly increase in the RAF 800 compare with raw ferronickel slag.

The leaching process causes the content of O, Na, Al, and Si to slightly decrease. It shows that these elements dissolved in the hot water and increasing some elements content that remained in the leaching residue such as Ca, Cr, and Fe. Moreover, some elements such as Cu, Zn, and Mn can also be observed.

RAF 900 shows the greatest change of elements content. The previous study also shows the greatest changes in the content of the element Al, Fe, and Mg with similar process conditions [14]. Liquid-solid reactions occurred since the process was performed at a temperature higher than the melting temperature of Na_2CO_3. The higher change of O content shows that RAF 900 is covered by oxide. Moreover, Ni and Co just can be observed on the RAF 900. Increasing elements content of Fe, Co, Cu, Cr, and Ni are in line with increasing O content. It indicates that these elements are in the form of oxide. However, increasing elements content might be causing the lower leaching percentage since more components are not dissolved in hot water. It can be proved by increasing elements content of Al,

Cr, Fe, and Mg in the leaching residue compared to RAF 900 or raw ferronickel slag. Decreasing O, Na, and Si elements in the leaching residue indicated that these elements dissolved in the hot water thus some elements contained in the leaching residue increase.

The element's content of RAF 1000 has a similar trend with RAF 900. The element content of Al, Fe, Mg, and Si in the leaching residue was higher than its RAF. However, the content of Cr, Na, and O in the leaching residue was decreased. It indicates a part of the dissolution of these components in the leachate. Increasing roasting temperature rises reaction rat, the content of Na in the leaching residue of RAF 1000 shows the highest content than RAF 800 and RAF 900, it indicates that more ferronickel slag reacts with Na_2CO_3.

3.3 Phase Transformation of RAF and Leaching Residue

XRD (x-ray diffraction) analysis was used to determine the phase transformation of the roasted product and the leaching residue. It carried out to the roasted product that was roasted at 1000 °C (RAF 1000) for 60 minutes and its leaching residue.

Figure 5(a) shows the XRD analysis of RAF 1000 °C. It shows olivine that is an original phase of ferronickel slag [12],[14] reacts with Na_2CO_3 forming $Na_2(MgSiO_4)$, Mg_2SiO_4, $NaAlSiO_4$, Na_4SiO_4, MgO, and Fe_3O_4. The proposed reactions are as follow [12], [14]:

$2[(Mg{\cdot}Fe)O{\cdot}SiO_2] + 3/2\ O_2 \rightarrow Mg_2SiO_4 + SiO_2 + Fe_2O_3$ (1)
$Mg_2SiO_4 + Na_2CO_3 \rightarrow 2MgO + Na_2SiO_3 + CO_{2(g)}$ (2)
$Fe_2SiO_4 + Na_2CO_3 + ½\ O_2 \rightarrow Na_4SiO_4 + Fe_2O_3 + CO_{2(g)}$ (3)
$Fe_2SiO_4 + Na_2CO_3 \rightarrow Na_2SiO_3 + Fe_2O_3 + CO_{(g)}$ (4)
$MgO + SiO_2 + Na_2CO_3 \rightarrow Na_2MgSiO_4$ (5)
$MgAl_2O_4 + Na_2CO_3 \rightarrow MgO + 2NaAlO_2 + CO_{2(g)}$ (6)
$NaAlO_2 + SiO_2 \rightarrow NaAlSiO_4$ (7)

Figure 5(b) shows the XRD analysis of the leaching residue from the leaching process at about 90 °C for 120 minutes of RAF 1000. It shows that Na_4SiO_4 was separated in the leachate since it is not presented on the XRD graph, Figure 5 (b), and leftover $Na_2(MgSiO_4)$, Mg_2SiO_4, $NaAlSiO_4$, MgO and Fe_3O_4. The formation of $Na_2(MgSiO_4)$ is similar to the reaction between ferronickel slag and Na_2O_2 [12]. The presence of Fe_3O_4 instead of Fe_2O_3 in the XRD graph might be caused a reduction of Fe_2O_3 by CO resulted from the reactions that occurred. Moreover, the presence of sodium aluminosilicate could prohibit the dissolution of silicon in the leaching process [17], resulted a lower leaching percentage of silicon.

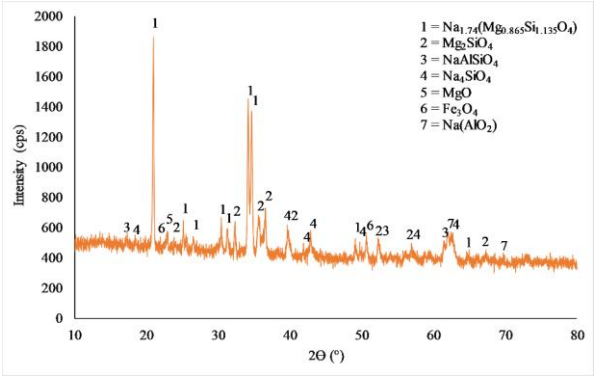

(a)

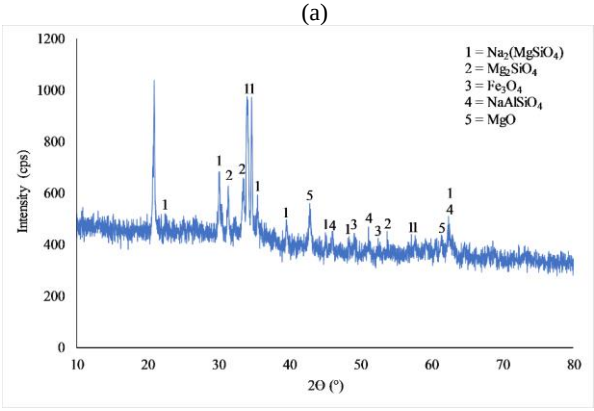

(b)

Figure 5. XRD analysis (a) roasted product at 1000 °C for 60 minutes and (b) the leaching residue

The semi-quantitative phases formed is tabulated in Table 3. The phases are dominated by $Na_2(MgSiO_4)$ and Mg_2SiO_4. It shows that SiO_2 does not liberate overall from olivine. The reaction might occur just at the surface since Mg_2SiO_4 is still presented. Moreover, the microstructure transformation of the RAF and its leaching residue show the surface differences.

Table 3. Phase compositions of roasted product and leaching residue

Phases	Roasted product (%)	Leaching residue (%)
Na_2MgSiO_4	43.8	54.7
Mg_2SiO_4	26.7	14.7
$NaAlSiO_4$	12.1	9.9
Na_4SiO_4	12.9	-
Fe_3O_4	2.7	7.3
MgO	1.7	13.3

3.4 Precipitation Process of the Leachate

Precipitations were conducted to the leachate that produced from leaching processes of RAF 800, RAF 900, and RAF 1000. The reaction mechanism for leaching and precipitation are shown on reaction (8) – (10).

$SiO_{2(s)} + 2Na_2CO_{3(s)} \rightarrow Na_4SiO_{4(s)} + 2CO_{2(g)}$ (8)
$Na_4SiO_{4(s)} + H_2O_{(l)} \rightarrow Na_4SiO_{4(aq)}$ (9)
$Na_4SiO_{4(aq)} + 4HCl_{(aq)} \rightarrow 4NaCl_{(aq)} + SiO_{2(s)} + 2H_2O_{(l)}$ (10)

Figure 6(a) shows the precipitate recovered from a series of roasting, leaching, and precipitation processes. It shows that the higher the roasting temperature and time, the higher silica recovered. Leaching followed by precipitation processes of roasted alkalinized ferronickel slag (RAF) with roasting temperature and time of 1000 °C and 240 minutes can recover precipitate up to 23.43 %. The low recovery of silica indicates the optimization of a series of processes needs to be carried out further. Decomposition of silica from olivine bonding to be sodium silicate must be optimum, therefore a high leaching percentage especially for Si can be obtained for the precipitation process further.

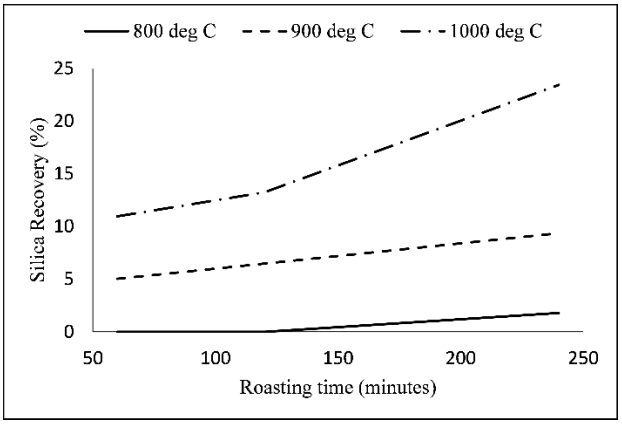

(a)

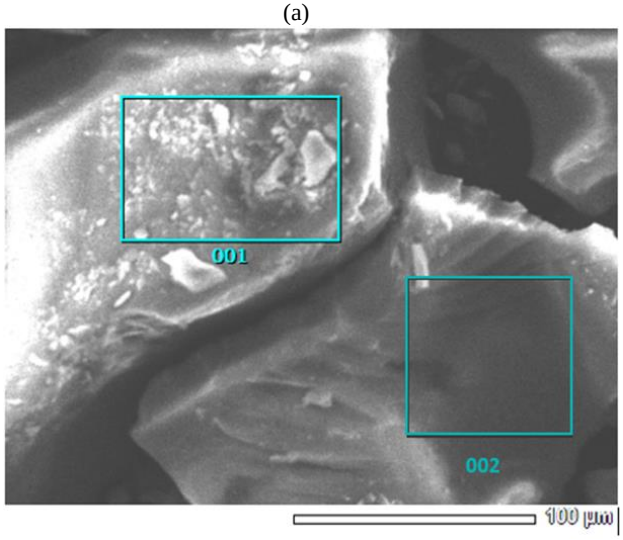

(b)

Figure 6. (a) Recovery of the precipitate (b) SEM analysis of the precipitate

Characterization of precipitate recovered is shown in Fig. 6(b) and its compositions in Table 4. SEM-EDS analysis shows the dark and compact particle with a particle size is more than 100 µm. The area 001 and 002 of EDS analysis show that the precipitate is silica. It shows that extraction of silica from ferronickel slag can be an option to provide added value for side products of nickel smelting.

Table 4. Compositions of silica precipitate

Compositions	Area 001	Area 002
Si	39.83	46.38
O	60.17	53.62
Total	100	100

4. CONCLUSIONS

The roasting process affects the content of the element of RAF and subsequently affects the leaching percentage of RAF. Roasting at 800 °C causes solid-solid reactions that generate low decomposition. Roasting at 900 °C causes massively decompositions, generating the lowest leaching percentage due to increasing some undissolved elements. Increasing roasting temperature to 1000 °C gains a higher leaching percentage. The higher the roasting temperature, the deeper reactions occurred, resulting from the smaller particle size of leaching residue. The reaction starts from the surfaces to the core. Sodium silicate (Na_4SiO_4) is formed as an effect of the roasting process and separated in the leachate when leaching using hot water performed. However, the presence of Na_2MgSiO_4, Mg_2SiO_4, and $NaAlSiO_4$ prevent the further dissolution of silica in the leaching process and cause low leaching percentage that trigger low recovery of the silica precipitate. Alkali roasting prior to the leaching process affects the recovery of silica precipitate, the higher the roasting temperature and the longer the roasting time, the more silica precipitate recovered. The particle size of silica precipitate is more than 100 µm.

ACKNOWLEDGEMENT

The authors would like to express their gratitude for the funding from PUTI 2020 Universitas Indonesia NKB-2028/UN2.RST/HKP.05.00/2020.

REFERENCES

[1] S. S. Kang, K. Park, and D. Kim, "Potential soil contamination in areas where ferronickel slag is used for reclamation work," *Materials*, vol. 7, no. 10, pp. 7157-7172, 2014. Doi: 10.3390/ma7107157

[2] C. Sagadin, S. Luidold, C. Wagner and C. Wenzl, "Melting behaviour of ferronickel slags," *The journal of the Minerals, Metals & Materials Society*, vol. 68, no. 07, pp. 3022-3028, 2016. Doi: 10.1007/s11837-016-2140-6

[3] Y. Cheol and S. Choi, "Alkali-silica reactivity of cementitious materials using ferro-nickel slag fine aggregates produced in different cooling conditions,"

Construction and Building Materials, vol. 99, pp. 279–281, 2015. Doi: 10.1016/j.conbuildmat.2015.09.039

[4] A. K. Saha, M. N. N. Khan, and P. K. Sarker, "Value added utilization of by-product electric furnace ferronickel slag as construction materials : A review," *Resources, Conservation & Recycling*, vol. 134, no. 7, pp. 10-24, 2018. Doi: 10.1016/j.resconrec.2018.02.034

[5] A. B. Prasetyo, A. Maksum, J. W. Soedarsono, and F. Firdiyono, "Thermal characteristics of ferronickel slag on roasting process with addition of sodium carbonate (Na_2CO_3)," in *International Seminar on Metallurgy and Materials 2019, OP Conf. Ser.: Mater. Sci. Eng*. 541 0120372019, 2020. Doi: 10.1088/1757-899X/541/1/012037

[6] A. K. Saha and P. K. Sarker, "Expansion due to alkali-silica reaction of ferronickel slag fine aggregate in OPC and blended cement mortars," *Construction and Building Materials*, vol. 123, pp. 135-142, 2016. Doi: 10.1016/j.conbuildmat.2016.06.144

[7] M. A. Rahman, P. K. Sarker, F. Uddin, A. Shaikh, and A. K. Saha, "Soundness and compressive strength of portland cement blended with ground granulated ferronickel slag," *Construction and Building Materials*, vol. 140, pp. 194-202, 2017. Doi: 10.1016/j.conbuildmat.2017.02.023

[8] Y. Huang, Q. Wang, and M. Shi, "Characteristics and reactivity of ferronickel slag powder," *Construction and Building Materials*, vol. 156, pp. 773-789, 2017. Doi: 10.1016/j.conbuildmat.2017.09.038

[9] A. Qi, X. Liu, Z. Wang, and Z. Chen, "Mechanical properties of the concrete containing ferronickel slag and blast furnace slag powder," *Construction and Building Materials*, vol. 231, pp. 117045, 2020. Doi:10.1016/j.conbuildmat.2019.117120

[10] J. Sun, J. Feng, and Z. Chen, "Effect of ferronickel slag as fine aggregate on properties of concrete," *Construction and Building Materials*, vol. 206, pp. 201-209, 2019. Doi: 10.1016/j.conbuildmat.2019.01.187

[11] D. Fang, J. Xue, and L. Xuan, "Recycling SiO_2 and Al_2O_3 from the laterite nickel slag in molten sodium hydroxides," in *9th International Symposium on High-Temperature Metallurgical Processing, The Minerals, Metals & Materials Series*, pp. 245-257, 2018.

[12] F. Gu, Y. Zhang, Z. Peng, Z. Su, H. Tang, W. Tian, G. Liang, J. Lee, M. Rao, G. Li, and T. Jiang, "Selective recovery of chromium from ferronickel slag via alkaline roasting followed by water leaching," *Journal of Hazardous Materials*, vol. 374, pp. 83-91, 2019. Doi: 10.1016/j.jhazmat.2019.04.002

[13] A. B. Prasetyo, R. Darmawansyah, W. Mayangsari, E. Febriana, S. Permana, A. Maksum, S. Oediyani, F. Firdiyono, J. W. Soedarsono, "Reverse leaching of magnesium from ferronickel slag using alkali," *Eastern-European Journal of Enterprise Technologies - Materials Science*, vol. 12, pp. 6-14, 2020. Doi: 10.15587/1729-4061.2020.193885

[14] W. Mayangsari, I. N. Avifah, A. B. Prasetyo, E. Febriana, and A. Maksum, "Decomposition of ferronickel slag thorugh alkali fusion in the roasting process," *Eastern-European Journal of Enterprise Technologie*, vol. 2, no. 6, pp. 44-51, 2021. Doi: 10.15587/1729-4061.2021.226342

[15] D. Fang, J. Xue, and L. Xuan, "Recycling SiO_2 and Al_2O_3 from the laterite nickel slag in molten sodium hydroxides," in *9th International Symposium on High-Temperature Metallurgical Processing, The Minerals, Metals & Materials Series*, pp. 245-257, 2018. Doi: 10.1007/978-3-319-72138-5_25

[16] Kirk-Othmer, *Encyclopedia of Chemical Technology, 4th edition*, vol. 1. John Willey & Sons Inc., USA, pp. 488, 1998.

[17] F. R. Mufakhir, M. Z. Mubarok, and Z. T. Ichlas, "Leaching of silicon from ferronickel (FeNi) smelting slag with sodium hydroxide solution at atmospheric pressure," *IOP Conference Series: Materials Science and Engineering, Mineral Processing and Technology International Conference 2017*, vol. 285, pp. 012003, 2018. Doi:10.1088/1757-899X/285/1/012003

METALURGI
Majalah Ilmu dan Teknologi
p-ISSN 0126-3188 | e-ISSN 2443-3926
www.ejurnalmaterialmetalurgi.com

ATMOSPHERIC PLASMA SPRAY COATING OF NI-AL AND Al-Si ON AUSTENITIC STAINLESS-STEEL CASING WITH LIMITED SHORT SPRAY DISTANCE

Ahmad Sahid[a,*], Ekavianty Prajatelistia[a], Ahmad Afandi[b]
[a]Material Science and Engineering Research Group
Faculty of Mechanical and Aerospace Engineering, Institut Teknologi Bandung
Jl. Ganesha 10 Bandung, Indonesia 40132
[b]Research Center for Physics, Indonesian Institute of Sciences
Gedung 440, Kawasan PUSPIPTEK Serpong, Banten, Indonesia 15314
*E-mail: ahmad.sahid.gerpasang@gmail.com

Masuk tanggal : 16-03-2021, revisi tanggal : 16-08-2021, diterima untuk diterbitkan tanggal 09-09-2021

Abstrak

Proses plasma spray atmosferik merupakan proses pelapisan yang banyak digunakan dalam aplikasi industri. Densitas dan kekuatan ikatan yang tinggi merupakan ciri utama dari proses ini dan diperlukan dalam hampir semua sifat lapisan untuk aplikasi-aplikasi khusus. Keterbatasan jarak semprot antara pistol nozel dan permukaan benda kerja pada saat proses plasma spray memerlukan modifikasi parameter proses standar. Pada penelitian ini, modifikasi parameter proses plasma spray lapisan Ni-Al dan Al-Si pada permukaan selubung baja tahan karat austenitik untuk mendapatkan hasil lapisan yang optimum. Lapisan diverifikasi dengan uji kekuatan ikatan tarik, uji keras, dan analisis struktur mikro. Dari modifikasi parameter yang dilakukan, penurunan kecepatan gerak pistol menunjukkan hasil yang paling optimum. Kekuatan ikatan tarik rata-rata yang diperoleh untuk lapisan Ni-Al dan Al-Si berturut-turut sebesar 9110 Psi dan 7283 Psi. Nilai kekerasan rata-rata yang diperoleh untuk lapisan Ni-Al dan Al-Si berturut-turut sebesar 77 HRB dan 106 HRH. Pengamatan struktur mikro lapisan Ni-Al menunjukkan struktur mikro yang lebih padat dibandingkan dengan struktur mikro lapisan dengan parameter standar. Untuk lapisan Al-Si, selain struktur mikro yang lebih padat, juga diperoleh fasa eutektik yang lebih proporsional dibandingkan dengan struktur mikro lapisan dengan parameter standar.

Kata Kunci: Plasma spray atmosferik, lapisan, Ni-Al, Al-Si, kecepatan lintas, kekuatan ikatan tarik, kekerasan

Abstract

The atmospheric plasma spray coating is a coating process that many used in industrial applications. High density and bond strength are the main features of this process. The limited spray distance between nozzle gun and workpiece surface during the plasma spray process requires standard process parameters modification. In the present study, an effort carried out a change of plasma spray process parameters of the Ni-Al and Al-Si coating on austenitic stainless steel casing for optimum results. Tensile bond strength, hardness, and microstructure tests were used to validate the coating. The Ni-Al and Al-Si layers had average tensile strengths of 9110 and 7283 Psi, respectively. The Ni-Al and Al-Si layers had average hardness values of 77 HR_B and 106 HR_H, respectively. When compared to the microstructure with standard parameters, the microstructure of the Ni-Al layer showed a denser microstructure. In addition to the denser microstructure of the Al-Si layer, a more proportional eutectic phase was obtained when compared to the microstructure of the layer with standard parameters.

Keywords: *Atmospheric plasma spray, coating, Ni-Al, Al-Si, traverse speed, tensile bond strength, hardness*

DOI : http://dx.doi.org/10.14203/metalurgi.v36i2.585

Metalurgi is Sinta 2 Journal (https://sinta.ristekbrin.go.id/journals/detail?id=3708) accredited by Ministry of Research & Technology, Republic Indonesia

1. INTRODUCTION

The APS (atmospheric plasma spray) coating is a thermal spray coating method that is widely used for a variety of protective coatings, including thermal barrier, corrosion-resistant, and wear-resistant surfaces [1]. The plasma arc used as an energy source can generate a very high temperature from the inert gas plasma jet [2]. This capability allows all types of feedstock materials to be melted during the coating process. This extremely high temperature will be decreased by increasing distance from the arc, thus keeping substrate material remains cool and have little or no changes in its microstructure [3]. The heated feedstock materials will form a molten or semi-molten state before being accelerated and propelled toward the cleaned and blasted surface [2]. Upon impact to the surface, a mechanical bond is created, resulting in splats and build-up layers with lamellar structure. The layers will then be cooled down and solidified [2]. Compare to another spray method, this atmospheric plasma spray offers a higher temperature, produces high density and tensile bond strength, and has uniform integrity. These properties will only be achieved by maintaining good substrate preparation, control environment, and process parameter. Process parameter standard in APS mostly was provided by the manufacturer as a complete package with its machine. However, it only works on a particular condition, such as the free distance between the spray gun and substrate. Changes in the shape, size, and geometrical workpiece lead to the change of the APS process parameter.

Two types of coating materials, nickel aluminum (Ni-Al) and aluminum-silicon (Al-Si), were selected. Ni-Al is the most widely used coating material for bond coat and has better suitability to apply in almost substrate [4]. It is used as a material for restoring worn components and as bond coats for specific and general industrial applications. Ni-Al coatings are self-bonding to steel substrates and have excellent oxidation resistance up to 800 °C (1470 °F). Mechanically clad aluminum and nickel composites provide this Ni-Al powder [5].

Another feedstock material, Al-Si, is mostly used as a structural material due to its better characteristics in wear resistance, lower thermal expansion coefficient, and high strength to wear ratio [6]-[10]. Al-Si is produced using gas atomized powders of aluminum alloyed with 12 wt.% silicon. These materials are excellent general-purpose materials for salvaging and rebuilding aluminum and magnesium alloy parts.

Plasma sprayed aluminum-silicon coatings are also used for the repair of worn jet engine components and the dimensional restoration of jet engine components that have been worn during manufacture. Aluminum with 12% silicon is a simple eutectic system with a low melting point. Silicon reduces the melting temperature to 577 °C (1071 °F) while increasing fluidity, specific gravity, and the coefficient of thermal expansion. It also decreases the contraction associated with solidification. The silicon present in the material is virtually pure, acting to increase the hardness of coatings produced from these materials and improving abrasion resistance. Aluminum silicon powders produce coatings that are harder and slightly denser than pure aluminum powder layers [11]. The purpose of choosing two coating materials was not to compare their mechanical properties or microscopic structure, but to learn about the trend that occurs when parameter changes are made to the metal powder group. In the present work, several parameters were investigated to find out the optimum result of coating on the substrate with limited geometry, followed by mechanical testing and microstructural examination.

2. MATERIALS AND METHODS

2.1 Material

As received substrate material of austenitic stainless steel 321 and two types of coating material Ni-Al and Al-Si with -90+45 μm particle size distribution was used in the present work. The substrate was prepared by solvent cleaning and grit blasting with aluminum oxide at 120 psi pressure.

The chemical compositions of each material are shown in Tables 1, 2, and 3, respectively.

Table 1. Chemical compositions of stainless steel substrate AISI 321 (in wt.%) [12]

Element	Composition (wt.%)
C	0.08
Mn	2.00
Si	1.00
Cr	18.00
Ni	11.00
P	0.05
S	0.03
Ti	0.40 (min)
Fe	Balance

2.2 APS Process Parameter

The atmospheric plasma spray coating process parameter was prepared based on the equipment guidance manufacturer and then modified to match the geometric condition. This geometric condition only allows a maximum spray distance of 2 inches, which differs from the standard parameter's amount of 9 inches. It will also increase the temperature of the base metal's surface and limit the amount of deposited dust that escapes from the spray area. The process parameter was limited to power as an output from ampere and voltage, speed of traverse gun and rotation of the workpiece, and feed rate of the powder. This study was prepared in accordance with the criteria listed in Table 4. The parameter is applied to the Al-Si and Ni-Al coating materials as a system on the AISI 321 stainless steel substrate.

Table 2. Chemical compositions of nickel aluminum (Ni-Al) coating material [5]

Element	Composition (wt%)
Ni	Balance
Al	4.5

Table 3. Chemical compositions of aluminum silicon (Al-Si) coating material [11]

Element	Composition (wt%)
Al	Balance
Si	12

2.3 Tensile Bond Strength Test

AISI 321 was prepared as a workpiece substrate for tensile bond strength testing in accordance with ASTM C-633, standard test method for adhesion or cohesion strength of thermal spray coatings, using a rod-type specimen with a diameter of 1 inch and a length of 2.5 inches [13]. A universal testing machine (Shimadzu) was then used to examine the sample. This testing method is used to determine the adhesive strength between the coating and the substrate, as well as the cohesive force within the coating. It had one coated surface and one blasted surface that were both sticky when combined with the adhesive film. All specimens were assembled in a special fixture before being cured in the oven. Following curing, excessive adhesion film was removed from the adjacent surface with grit abrasive paper or cloth. At room temperature, the specimen was mounted to the tensile testing machine with a fixture to allow for handling during the process. Each sample was tested until rupture occurred at a constant stress rate and crosshead travel. Each specimen's rupture surface was examined to determine the type of failure of each coating. If the failure occurs between the coating and the substrate, the strength is referred to as adhesive strength. If it occurs within the coating, the strength is referred to as cohesive strength.

2.4 Hardness Test

The hardness specimen was created using the ASTM E18-20 standard test methods for Rockwell hardness of metallic materials [14]. The sample measured 3 inches in length, 1 inch in width, and 0.2 inch in thickness. The sample was then examined using a Rockwell hardness testing machine (Matsuzawa) and the Rockwell H (HR_H) and B values (HR_B). The goal of this test was to see how parameter changes affected the hardness of the coating.

2.5 Metallographic Test

Metallographic specimens were prepared in accordance with ASTM E1920, the standard guide for metallographic preparation of thermal sprayed, with specimens measuring 3 inches in length, 1 inch in width, and 0.2 inch in thickness [15]. The sample was then examined under a 100X magnification optical microscope (Nikon Microphot-FX). The goal of this microstructure evaluation is to determine the impact of parameter changes on the structure of Ni-Al and Al-Si coatings.

Table 4. Atmospheric plasma spray parameter modification for Ni-Al and Al-Si coating materials applied on AISI 321 stainless steel casing substrate

Parameter	Specimen A1 / B1[a]	Specimen A2 / B2	Specimen A3 / B3	Specimen A4 / B4	Specimen A5 / B5
Power (kW)	35	30	35	35	35
Spray Distance (inches)	4	2	2	2	2
Powder Feed Rate (lb/hr)	10	10	5	10	10
A traverse speed of gun (mm/s)	10	10	10	7.5	10
A rotation speed of workpiece (RPM)	60	60	60	60	160

3. RESULTS AND DISCUSSIONS

3. 1. Tensile Bond Strength Test

The failure feature of the tensile bond strength test specimen is shown in Figs. 1 and 2 for Ni-Al and Al-Si coating, respectively. There are two modes of failure resulted; the first one is an adhesive failure where the coating failed between coating and substrate. The second one is a cohesive failure where the failure occurred within the coating [13]. Adhesive failure may occur between substrate and bond coat which remain the grey colour of the substrate after failure. The adhesive failure occurred in three different parameters, which was selected based on the most failure occur in one set of specimens as shown in Figure 1. While in Fig. 2, adhesive failure occurs between the coating and adhesive film, which remain white colour after failure or between adhesive film and substrate, which remain the white colour of the adhesive film after failure. The first one was in the standard parameter, either A1 or B1. The Second one was obtained by reducing 50% of the powder feed rate from 10 lbs/hr to 5 lbs/hr with a spray distance of 2 inches for both A3 and B3. This was the maximum space that was available due to the limited geometry of the casing. The last was obtained by reducing the 25% traverse speed of the gun from 10 mm/s to 7.5 mm/s with the same spray distance for specimens A4 and B4. In the meantime, cohesive failure was obtained when the parameter of the process was reduced power to 30 kW from 35 kW and increased RPM of the workpiece to 160 RPM from 60 RPM standard parameter. From these results, reducing powder feed rate and traverse speed led to adhesive failure, while reducing power led to cohesive failure.

Tensile Test Bond Strength results of Ni-Al and Al-Si coating are shown in Figs. 3 and 4, respectively. Reducing traverse speed from 10 mm/s to 7.5 mm/s and spray distance from 4 inches to 2 inches in both A4 and B4 resulted in the highest tensile bond strength. The same result was found during the deposition process powder feed rate affect the mechanical properties [16]. There was an optimum powder feed rate in a certain value for a specific type of coating. This was found clearly in specimen A4, which had the highest tensile bond strength value. The lower spray rate tends to be more homogeneous particle heated and improve bonding. In the meantime, the deposition rate will be slower. While reducing power from 35 kW to 30 kW with the same spray distance, 2 inches, obtained the lower result. This was related to unmelted and partially melted particles that were found in the coating that led to low tensile bond strength [17].

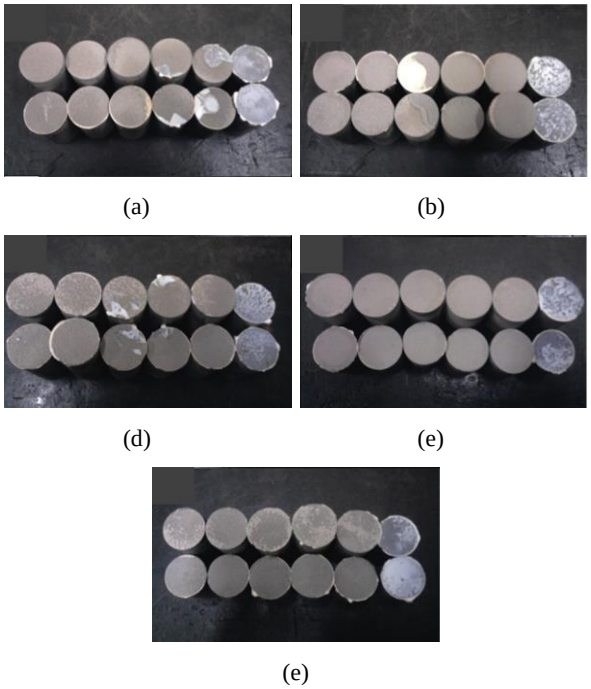

Figure 1. Failure feature of tensile bond strength Ni-Al coating specimen (a) A1, (b) A2, (c) A3, (d) A4, (e) A5

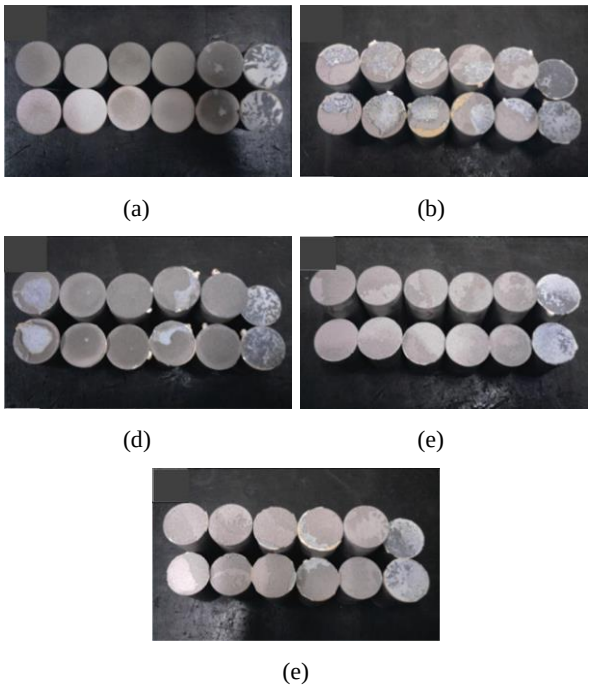

Figure 2. Failure feature of tensile bond strength Al-Si coating specimen (a) B1, (b) B2, (c) B3, (d) B4, (e) B5

Failure modes and tensile bond strength result indicated modification of spraying parameter affected to the result of coating properties. Reducing powder feed rate became a small amount of particle allowed heat absorbed almost of each particle and led to the optimum heating required by each particle.

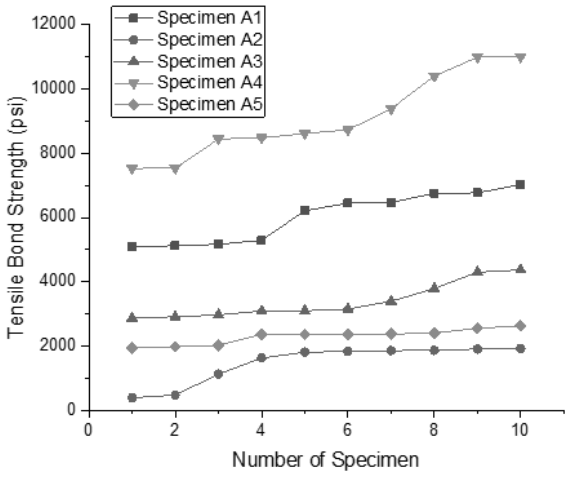

Figure 3. Tensile bond strength test result of Ni-Al coating

The other way was by making slower traverse speeds of the gun to maintain particle and workpiece heating at the same time. Having both in the same hot condition led particles and prepared substrate better mechanically bonded.

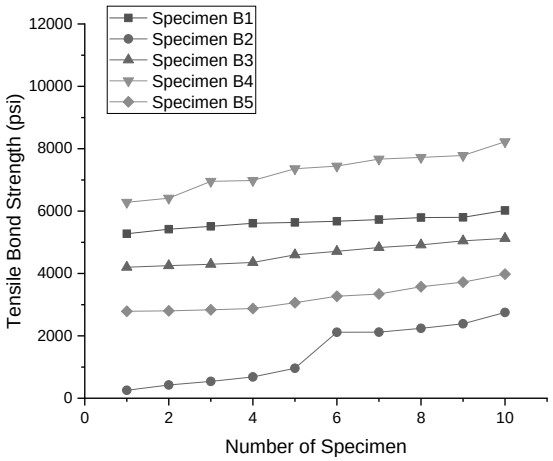

Figure 4. Tensile bond strength of Al-Si Coating

It was supported by the characteristic of Ni-Al particle that can create an exothermic reaction during processing, resulting in a quasi-metallurgical bond with stainless steel substrate. In Al-Si coating, higher bond strength was promoted by silicon element with 12% during the eutectic reaction.

3. 2. Hardness Test Result

Modification of parameter also affected the hardness properties of both coating, as shown in Fig. 5 and Fig. 6. In Ni-Al coating, the highest hardness value was obtained by reducing the traverse speed of gun from 10 mm/s to 7.5 mm/s (A4). However, reducing power and keeping the feed rate higher led to lower hardness results (A2). The higher amount of heated particle with lower power led to partially melted particle that affect to the hardness value [18].

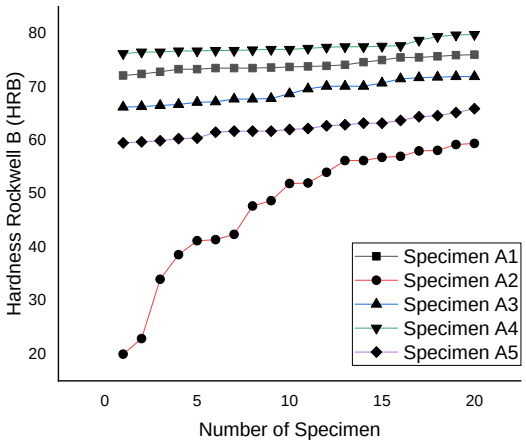

Figure 5. Hardness test result of Ni-Al coating

The exothermic reaction during spraying produced self-bonding of the dense and high structural integrity of Ni-Al coating [18]. Different from Ni-Al, in Al-Si, coating the amount of hardness is promoted by the number of eutectic phases that formed during spraying and high cooling rate [16]. Lesser spray distance, high heat input, and lower powder feed rate, a located particle of powder in the melting state that was suddenly cooled to ambient temperature, formed the more possibility to create the eutectic phase.

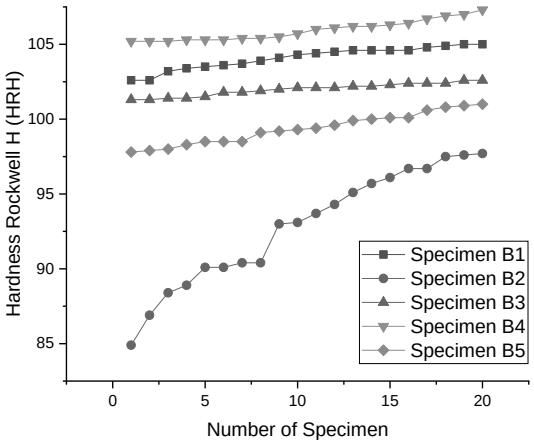

Figure 6. Hardness test result of Al-Si coating

3. 3. Microstructure

Microstructure examinations for Ni-Al and Al-Si coating were shown in Fig. 7 and Fig. 8, respectively. Starting from specimen A1 which followed the standard parameter, it has a moderate density of Ni-Al. A higher density of

Ni-Al was obtained for A4 from modification of spray distance and traverse speed of gun. However, lower density was also obtained for A2 from modification of power output. The degree of the high density of coating contributed to mechanical properties as confirmed in the above result of tensile bond strength and hardness, where dense coating resulted in high of mechanical properties [18].

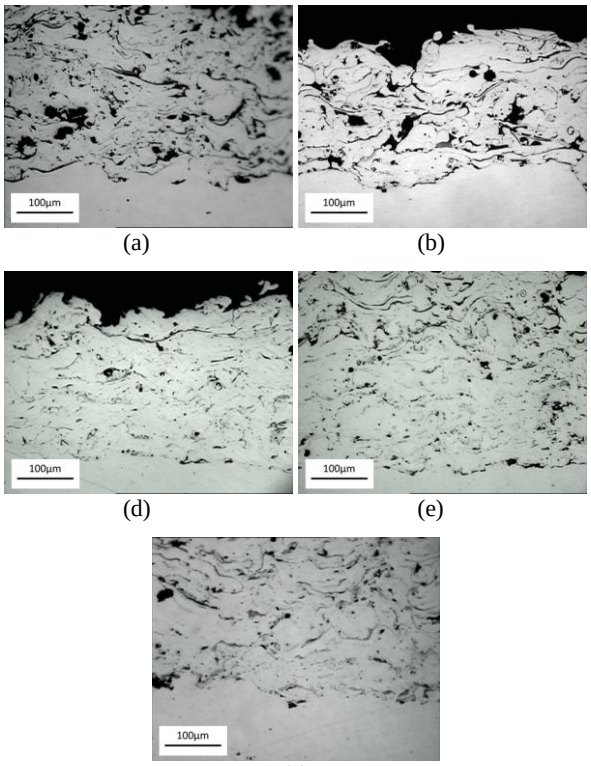

(a) (b) (d) (e) (e)

Figure 7. Microstructure of Ni-Al coating (a) A1, (b) A2, (c) A3, (d) A4, (e) A5

In another case, the initial Al-Si coating parameter B1 has a microstructure with the highest density and a small amount of eutectic phase. However, many pores were obtained for B2 with low power input. High density was mostly affected by heat input as a function of power. Besides the density, the eutectic phase was formed through a eutectic reaction during high solidification. It contributed to mechanical properties, mainly hardness and tensile bond strength, as discussed above [16]. It is confirmed by B4 that it has the highest mechanical properties.

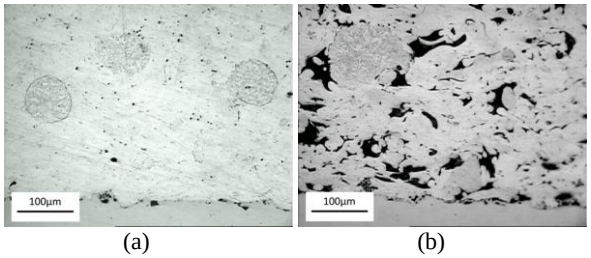

(a) (b)

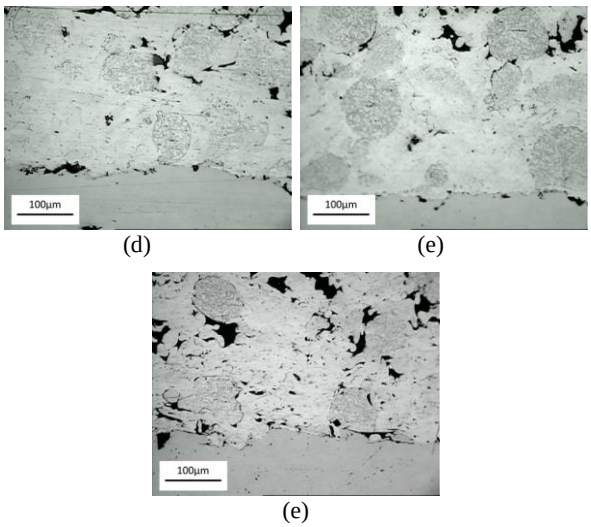

(d) (e) (e)

Figure 8. The microstructure of Al-Si coating (a) B1, (b) B2, (c) B3, (d) B4, (e) B5

4. CONCLUSIONS

To increase the mechanical properties and to improve the microstructure of the coating under a limited condition where the distance was less than guidance requirement, modification parameter by lowering traverse speed of gun could be considered to maintain the mechanical properties and improve the integrity of microstructure. Lowering traverse speed of gun showed better coating microstructure for both Ni-Al with less porosity and Al-Si with denser microstructure and moderate eutectic phase formation. This experimental research is useful for the industry that cannot invest in new equipment that was developed specifically for a limited purpose. This research was only focused on coating under the metal alloys group. Future work must identify the modification parameter to other groups, such as carbide, self-fluxing, abradable, and ceramic coating.

ACKNOWLEDGEMENT

This research was supported by PT Nusantara Turbin dan Propulsi.

REFERENCES

[1] A. Alian dan I. S. Jalham, "Abrasive wear resistance comparative study of plasma-sprayed steel by magnesium zirconate, aluminum-bronze, molybdenum, and mixtures of them as coating materials," *Arab. J. Sci. Eng. (Springer Sci. Bus. Media BV)*, vol. 31, pp. 27-34, 2006.

[2] J. R. Davis dan D. & Associates, *Handbook of Thermal spray technology*, vol. 1, no. 6. ASM International, 2004.

[3] G. Singh dan N. Bala, "Nanocomposites coatings by thermal spraying technique : A review," *Int. Conf. Adv. Futur. Trends Mech. Mater. Eng.*, pp. 643-648, 2012.

[4] M. Zandrahimi, J. Vatandoost, dan H. Ebrahimifar, "Al, Si, and Al-Si coatings to improve the high-temperature oxidation resistance of AISI 304 stainless steel," *Oxid. Met.*, vol. 76, no. 3-4, pp. 347-358, 2011. Doi: 10.1007/s11085-011-9259-1

[5] O. Metco, "Material product data sheet nickel-aluminum materials," 2020. https://www.oerlikon.com (accessed 16 Feb, 2021).

[6] J. Clarke dan A. D. Sarkar, "Wear characteristics of as-cast binary aluminium-silicon alloys," *Wear*, vol. 54, no. 1, pp. 7-16, 1979. Doi: 10.1016/0043-1648(79)90044-9

[7] Q. Xu, B. Gabbitas, dan S. Matthews, "Titanium compacts with controllable porosity by slip casting of binary powder mixtures," *Powder Technol.*, vol. 266, pp. 396-406, 2014. Doi: 10.1016/j.powtec.2014.06.042

[8] M. Qian, D. Li, S. B. Liu, dan S. L. Gong, "Corrosion performance of laser-remelted Al–Si coating on magnesium alloy AZ91D," *Corros. Sci.*, vol. 52, no. 10, pp. 3554-3560, 2010. Doi: https://doi.org/10.1016/j.corsci.2010.07.010

[9] M. Gurutze Pérez Artieda, A. Cortiella, N. R. Harlan, F. Zapirain, dan F. Zubiri, "Two step coating of a hypereutectic PM Al-Si alloy," *Mater. Lett.*, vol. 64, no. 13, pp. 1458-1461, 2010. Doi: 10.1016/j.matlet.2010.03.056

[10] J. Wang, L. Kong, J. Wu, T. Li, dan T. Xiong, "Microstructure evolution and oxidation resistance of silicon-aluminizing coating on γ-TiAl alloy," *Appl. Surf. Sci.*, vol. 356, pp. 827-836, 2015. Doi: 10.1016/j.apsusc.2015.08.204

[11] O. Metco, "Material product data sheet aluminum 12% silicon thermal spray powders," 2016. https://www.oerlikon.com (accessed 16 Feb, 2021).

[12] J. R. Davis, *Metals Handbook Desk Edition*, Third. ASM International, 2001.

[13] A. Standard, "ASTM C633-13: Standard Test Method for Adhesion or Cohesion Strength of Thermal Spray Coatings," *ASTM Int.*, pp. 4, 2008.

[14] A. Standard, "ASTM E18-03: Standard test methods for rockwell hardness and rockwell superficial hardness of metallic materials," *Annu. B. ASTM Stand.*, no. 08b, pp. 1-37, 2003.

[15] A. Standard, "ASTM E1920-03: guide for metallographic preparation of thermal sprayed coatings," no. 03, pp. 1-8, 2014.

[16] M. Mrdak, B. Medjo, D. Veljić, M. Arsić, dan M. Rakin, "The influence of powder feed rate on mechanical properties of atmospheric plasma spray (APS) Al-12Si coating," *Rev. Adv. Mater. Sci.*, vol. 58, no. 1, pp. 75-81, 2019. Doi: 10.1515/rams-2019-0007

[17] X. C. Zhang, B. S. Xu, S. T. Tu, F. Z. Xuan, H. D. Wang, dan Y. X. Wu, "Effect of spraying power on the microstructure and mechanical properties of supersonic plasma-sprayed Ni-based alloy coatings," *Appl. Surf. Sci.*, vol. 254, no. 20, pp. 6318-6326, 2008. Doi: 10.1016/j.apsusc.2008.03.148

[18] L. Zhang, X. J. Liao, S. L. Zhang, X. T. Luo, dan C. J. Li, "Effect of powder particle size and spray parameters on the Ni/Al reaction during plasma spraying of Ni-Al composite powders," *J. Therm. Spray Technol.*, vol. 30, no. 1-2, pp. 181-195, 2021. Doi: 10.1007/s11666-020-01150-2

Metalurgi (2021) 2: 59 - 68

LIPI

METALURGI
Majalah Ilmu dan Teknologi
p-ISSN 0126-3188 | e-ISSN 2443-3926
www.ejurnalmaterialmetalurgi.com

PERAN N-DOPING TERHADAP KARAKTERISTIK PORI KARBON AKTIF YANG DIHASILKAN DARI LIMBAH DESTILASI AKAR WANGI

Yohana Fransiska Ferawati dan Ratna Frida Susanti*
Jurusan Teknik Kimia, Fakultas Teknologi Industri, Universitas Katolik Parahyangan
Jln. Ciumbuleuit No. 94, Bandung, Indonesia 40141
*E-mail: santi@unpar.ac.id

Masuk tanggal : 05-08-2021, revisi tanggal : 18-08-2021, diterima untuk diterbitkan tanggal 09-09-2021

Abstrak

Pada penelitian ini modifikasi gugus fungsi permukaan nitrogen pada karbon aktif dari limbah akar wangi diteliti pengaruhnya terhadap pengembangan pori karbon aktif. Sintesis karbon aktif dilakukan dengan cara karbonisasi hidrotermal LAW (limbah akar wangi) pada suhu 225 °C selama 18 jam dilanjutkan dengan aktivasi menggunakan tungku tabung dalam atmosfer nitrogen dengan laju 100 mL/menit pada suhu 800 °C selama 2 jam dengan bahan pengaktivasi K_2FeO_4. Urea digunakan sebagai sumber nitrogen. Variasi konsentrasi urea yang diteliti adalah 1:0 (AC–0), 1:3 (AC–3) dan 1:5 (AC–5). Hasil yang diperoleh menunjukkan bahwa ketiga karbon aktif ini memiliki karakteristik mesopori dengan luas permukaan S_{BET} (*brunauer emmett teller*) terbesar yaitu 552,90 m^2g^{-1} dan diameter pori rata-rata 3,43 nm. Keberadaan gugus fungsi nitrogen juga tampak pada analisa FTIR (*fourier transform infrared spectrometer).* Berdasarkan hasil analisa SEM-EDX (*scanning electron microscope-energy dispersive x-ray*), semakin besar rasio penambahan urea maka unsur N yang terkandung pada karbon aktif semakin meningkat. Sintesis karbon aktif dari limbah akar wangi dengan penambahan urea merupakan metode terbaru untuk menghasilkan karbon aktif mesopori yang nantinya dapat digunakan dalam aplikasi elektroda dan katalis pendukung.

Kata Kunci: Doping nitrogen, urea, limbah akar wangi, karbon aktif

Abstract

This work studied the effect of nitrogen functional group modification on activated carbon synthesized from vetiver root waste on pores development. Synthesis of activated carbon was carried out by hydrothermal carbonization of vetiver root waste at a temperature of 225 °C for 18 hours followed by chemical activation using K_2FeO_4 as an activated agent in a tubular furnace at a temperature of 800 °C for 2 hours with nitrogen atmosphere flowed at a rate of 100 mL/minute. Urea was used as a nitrogen source. The variation of urea concentration was 1:0 (AC–0), 1:3 (AC–3), and 1:5 (AC–5). The results showed that these activated carbons have mesoporous characteristics with the largest S_{BET} (brunauer emmett teller) surface area of 552.90 m^2g^{-1} and average pore width 3.43 nm. The presence of the nitrogen functional group was observed in the FTIR (fourier transform infrared spectrometer) analysis. Based on SEM-EDX (scanning electron microscopy-energy dispersive x-ray) analysis, a higher amount of urea addition will increase the nitrogen content in activated carbon. Synthesis of activated carbon from vetiver root waste with an addition of urea is the newest method to produce mesoporous activated carbon for electrode and support catalyst purposes.

Keywords: *Nitrogen doping, urea, vetiver root waste, activated carbon*

1. PENDAHULUAN

Pengolahan limbah biomasa menjadi material kaya manfaat masih menjadi problem dalam masyarakat. Jika dilihat secara umum, limbah biomasa mengandung lignoselulosa dengan komponen terbesar yaitu selulosa 30-55 %berat, lignin 25-30 %berat dan hemiselulosa 25-30 %berat [1]-[2]. Ketiga komponen ini berpotensi untuk dimanfaatkan dalam berbagai produk salah satunya adalah karbon aktif. Pembuatan karbon aktif dari limbah biomasa juga dapat menjadi solusi dari permasalahan lingkungan dan menekan biaya proses karena sumber bahan baku yang berlimpah dan terkadang menjadi limbah.

DOI : http://dx.doi.org/10.14203/metalurgi.v36i2.595

Metalurgi is Sinta 2 Journal (https://sinta.ristekbrin.go.id/journals/detail?id=3708) accredited by Ministry of Research & Technology, Republic Indonesia

Limbah akar wangi (*vetiveria zizanioides*) sebagai hasil samping dari proses ekstraksi minyak akar wangi menjadi komoditas berlimpah di Kabupaten Garut. Luas lahan akar wangi sebesar 2.341 hektar dengan produktivitas 11-12 ton akar wangi per hektar per tahun. Komponen minyak akar wangi yang disuling hanya sekitar 0,4-0,5 %b. Dengan demikian industri pengolahan minyak akar wangi di Kabupaten Garut akan menyisakan sekitar 25.622 ton limbah akar wangi setiap tahunnya [3]. Sebagian besar limbah hanya dibiarkan teronggok di sekitar industri penyulingan dan belum dimanfaatkan secara maksimal. Selain itu, kandungan selulosa sebesar 24,51 %berat, hemiselulosa 33,07 %berat dan lignin 20,09 %berat mendukung potensi akar wangi untuk diolah menjadi karbon aktif [4]. Oleh karena itu sintesis limbah akar wangi menjadi karbon aktif dapat menjadi alternatif pemanfaatan limbah biomasa ini.

Karbon aktif merupakan material dengan porositas dan luas permukaan yang besar. Aplikasi karbon aktif sangat luas seperti elektroda dalam media penyimpan energi [5]-[6], adsorben [7]-[8], dan *support catalyst* [9]. Karakteristik karbon aktif selain luas permukaan besar, juga didukung oleh gugus fungsi permukaan. Gugus fungsi permukaan pada karbon aktif didominasi oleh OFG (*oxygenated functional group*) yang berfungsi sebagai daerah aktif untuk reaksi redoks [10]. Penambahan *heteroatom doping* dapat meningkatkan distribusi elektron yang berdampak positif terhadap nilai konduktivitas. Modifikasi ini juga berpengaruh terhadap kemampuan terbasahi (*wettability*) karbon aktif [6], [11]. *Heteroatom doping* yang dapat ditambahkan dalam karbon aktif antara lain nitrogen, sulfur, fosfor dan boron [12]-[13]. Modifikasi dapat dilakukan secara *self-doping* dimana heteroatom sudah secara alami ada dalam biomasa mentah, maupun *artificial doping* yaitu dengan cara menambahkan bahan kimia selama proses sintesis.

Sintesis karbon aktif terdiri atas dua tahap yaitu karbonisasi dan aktivasi. Karbonisasi hidrotermal merupakan proses karbonisasi menggunakan media air pada kondisi subkritik dengan hasil produk padat yang disebut *hydrochar* [14]. Proses dilakukan pada suhu 150-350 °C dalam reaktor bertekanan untuk menjaga agar air tetap berada pada fasa cair. Pada kondisi tersebut, air yang bertindak sebagai pelarut juga dapat terionisasi menjadi H_3O^+ dan menjadi aktivator asam ataupun basa untuk reaksi hidrolisis [1], [14]-[15]. Hal ini yang menjadikan karbonisasi hidrotermal bersifat ramah lingkungan karena tidak diperlukan tambahan aktivator kimia. Karbonisasi hidrotermal juga cocok untuk biomasa dengan kandungan air yang tinggi tanpa diperlukan proses pengeringan terlebih dahulu. *Hydrochar* yang dihasilkan memiliki OFG lebih besar jika dibandingkan dengan *biochar*, yaitu material karbon padat hasil pirolisis [15]. Selain itu, temperatur proses yang lebih rendah daripada proses pirolisis juga dapat menghemat waktu dan biaya.

Proses aktivasi dilakukan secara kimia yaitu dengan penggunaan aktivator K_2FeO_4 (potasium ferat). Aktivator K_2FeO_4 sudah digunakan pada proses pembuatan karbon aktif pada berbagai bahan baku antara lain daun phoenix [16], *black locust* [17] dan serbuk gergaji [18]. Penggunaan aktivator logam ini dapat meningkatkan derajat grafitisasi dari karbon aktif sehingga dapat berdampak positif pada konduktivitas. Menurut Zhou [18], aktivator K_2FeO_4 dapat dapat berperan dalam meningkatkan grafitisasi, memperluas pori dan menambah daya magnetisasi karbon aktif karena kandungan senyawa Fe, KOH dan Fe_2O_3 sehingga hasilnya dapat diaplikasikan sebagai adsorben. Selain itu, dengan adanya aktivator logam maka tidak diperlukan suhu aktivasi yang terlalu tinggi guna mendapatkan karbon aktif [16], [19].

Fokus penelitian kali ini adalah sintesis dan modifikasi karbon aktif dengan menggunakan bahan baku LAW (limbah akar wangi). Urea ditambahkan sebagai sumber nitrogen pada proses karbonisasi LAW yang bertujuan untuk pembentukan gugus fungsi nitrogen pada *hydrochar*. Nitrogen atom doping dengan urea sebagai sumber nitrogen dipilih karena stabil serta mudah didapat dengan harga yang relatif murah. Proses dilanjutkan dengan aktivasi kimia menggunakan aktivator K_2FeO_4. Karbon aktif yang dihasilkan dianalisa luas permukaan, distribusi pori, dan gugus fungsi permukaan. Sejauh pengamatan yang kami lakukan pada beberapa literatur, belum ada hasil penelitian mengenai sintesis karbon aktif terdoping nitrogen dari limbah akar wangi dengan K_2FeO_4 sebagai agen pengaktivasi, sehingga hasil penelitian ini bisa memberi kontribusi terhadap ilmu pengetahuan khususnya sintesis material karbon berbasis limbah biomassa

2. PROSEDUR PERCOBAAN

2.1 Bahan

LAW (limbah akar wangi) sebagai bahan baku diperoleh dari daerah Kabupaten Garut, Jawa Barat. Bahan baku ini dikeringkan dengan

menggunakan oven pada suhu 110 °C selama 24 jam. Limbah akar wangi kering digiling lalu diayak menggunakan mesh -10+120 M (± 1,0625 mm). Selanjutnya bahan baku dianalisa kadar air dan kadar abu menggunakan TGA (*thermal gravimetry analysis*), kandungan ekstraktif menggunakan metode ekstraksi soxhlet, serta kandungan lignoselulosa (selulosa, hemiselulosa dan lignin) awal dengan menggunakan metode Klason Lignin dan Van Soest [20]. Aktivator potasium ferat (K_2FeO_4) diperoleh dari GK Chem Technology, Cina. Bahan-bahan lain yang digunakan adalah urea grade teknis sebagai sumber nitrogen, etanol 96% dan asam klorida (HCl) sebagai bahan pencuci.

2.2 Sintesis karbon aktif

LAW sebanyak 4 gram diimpregnasi dalam larutan urea dengan perbandingan LAW:urea sebanyak 1:3 dan 1:5. Proses impregnasi dilakukan dengan pengadukan selama 15 menit dilanjutkan dengan sonikasi selama 30 menit. Bubur LAW kemudian dimasukkan dalam reaktor autoklaf untuk dikarbonisasi pada suhu 225 °C selama 18 jam menggunakan oven. *Hydrochar* selanjutnya disaring dan dibilas dengan menggunakan air demineralisasi dan etanol, lalu dikeringkan dalam oven selama 24 jam pada suhu 105 °C. Sampel *hydrochar* yang diperoleh diberi kode sampel HC–3 dan HC–5. Selain itu dilakukan juga sintesis *hydrochar* tanpa doping urea dengan kode HC–0 sebagai pembanding.

Proses selanjutnya 2 gram *hydrochar* diimpregnasi dengan larutan K_2FeO_4 20% dengan rasio 1:4 melalui pengadukan secara terus-menerus selama 24 jam. Sampel dikeringkan dalam oven selama 24 jam pada suhu 105 °C. Selanjutnya dilakukan proses aktivasi pada suhu 800 °C selama 2 jam menggunakan tungku tabung dalam atmosfer nitrogen. Laju alir nitrogen dijaga konstan pada 100 mL/min. Karbon aktif yang diperoleh dicuci dengan cara direndam HCl 1 M selama 24 jam, lalu disaring dan dibilas dengan menggunakan air demineralisasi hingga pH netral. Karbon aktif kemudian dikeringkan dalam oven pada suhu 105 °C selama 24 jam dan diperoleh sampel AC-0, AC-3 dan AC-5. Sebagai pembanding, karbon aktif juga disintesis tanpa agen pengaktivasi menggunakan *hydrochar* yang disintesis tanpa doping urea. Sampel ini diberi kode AC–0P.

2.3 Karakterisasi Karbon Aktif

Karakterisasi karbon aktif yang diperoleh meliputi morfologi, kandungan unsur, luas permukaan, distribusi pori dan gugus fungsi permukaan. Analisa SEM-EDX (*scanning electron microscope-energy dispersive x-ray*) menggunakan SU3500 (Hitachi, Jepang) untuk mengetahui morfologi dan kandungan unsur dari karbon aktif, analisa adsorpsi-desorpsi nitrogen pada suhu 77 K dengan metode BET (*brunauer emmett teller*) menggunakan Nova 4200e (Quantachrome, USA) untuk mengetahui luas permukaan serta metode BJH (*barrett joyner halenda*) untuk penentuan distribusi pori. Analisa kualitatif gugus fungsi nitrogen dilakukan dengan instrumen FTIR (*fourier transform infrared spectrometer*) IRPrestige21 (Shimadzu, Jepang).

3. HASIL DAN PEMBAHASAN

3. 1. Analisa Lignoselulosa

Pada akar wangi mentah, kandungan lignin lebih besar jika dibandingkan dengan selulosa dikarenakan akar wangi merupakan kategori rerumputan sehingga berpotensi untuk diolah menjadi karbon aktif [4], [21]. Setelah melalui proses penyulingan, kadar ekstraktif menurun dari 20,6% menjadi 12,16%, begitu pula dengan kandungan hemiselulosa (Tabel 1).

Tabel 1. Kandungan akar wangi mentah dan limbah akar wangi (LAW)

Komposisi	Akar wangi mentah[a]	LAW
Kadar air[b]	TD[h]	5,2
Kadar abu[c]	1,67	3,25
Ekstraktif[d]	20,6	12,16
Lignin[e]	20,09	37,8
Hemiselulosa[f]	33,07	1,05
Selulosa[g]	24,51	43,79

[a] Hasil analisis dari Gaspard, S., dkk [4] menggunakan bahan baku akar wangi yang belum didistilasi.
[b] Kadar air diperoleh melalui *thermal gravimetry analysis* (TGA).
[c] Kadar abu diperoleh melalui *thermal gravimetry analysis* (TGA).
[d] Kandungan ekstraktif ditentukan dengan ekstraksi LAW metode Soxhlet menggunakan pelarut toluene:etanol (1:1 v/v).
[e] Kandungan lignin ditentukan dengan menggunakan metode Klason [20].
[f] Kandungan hemiselulosa dihitung melalui pengurangan *acid detergent fiber* terhadap *neutral detergent fiber* pada metode Van Soest.
[g] Kandungan selulosa dihitung melalui pengurangan *neutral detergent fiber* dengan kandungan hemiselulosa dan lignin.
[h] Tidak tersedia.

Ekstraktif merupakan zat yang mudah larut dalam pelarut seperti air, alkohol dan eter, termasuk di dalamnya adalah minyak, resin, lemak, lilin, pati, dan zat warna. Penurunan ekstraktif merupakan dampak dari proses penyulingan komponen sekuisterpen,

sekuisterpenol dan sekuisterpenon yang terkandung dalam minyak akar wangi [22]. Komponen minyak akar wangi ini terletak pada bagian dalam jaringan akar yang keras sehingga proses difusi berjalan dengan lambat hingga ke permukaan. Hal ini diduga menjadi penyebab kandungan ekstraktif pada limbah akar wangi masih relatif besar.

Kandungan hemiselulosa juga menurun drastis sekitar 19%. Proses penyulingan mempunyai andil dalam penurunan kandungan hemiselulosa. Penyulingan minyak akar wangi di daerah Kabupaten Garut, tempat asal bahan baku LAW (limbah akar wangi), mayoritas masih menggunakan metode air dan uap (*water and steam distillation*) serta beberapa menggunakan metode uap (*steam distillation*). Metode *water and steam distillation* atau sistem kukus memanfaatkan uap jenuh pada proses penyulingan selama lebih dari 24 jam sedangkan *steam distillation* memanfaatkan uap bertekanan (2-4 bar) selama 24 jam [22]. Demi menghemat biaya, proses penyulingan ini dimodifikasi oleh petani menjadi tekanan 5 bar dalam waktu 15-18 jam. Kenaikan tekanan dan waktu proses diduga menyebabkan penurunan hemiselulosa yang signifikan. Seperti diketahui bahwa hemiselulosa merupakan komponen lignoselulosa yang paling mudah terdegradasi secara termal [23].

3. 2. *Yield Hydrochar*

Selama proses karbonisasi hidotermal, komponen utama lignoselulosa yaitu selulosa, hemiselulosa dan lignin akan mengalami beberapa reaksi seperti hidrolisis, dehidrasi, polimerisasi dan kondensasi yang diaktivatori oleh ion hidronium sebagai hasil autoaktivatoris air [24].

Selulosa akan terhidrolisis membentuk beberapa oligomer serta monomer glukosa dan fruktosa. Dekomposisi dari monomer tersebut akan menghasilkan asam-asam organik seperti asam asetat, asam laktat, asam levulenat dan asam format. Oligomer juga terhidrolisis membentuk monomer disertai reaksi dehidrasi dan fragmentasi yang akan menghasilkan produk-produk larut air misalnya 1,6-anhidroglukosa, eritrosa, senyawa furfural termasuk HMF (hidroksi metil furfural). Dekomposisi senyawa furfural juga menghasilkan senyawa asam, aldehid dan fenol. Reaksi selanjutnya adalah polimerisasi atau kondensasi yang akan menghasilkan polimer larut air. Reaksi ini disebabkan oleh dehidrasi intermolekular atau kondensasi aldol. Ketika konsentrasi senyawa aromatik sudah melebihi titik supersaturasi maka akan terbentuk inti kristal yang terus berkembang dan berikatan dengan gugus fungsi oksigen (hidroksil, karbonil, karboksilat). Permukaan *hydrochar* akan dipenuhi dengan gugus fungsi oksigen yang reaktif dibandingkan dengan gugus fungsi oksigen di dalam inti *hydochar* [14] .

Pembentukan *hydrochar* dari hemiselulosa dimulai dari pelarutan hemiselulosa pada suhu 180 °C selama proses karbonisasi. Xylan yang merupakan komponen dari polimerisasi hemiselulosa akan terhidrolisis membentuk D-xilosa dan selanjutnya terdekomposisi menjadi furfural. Senyawa ini akan mengalami polimerisasi membentuk *hydrochar*. Di sisi lain, pembentukan *hydrochar* dari lignin terjadi melalui 2 mekanisme, yaitu fraksi lignin terlarut dan tidak terlarut. Fraksi lignin yang tidak terlarut akan mengalami reaksi pembentukan *hydrochar* yang lebih cepat dibandingkan fraksi terlarut. Pada fraksi terlarut terjadi reaksi repolimerisasi antar fragmen sehingga terbentuk *hydrochar* [15].

Di sisi lain, urea akan terdekomposisi membentuk karbon dioksida dan amonia menurut reaksi berikut :

$$2NH_3 + CO_2 + H_2O \leftrightarrow NH_4^+ + HCO_3^- + NH_3 \quad (1)$$

$$NH_4^+ + HCO_3^- + NH_3 \leftrightarrow 2NH_4^+ + CO_3^{2-} \quad (2)$$

NH^3/NH^{4+} hasil degradasi urea mempunyai dua peranan yaitu sebagai reaktan organik yang mengandung nitrogen serta berkontribusi terhadap pH larutan yang nantinya akan memberikan efek terhadap beberapa reaksi secara tidak langsung.

Degradasi glukosa dan fruktosa sebagai penyusun utama selulosa dan hemiselulosa dipengaruhi oleh aktivator asam dan basa. Pada kondisi asam, reaksi hidrolisis dan dehidrasi lebih dominan dimana fruktosa akan membentuk HMF dan terhidrasi membentuk asam levulenat dan asam format. Sebaliknya, jika kondisi basa maka akan terjadi reaksi fragmentasi membentuk gliseraldehid, glikolaldehid, eritros, dihidroksiaseton dan piruvaldehid [25]. Urea yang cenderung bersifat basa mendominasi reaksi fragmentasi sehingga menurunkan pembentukan *hydrochar*. Selain itu, gugus amina pada urea akan bereaksi dengan gula pereduksi sehingga terjadi reaksi Maillard. Reaksi Maillard menghasilkan polimer dan kopolimer nitrogen seperti melanoid. Peningkatan pH akan mendorong pembentukan senyawa ini sehingga dengan adanya gugus amina pada proses karbonisasi hidrotermal dapat menghambat pembentukan *hydrochar* dan menurunkan *yield*. *Yield* dihitung menggunakan rumus sebagai berikut

$$\text{Yield hydrochar} = \frac{M_{HC}}{M_{I.AW}} \text{ x } 100\% \quad (1)$$

$$\text{Yield karbon aktif} = \frac{M_{AC}}{M_{I.AW}} \text{ x } 100\% \quad (2)$$

Dimana M_{HC} adalah massa *hydrochar* (gram), M_{LAW} adalah massa limbah akar wangi (gram) dan M_{AC} adalah massa karbon aktif (gram).

Sampel HC-5 memiliki *yield* paling kecil jika dibandingkan dengan HC-3 dan HC-0. Dalam hal ini, semakin besar konsentrasi urea yang digunakan maka semakin rendah *yield hydrochar* yang diperoleh sebagaimana tersaji pada Tabel 2.

Tabel 2. *Yield hydrochar* dan karbon aktif dari limbah akar wangi

Kode Sampel	Yield (%)
HC–0	49,56
HC–3	49,06
HC–5	45,42
AC–0	21,59
AC–3	21,46
AC–5	20,74
AC–0P	28,30

Pada sampel karbon aktif, *yield* sampel AC–0P lebih besar jika dibandingkan dengan karbon aktif lainnya karena aktivator K_2FeO_4 dapat terdegradasi membentuk KOH menurut reaksi:

$$4K_2FeO_4 + 10H_2O \rightarrow 8KOH + 4Fe(OH)_3\downarrow + 3O_2\uparrow \quad (3)$$

Senyawa KOH yang terbentuk merupakan aktivator reaksi oksidasi. Sehingga *yield* karbon aktif dengan aktivator lebih rendah jika dibandingkan tanpa aktivator.

3. 3. Gugus Fungsi Permukaan

Karbonisasi hidrotermal juga memberikan efek perubahan struktur kimia dari LAW dan *hydrochar* yang dihasilkan, seperti terlihat dalam hasil analisa FTIR (Gambar 1). Spektrum FTIR (*fourier transform infrared spectrometer*) LAW berbeda dengan HC-3 dan HC-5 yang menandakan adanya peregangan beberapa ikatan kimia akibat reaksi aromatisasi dan heteroatom doping. Gugus fungsi oksigen terlihat pada ikatan O-H, C=O dan C-O sedangkan gugus fungsi nitrogen terlihat pada ikatan N-H dan C-N. Penambahan doping nitrogen dapat berdampak positif pada kemampuan terbasahi (*wettability*) dari karbon aktif serta peningkatan sifat elektrokimia pada aplikasi elektroda media penyimpan energi [26].

Intensitas ikatan O-H pada HC–0, HC–3 dan HC–5 terlihat menurun jika dibandingkan dengan LAW karena adanya reaksi dehidrasi, selain itu intensitas C-O dan C-H juga menurun karena reaksi dekarboksilasi [14]. Pada saat karbonisasi hidrotermal juga terjadi reaksi aromatisasi yang terlihat dari keberadaan ikatan C=C pada sampel HC–0, HC–3 dan HC–5. Peregangan ikatan C-N terjadi pada 1270 cm^{-1} kemudian ikatan N-H dan atau O-H terjadi pada 3200-3400 cm^{-1} [14], [27]-[28]. Hal ini menunjukan adanya reaksi antara gugus fungsi nitrogen dalam urea dengan gugus fungsi oksigen yang terkandung dalam LAW selama proses karbonisasi. Senyawa antara dari reaksi tersebut adalah 1-deoksi-2-amino-1-ketosa yang selanjutnya dapat mengalami dehidrasi dan deaminasi menghasilkan gugus fungsi N pada karbon yaitu C-N dan atau N-H [29].

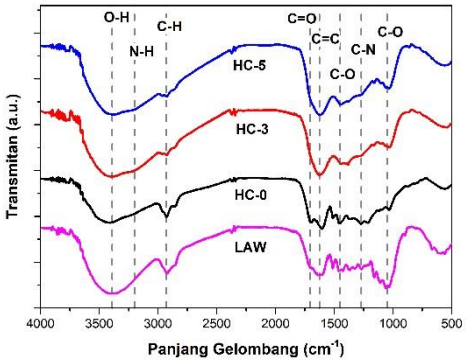

Gambar 1. Analisa FTIR karbon aktif LAW, HC-0, HC-3 dan HC-5

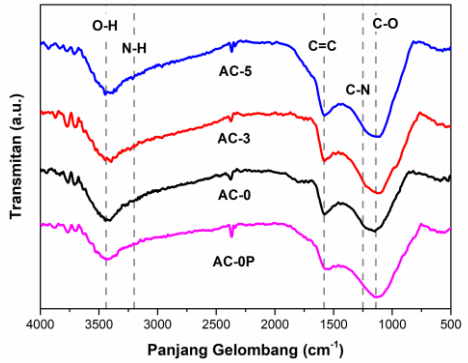

Gambar 2. Analisa FTIR karbon aktif AC–0, AC–3, AC–5 dan AC–0P

Setelah diaktivasi dengan menggunakan aktivator K_2FeO_4, terlihat bahwa intensitas ikatan C-O dan atau ikatan C-N (1000-1300 cm^{-1}) pada AC–5 meningkat jika dibandingkan dengan AC-3 dan AC0 [27]. Peningkatan juga terlihat pada ikatan C=C sampel AC-5. Sebaliknya, intensitas O-H dan atau ikatan N-H (3000-3400 cm^{-1}) pada sampel AC-5 mengalami penurunan jika dibandingkan dengan sampel AC-3 dan AC-0. Hasil analisa FTIR karbon aktif dapat dilihat pada Gambar 2.

3. 4. Morfologi dan Komposisi Unsur

Morfologi dan komposisi unsur karbon aktif dianalisa menggunakan SEM-EDX (*scanning electron microscope-energy dispersive x-ray*). Pada Gambar 3 terlihat bahwa morfologi semua sampel karbon aktif mirip dengan LAW. Struktur LAW lebih tidak berpori (Gambar 3(a)-3(b) jika dibandingkan dengan karbon aktif (Gambar 3(c)-3(f)). Sampel AC-0P, AC-0, AC-3 dan AC-5 mempunyai struktur pori yang seragam dengan perbedaan ada pada volume pori. Pengecilan struktur pori menjadi lebih kecil terjadi pada sampel AC-3 (Gambar 3(e)) yang nantinya akan berpengaruh terhadap peningkatan luas permukaan. Pada rasio doping nitrogen terbesar yaitu sampel AC-5 (Gambar 3(f)) terlihat beberapa pori mulai tertutup. Hal ini ditegaskan dalam tren hasil analisa luas permukaan (Tabel 5).

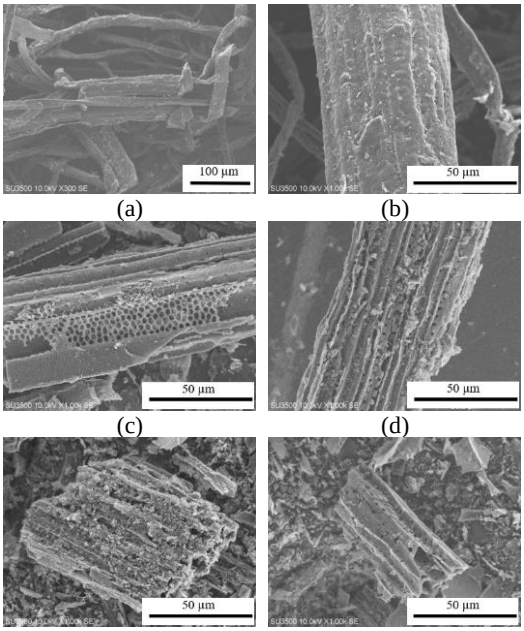

Gambar 3. Analisa SEM karbon aktif (a)-(b) LAW, (c) AC-0P, (d) AC-0, (e) AC-3 dan (f) AC-5

Penambahan urea dengan berbagai rasio berpengaruh terhadap kandungan unsur N yang ada pada karbon aktif. Tabel 3 menyajikan hasil analisa kandungan unsur dengan menggunakan SEM-EDX. Sampel AC-5 dengan rasio urea terbesar mempunyai kandungan N paling tinggi jika dibandingkan dengan ketiga sampel lainnya. Hal ini juga menegaskan hasil analisa kualitatif FTIR (Gambar 2) yaitu peningkatan intensitas ikatan C-N seiring dengan penambahan rasio urea yang digunakan.

Tabel 3. Komposisi unsur karbon aktif dari limbah akar wangi

Kode Sampel	Komposisi Unsur (%berat)			
	C	N	O	S
AC–0	85,84	0,02	10,39	3,75
AC–3	83,75	2,86	10,99	2,4
AC–5	83,66	3,73	10,25	2,36
AC–0P	88,96	0,83	9,07	1,14

3. 5. Luas Permukaan dan Distribusi Pori

Untuk mendukung pembahasan lebih lanjut mengenai pori dan luas permukaan karbon aktif, dilakukan analisa dengan metode BET (*brunauer emmett teller*) yang memanfaatkan proses adsorpsi desorpsi nitrogen pada suhu 77 K. Proses fisiosorpsi nitrogen ke dalam pori-pori karbon aktif dapat digunakan untuk mengetahui luas permukaan, volume pori dan distribusi ukuran pori yang diolah lebih lanjut dengan metode BJH (*barrett joyner halenda*).

Karbon aktif yang dihasilkan dominan memiliki struktur mesopori yang dibuktikan dengan grafik isothermal adsorpsi-desorpsi nitrogen. Jika dilihat pada Gambar 4. Karbon aktif AC-0, AC-3 dan AC-5 menunjukkan kurva isothermal tipe IV sesuai dengan klasifikasi IUPAC dengan adanya histeresis pada nilai P/P_0 yaitu 0,4-0,9. Sedangkan sampel AC-0P menunjukan kurva isothermal type I yang menunjukkan dominasi mikropori [30].

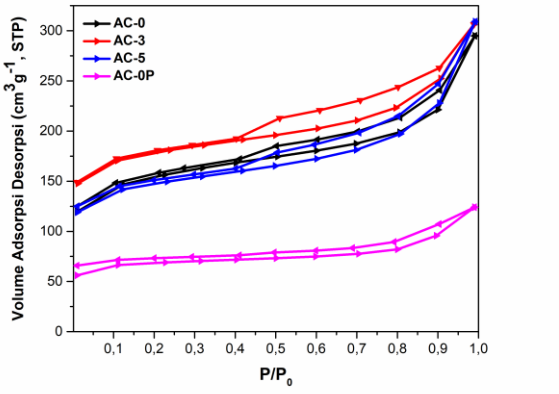

Gambar 4. Grafik isotermal adsorpsi desorpsi N_2 sampel AC-0, AC-3, AC-5 dan AC-0P

Peningkatan luas permukaan karbon aktif terhadap *hydrochar* (Tabel 4 dan 5) menunjukan bahwa aktivator bekerja dengan baik, Luas permukaan *hydrochar* sangat kecil karena pada proses karbonisasi hidrotermal belum terbentuk banyak pori.

Tabel 4. Karakteristik fisik dari *hydrochar* limbah akar wangi

Karakteristik	Kode Sampel		
	HC-0	HC-3	HC-5
S_{BET} (m^2g^{-1})	27,08	116,62	112,64
Ukuran partikel (nm)	221,58	51,45	53,27
Diameter pori rata-rata (nm)	17,66	10,54	10,96
Volume Pori (cm^3g^{-1})	0,1195	0,3075	0,3088
Volume Mikropori (%)	0,83	0,41	0,91
Volume Mesopori (%)	99,17	99,59	99,09

Berbeda dengan *hydrochar*, penggunaan aktivator K_2FeO_4 berdampak positif pada peningkatan luas permukaan. Jika dilihat, AC-0P hanya memiliki luas permukaan 212,36 m^2g^{-1} dengan volume pori 0,1918 cm^3g^{-1}. Nilai ini jauh lebih kecil jika dibandingkan dengan AC-0, AC-3 dan AC-5 sebesar 489,22 m^2g^{-1}; 552,90 m^2g^{-1} dan 463,68 m^2g^{-1}. Selama proses aktivasi dengan K_2FeO_4, bahan ini akan bereaksi dengan atom C sesuai dengan reaksi sebagai berikut:

$$K_2FeO_4 \rightarrow Fe_2O_3 + 2K_2O \quad (4)$$
$$K_2O + C \rightarrow 2K + CO \quad (5)$$
$$Fe_2O_3 + 3CO \rightarrow 2Fe + 3CO_2 \quad (6)$$

Tabel 5. Karakteristik fisik dari karbon aktif limbah akar wangi

Karakteristik	Kode Sampel			
	AC-0	AC-3	AC-5	AC-0P
S_{BET} (m^2g^{-1})	489,22	552,9	463,68	212,36
Ukuran partikel (nm)	12,26	10,85	12,94	28,25
Diameter pori rata-rata (nm)	3,73	3,43	4,12	3,61
Volume Pori (cm^3g^{-1})	0,4562	0,4737	0,478	0,1918
Volume Mikropori (%)	31,6	41,6	32,66	43,41
Volume Mesopori (%)	68,4	58,7	67,34	56,59

Dari keempat karbon aktif, AC-3 memiliki luas permukaan terbesar yaitu sebesar 552,90 m^2g^{-1} dengan volume pori 0,4730 cm^3g^{-1}. Penambahan luas permukaan terjadi karena semakin banyak K_2O yang bereaksi dengan atom C sehingga menghasilkan gas CO dan CO_2 yang nantinya akan menguap dan membentuk struktur pori. Peningkatan luas area ini juga dikarenakan meningkatnya pembentukan mikropori. Namun ketika variasi nitrogen diperbesar justru terjadi penurunan luas permukaan seperti terlihat pada AC-5 yang hanya mempunyai luas sebesar 463,48 m^2g^{-1}. Hal ini diduga karena semakin banyak nitrogen yang ditambahkan maka akan menghambat pembentukan mikropori [31]. Penurunan luas permukaan pada HC-5 dan AC-5 dimungkinkan karena urea yang dipergunakan berlebih, sehingga dimungkinkan nitrogen yang terdoping menyumbat pori-pori yang terbentuk. Hal ini terjadi pula pada penelitian Sun, L., dkk [32].

Data grafik distribusi pori dengan metode BJH (*barrett joyner halenda*) tersaji dalam Gambar 5. Ukuran pori pada karbon aktif terdiri atas 3 jenis yaitu mikropori (< 2nm), mesopori (2-50 nm) dan makropori (>50 nm). *Hydrochar* dengan dominasi makropori berukuran 50-221 nm sedangkan karbon aktif dengan ukuran mesopori 1,5-11 nm. Makropori dengan ukuran paling besar tidak berdampak langsung terhadap luas permukaan karbon aktif. Pori jenis ini hanya sebagai tempat penampungan ion/adsorben. Lain halnya dengan mesopori. Ukuran pori yang sedang ini berfungsi sebagai akses dan jalur ion atau adsorben untuk bergerak ke daerah aktif. Mikropori dengan ukuran paling kecil mempunyai dampak langsung terhadap luas permukaan karbon aktif. Namun karena ukurannya yang kecil, mikropori mudah tertutup oleh molekul besar.

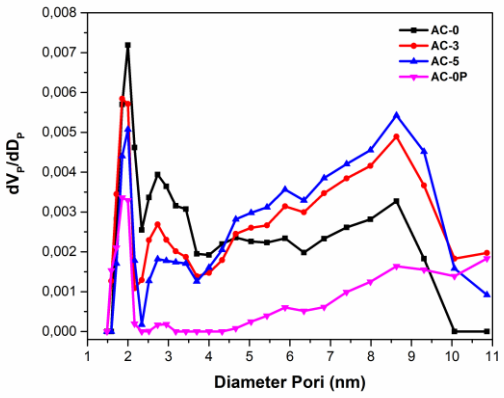

Gambar 5. Grafik distribusi pori sampel AC-0, AC-3, AC-5 dan AC-0P

Karbon aktif yang diaktivasi dengan K_2FeO_4 mempunyai distribusi dominan mesopori. Beberapa penelitian menunjukan bahwa pembentukan mesopori pada karbon aktif dapat diaplikasikan sebagai elektroda dalam media penyimpan energi maupun sebagai support katalis. Borisov, dkk., [9] meneliti tentang sibunit *carbon support* pada reaksi dekomposisi ammonia dengan katalis ruthenium. Keberadaan mesopore pada sibunit *carbon support* membantu proses pelepasan katalis sehingga reaksi berjalan lebih baik. Pada aplikasi elektroda, mesopori memfasilitasi pergerakan ion dengan cepat sehingga dapat meningkatkan *rate capability*. Hal ini ditemukan dalam penelitian

Hou, dkk., [17] yang mensitesis karbon aktif dari biji *black locust* dan mengaplikasikan sebagai elektroda pada superkapasitor.

4. KESIMPULAN

Konversi limbah akar wangi menjadi karbon aktif dapat menjadi solusi alternatif dalam pengolahan limbah yang selama ini belum dimanfaatkan secara maksimal. Kandungan lignoselulosa yang tinggi mendukung potensi limbah akar wangi untuk disintesis menjadi karbon aktif dengan banyak bidang aplikasi.

Modifikasi heteroatom doping dilakukan dengan menambahkan urea pada saat karbonisasi hidrotermal dalam berbagai rasio (1:0, 1:3, 1:5). Penggunaan urea sebagai sumber atom nitrogen saat pross karbonisasi hidrotermal dan aktivator K_2FeO_4 berhasil mendapatkan karbon aktif dengan karakteristik mesopori dan luas permukaan yang cukup besar. Penambahan urea yang berlebih menyebabkan penurunan yield *hydrochar*. Begitu pula dengan *yield* karbon aktif yang semakin menurun seiring peningkatan kandungan nitrogen doping dalam *hydrochar*. Perbandingan rasio urea terhadap luas permukaan yang optimal ada pada rasio 1:3 (AC-3) dengan S_{BET} sebesar 552,90 m^2g^{-1} dengan volume pori 0,4737 cm^3g^{-1} dan diameter pori rata-rata 3,43 nm. Gugus fungsi nitrogen terlihat pada hasil analisa FTIR baik bahan baku, *hydrochar* maupun karbon aktif, dimana intensitas semakin tinggi seiring peningkatan rasio urea yang digunakan. Ke depannya, karbon aktif dengan ukuran mesopori bisa dijajaki untuk aplikasi elektroda dalam media penyimpan energi maupun sebagai *support catalyst*.

UCAPAN TERIMA KASIH

Penelitian ini didanai oleh Hibah Kementerian Riset dan Teknologi (KEMENRISTEK) dan Badan Ristek dan Inovasi Nasional (BRIN) melalui skema World Class Research (WCR) 2021 dan dana pendamping LPPM UNPAR.

REFERENCES

[1] R. F. Susanti, G. Kevin, M. Erico, Kevien, A. A. Arie, H. Kristianto and T. Handoko, "Delignification, carbonization temperature and carbonization time effects on the hydrothermal conversion of salacca peel," *Journal of Nanoscience and Nanotechnology*, vol. 18, pp. 7263-7268, 2018. Doi: 10.1166/jnn.2018.15724

[2] O. Bobleter, "Hydrothermal degradation of polymers derived from plants," *Prog. Polym. Sci.*, vol. 19, pp. 797-841, 1994. Doi: 10.1016/0079-6700(94)90033-7

[3] F. A. Syamani, "Rekayasa proses fibrilasi selulosa untuk penguat dan pengisi komposit polimer," Doctor. Disertasi, Sekolah Pascasarjana, Institut Pertanian Bogor, Bogor, pp. 1-2, 2015.

[4] S. Gaspard, S. Altenor, E. A. Dawson, P. A. Barnes, and A. Ouensanga, "Activated carbon from vetiver roots: Gas and liquid adsorption studies," *Journal of Hazardous Material*, vol. 144, pp. 73-81, 2006. Doi: 10.1016/j.jhazmat.2006.09.089

[5] R. F. Susanti, A. A. Arie, H. Kristianto, M. Erico, G. Kevin, and H. Devianto, "Activated carbon from citric acid catlyzed hydrothermal carbonization and chemical activation of salacca peel as potential electrode for lithium ion capacitor's cathode," *Ionics*, vol. 25, pp. 3915-3925, 2019. Doi: 10.1007/s11581-019-02904-x

[6] D. Chen, L. Yang, J. Li, and Q. Wu, "Effect of self-doped heteroatoms in biomass-derived activated carbon for supercapacitor applications," *Chemistry Select*, vol. 4, pp. 1586-1595, 2019. Doi: 10.1002/slct.201803413

[7] A. A. Arie, Vincent, and A. Putranto, "Activated carbons from KOH-activation of salacca peels as low cost potential adsorbents for dye removal," *Advanced Materials Letters*, vol. 7, 3, pp. 226-229, 2016. Doi: 10.5185/amlett.2016.6194

[8] C. Quan, X. Jia, and N. Gao, "Nitrogen-doping activated biomass carbon from tea seed shell for CO2 capture and supercapacitor," *International Journal of Energy Research*, vol. 44, pp. 1-15, 2019. Doi: 10.1002/er.5017

[9] V. A. Borisov, K. N. Iost, V. L. Temerev, N. N. Leont'eva, I. V. Muromtsev, A. B. Arbuzov, M. V. Trenikhin, G. G. Savel'eva, N. S. Sminorva and D. A. Shlyapin, "The influence of the specific surface area of the carbon support on the activity of ruthenium catalysts for the ammonia-decomposition reaction," *Kinetics and Catalysis*, vol. 59, 2, pp. 136-142, 2018. Doi: 10.1063/5.0027083

[10] K. Zou, P. Cai, X. Cao, G. Zou, H. Hou, and X. Ji, "Carbon materials for high-performance lithium-ion capacitor," *Current Opinion in Electrochemistry*, vol. 21, pp. 31-39, 2020. Doi: 10.1016/j.coelec.2020.01.005

[11] W. Si, J. Zhoua, S. Zhanga, S. Lia, W. Xinga, and S. Zhuoa, "Tunable N-doped or

dual N, S-doped activated hydrothermal carbons derived from human hair and glucose for supercapacitor applications," *Electrochimica Acta*, vol. 107, pp. 397-405, 2013. Doi: 10.1016/j.electacta.2013.06.065

[12] S. Yan, J. Lin, P. Liu, Z. Zhao, J. Lian, W. Chang, L. Yao, Y. Liu, H. Liu and S. Han, "Preparation of nitrogen-doped porous carbons for high-performance supercapacitor using biomass of waste lotus stems," *Royal Society of Chemistry Advance*, vol. 8, pp. 6806-6813, 2018. Doi: 10.1039/C7RA13013A

[13] S. Liu, Y. Cai, X. Zhao, Y. Liang, M. Zheng, H. Hu, H. Dong, S. Jiang, Y. Liu and Y. Xiao, "Sulfur-doped nanoporous carbon spheres with ultrahigh specific surface area and high electrochemical activity for supercapacitor," *Journal of Power Source*, vol. 360, pp. 373-382, 2017. Doi: 10.1016/j.jpowsour.2017.06.029

[14] M. Sevilla and A. B. Fuertez, "The production of carbon materials by hydrothermal carbonization of cellulose," *Carbon*, vol. 47, pp. 2281-2289, 2009. Doi: 10.1016/j.carbon.2009.04.026

[15] T. Wang, Y. Zhai, Y. Zhu, C. Li, and G. Zeng, "A review of the hydrothermal carbonization of biomass waste for hydrochar formation: Process conditions, fundamentals, and physicochemical properties," *Renewable and Sustainable Energy Reviews*, vol. 90, pp. 223-247, 2018. Doi: 10.1016/j.rser.2018.03.071

[16] J. He, D. Zhang, Y. Wang, J. Zhang, B. Yang, H. Shi, K. Wang and Y. Wang, "Biomass-derived porous carbons with tailored graphitization degree and pore size distribution for supercapacitors with ultra-high rate capability," *Applied Surface Science*, vol. 515, pp. 146020, 2020. Doi: 10.1016/j.apsusc.2020.146020

[17] L. Hou, Z. Hu, X. Wang, L. Qiang, Y. Zhou, L. Lv and S. Li, "Hierarchically porous and heteroatom self-doped graphitic biomass carbon for supercapacitors," *Journal of Colloid and Interface Science*, vol. 540, pp. 88-96, 2019. Doi: 10.1016/j.jcis.2018.12.029

[18] Y. Zhou, S. Liu, Y. Liu, X. Tan, N. Liu, and J. Wen., "Efficient removal 17-estradiol by graphene-like magnetic sawdust biochar: Preparation condition and adsorption mechanism," *International Journal of Environmental Research and Pablic Health*, vol. 17, pp. 8377, 2020. Doi: 10.3390/ijerph17228377

[19] B. Gang, F. Zhang, X. Li, B. Zhai, X. Wang, and Y. Song, "A ulva lactuca-derived porous carbon for high-performance electrode materials in supercapacitor: Synergistic effect of porous structure and graphitization degree " *Journal of Energy Storage*, vol. 33, pp. 102132, 2021. Doi: 10.1016/j.est.2020.102132

[20] R. F. Susanti, S. Alvin, and J. Kim, "Toward high-performance hard carbon as an anode for sodium-ion batteries: Demineralization of biomass as a critical step," *Journal of Industrial and Engineering Chemistry*, vol. 91, pp. 317-329, 2020. Doi: 10.1016/j.jiec.2020.08.016

[21] T. Iskandar and U. Rofiatin, "Biochar characteristics based on biomass types and pyrolysis process parameters " *Jurnal Teknik Kimia*, vol. 12, 1, pp. 28-34, 2017. Doi: 10.33005/tekkim.v12i1.843

[22] E. Mulyono, D. Sumangat, and T. Hidayat, "Peningkatan mutu dan efisiensi produksi minyak akar wangi melalui teknologi penyulingan dengan tekanan uap bertahap," *Buletin Teknologi Pascananen Pertanian*, vol. 8, 1, pp. 35-47, 2012.

[23] W.-H. Chen, C.-W. Wang, H. C. Ong, P. L. Show, and T.-H. Hsieh, "Torrefaction, pyrolysis and two stage thermodegradation of hemicellulose, cellulose and lignin," *Fuel*, vol. 258, pp. 116-168, 2019. Doi: 10.1016/j.fuel.2019.116168

[24] S. A. Nicolae, H. Au, P. Modugno, H. Luo, A. E. Szego, M. Qiao, L. Li, W. Yin, H. J. Heeres, N. Berge, and M. M. Titirici, "Recent advances in hydrothermal carbonisation: from tailored carbon materials and biochemicals to applications and bioenergy," *Green Chemistry*, vol. 22, pp. 4747-4800, 2020. Doi: 10.1039/D0GC00998A

[25] M. J. Alhnidi, P. Körner, D. Wüst, J. Pfersich, and A. Kruse, "Nitrogen-containing hydrochar: the influence of nitrogen containing compounds on the hydrochar formation," *Chemistry Open*, vol. 9, pp. 864-873, 2020. Doi: 10.1002/open.202000148

[26] Q. Abbas, R. Raza, I. Shabbir, and A. G. Olabi, "Heteroatom doped high porosity carbon nanomaterials as electrodes for energy storage in electrochemical capacitors: A review," *Journal of Science: Advanced Materials and Devices*, vol. 4, pp. 341-352, 2019. Doi: 10.1016/j.jsamd.2019.07.007

[27] J. Chen, J. Yang, G. Hu, X. Hu, Z. Li, S. Shen, M. Radoz and M. Fan, "Enhanced CO_2 capture capacity of nitrogen-doped biomass-derived porous carbons," *ACS Sustainable Chemistry & Engineering*, vol. 4, pp. 1439-1445, 2016. Doi: 10.1021/acssuschemeng.5b01425

[28] Y. Lin, Z. Chen, C. Yu, and W. Zhong, "Heteroatom-doped sheet-like and hierarchical porous carbon based on natural biomass small molecule peach gum for high performance supercapacitors," *ACS Sustainable Chemistry & Engineering*, vol. 7, pp. 3389–3403, 2019. Doi: 10.1021/acssuschemeng.8b05593

[29] Q. Wu, W. Li, S. Liu, and C. Jin, "Hydrothermal synthesis of N-doped spherical carbon from carboxymethylcellulose for CO_2 capture," *Applied Surface Science*, vol. 369, pp. 101-107, 2016. Doi: 10.1016/j.apsusc.2016.02.022

[30] M. Thommes, K. Kaneko, A. V. Neimark, J. P. Oliver, F. R. Reinoso, J. Rouquerol and K. S. W. Sing, "Physisorption of gases, with special reference to the evaluation of surface area and pore size distribution (IUPAC Technical Report)," *Pure Appl. Chem*, vol. 87, pp. 9-10, 2015. Doi: 10.1515/pac-2014-1117

[31] J. Han, L. Zhang, B. Zhao, L. Qin, Y. Wang, and F. Xing., "The N-Doped activated carbon derived from sugarcane bagasse for CO_2 adsorption," *Industrial Crops and Product*, vol. 128, pp. 290-297, 2019. Doi: 10.1016/j.indcrop.2018.11.028

[32] L. Sun, C. Tian, Y. Fu, Y. Yang, J. Yin, L. Wang and H. Fu, "Nitrogen-doped porous graphitic carbon as an excellent electrode material for advanced supercapacitors," *Chemsitry European Journal*, vol. 20, pp. 564-574, 2014. Doi: 10.1002/chem.201303345

METALURGI
Majalah Ilmu dan Teknologi
p-ISSN 0126-3188 | e-ISSN 2443-3926
www.ejurnalmaterialmetalurgi.com

THE EFFECT OF ECAP PROCESSING ON HARDNESS, SURFACE MORPHOLOGY, AND CORROSION RESISTANCE OF 6061 ALLOYS

I Nyoman Gede Putrayasa Astawa, Vinda Puspasari*, Efendi Mabruri, Satrio Herbirowo, Edi Priyanto Utomo
[a]Pusat Penelitian Metalurgi dan Material-LIPI
Gedung 470, Kawasan Puspiptek Serpong, Indonesia 15343
*E-mail: vindapuspa13@gmail.com

Masuk tanggal : 07 Juni 2021, revisi tanggal : 24 Agustus 2021, diterima untuk diterbitkan tanggal 09-09-2021

Abstrak

Paduan aluminum Al-Mg-Si (6xxx) telah banyak digunakan sebagai material struktural untuk bangunan dan kendaraan bermotor karena memiliki kekuatan mekanik dan ketahan korosi yang baik. Proses ECAP (*equal channel angular pressing*) merupakan metode yang paling menjanjikan dengan mengaplikasikan deformasi plastis yang memproduksi material utuh dengan butir yang halus tanpa porositas sisa. Penelitian ini mempelajari tentang pengaruh jumlah pass pada proses ECAP terhadap kekerasan, struktur mikro, dan perilaku korosi pada paduan aluminum 6061. Material paduan terlebih dahulu dilakukan proses aniling di dalam tungku dengan lingkungan gas argon pada T = 530 °C selama 4 jam kemudian dicelupkan pada nitrogen cair selama 5 menit sebelum proses ECAP. Proses ECAP dilakukan melalui rute Bc dengan cetakan yang memiliki lubang dalam bersudut 120° dan variasi pass dari 1, 2, 3, dan 4. Kekerasan optimal yang diperoleh yaitu 107,58 HB pada paduan Al 6061 dengan 3 pass ECAP. Peningkatan jumlah pass pada ECAP menyebabkan adanya pengurangan ukuran butir dari ukuran 10 µm pada paduan hasil aniling menjadi ukuran 2,5 µm pada paduan dengan 4 pass. Ketahanan korosi meningkat seiring dengan peningkatan jumlah ECAP pass.

Kata Kunci: Paduan Al-Mg-Si, *ECAP*, kriogenik, struktur mikro, ketahanan korosi

Abstract

Al-Mg-Si alloys (6xxx) have been widely used as structural materials in buildings and vehicles because of their excellent strength and corrosion resistance. ECAP (equal channel angular pressing) is the most promising method to apply SPD (severe plastic deformation), producing ultra-fine grain in the bulk material without residual porosity. This study presents some experiments results on the effect of ECAP number of passes variation on the hardness, microstructure, and corrosion behavior of Al 6061 alloys. The alloy was annealed in the furnace with an argon gas environment at 530°C for 4 hours and then immersed in liquid nitrogen for 5 minutes before the ECAP process. The ECAP process was carried out via the Bc route, with dies with an internal channel angle of 120° and pass variations of 1, 2, 3, and 4. The optimum hardness was 107.58 HB in Al 6061 alloy with three passes of ECAP. The increasing ECAP number of passes leads to a significant grain size reduction from the 0-way pass; the grain size was around 10 µm, while for a 4-way pass, the grain size was around 2.5 µm. The corrosion resistance of Al 6061 alloys increased with the increasing number of passes in the ECAP process.

Keywords: *Al-Mg-Si alloys, ECAP, cryogenic, hardness, microstructure, corrosion resistance*

1. INTRODUCTION

Aluminum alloys are widely used due to increasing demand for improving construction and automotive performance using lightweight materials [1]. The 6xxx series Al-Mg-Si alloys are heat treatable and maintain high mechanical properties. Al-Mg-Si alloys (6xxx) have been widely used as structural materials in buildings and vehicles, such as vessels, engine blocks, and pistons, because of their excellent strength and corrosion resistance [2]. The improved fine-grain microstructure, which can increase mechanical and physical properties, has become an exciting field in recent research [3]. The combination of nanostructured and sub-micrometer materials will produce high performances because of their small

DOI : http://dx.doi.org/10.14203/metalurgi.v36i2.589

Metalurgi is Sinta 2 Journal (https://sinta.ristekbrin.go.id/journals/detail?id=3708) accredited by Ministry of Research & Technology, Republic Indonesia

grain size [4]. The deformation process to refining the microstructure of Al 6061 (6061 aluminum alloys) has effectively improved physical-mechanical properties such as ductility, strength, toughness, strain, elongation, and corrosion resistance [5].

Equal channel angular press is the most promising method to apply severe plastic deformation (SPD), producing ultra-fine grain in the bulk material without residual porosity [6]. The large bulk sizes of ECAP processing materials become an advantage to obtain nano and ultra-fine structured mechanical parts and offer the opportunity to scale up the process to an industrial level [7]. The ECAP process utilized a sample that pressed through a die with two intersecting channels equal in the cross-section. The ECAP process uses shear force to deform the materials through the intersection of the angular channels [8]. The other advantage of the ECAP process is that the sample holds a similar cross-sectional area after pressing so that it is feasible to repeat the pressing a few times [9]. The improved material properties are the result of the ECAP process, which is dependent on the geometry of the channels and the number of passes. [10]. Furthermore, some parameters such as die geometry and channel angle of ECAP can influence the induced equivalent plastic strain, which improves mechanical properties in the materials [11].

Aluminum alloys are well known for their high corrosion resistance because of their oxide film in the atmospheric environment [12]. Uniform, localized and pitting corrosions are the most common corrosion founded in aluminum alloys with a halide ion environment. Recently, the effect of grain refinement on the hardness and corrosion properties has attracted much attention. Some researchers revealed that decreasing grain size using ECAP could increase the corrosion resistance of Al-Mg and pure Mg alloys [13]. It also reported that the decreasing hardness properties resulted from the increasing number of ECAP passes [14]. In this paper, the effect of ECAP number of the pass in the cryogenic environment has been investigated on hardness, microstructure, and corrosion properties of Al 6061.

2. MATERIALS AND METHODS

The element percentage in the Al 6061 was determined using OES (optical emission spectroscopy) on a commercial billet of 6061 aluminum alloys. For the ECAP process, the Al 6061 billets were machined into cylindrical specimens with dimensions of 65 mm length and 13.55 diameters. Figure 1 showed the flow diagram of the ECAP (equal channel angular pressing) process and the characterization after the ECAP process. Before the ECAP process, the samples were annealed in an argon gas environment for 4 hours at 530 °C to homogenize the microstructure and remove internal stress [15]. The samples were immersed in liquid nitrogen for 5 minutes before the ECAP process to obtain the cryogenic temperature in the samples. The immersion of samples in liquid nitrogen was done before the addition of the ECAP pass. The immersion of sample in liquid nitrogen was done in every each ECAP pass addition.

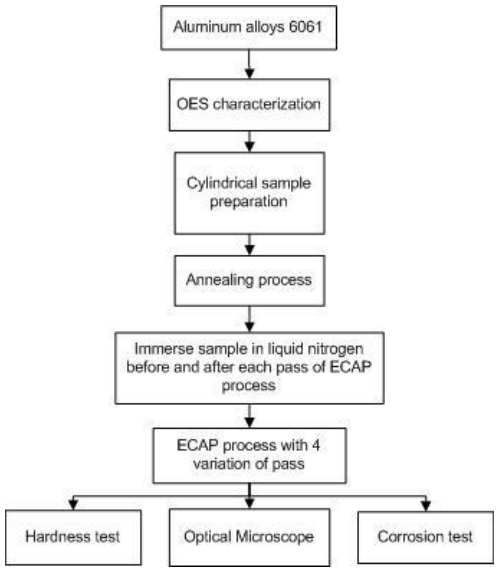

Figure 1. The flow diagram of ECAP process and characterization

After the nitrogen immersion of the sample, the ECAP process was done using the Bc route using 120° of internal channel angle with pass variations of 1, 2, 3, and 4. The Bc deformation was done by rotating the sample orientation of 90° before each new ECAP pass. After the ECAP process was done, the hardness properties were characterized using a hardness test, and the microstructure of the ECAP-processed sample was also evaluated using an optical microscope. The corrosion properties such as open circuit potential and Tafel polarization were characterized using CMS (corrosion measurement system). The morphology of corrosion products was also investigated using an optical microscope.

The hardness test was held using Hardness Brinnel in 5 varied points and the values obtained are averaged to obtain the hardness number. The hardness test was done on annealed samples and ECAP-processed samples. The ECAP-processed pieces were cut along their longitudinal cross-section, ground, polished, and etched using

Poulton's reagent. After that, the samples were characterized using an optical microscope to analyze the microstructure which has been formed.

The corrosion testing of Al 6061 samples was held using a 3-electrode flat corrosion cell in a 3.5% NaCl with Gamry Reference potentiostat. The platinum electrode was utilized as the counter electrode, the saturated calomel (SCE) was used as the reference electrode, and the Al 6061 sample was used as the working electrode. The samples were wet ground using 240, 600, 800, 1000, 1200 SiC abrasive paper followed by degreasing with distilled water and acetone and then blow-dried with compressed air. The OCP characterization was done by immersed the sample in the NaCl solution in 1 hour. Tafel polarization was then investigated against the OCP at a scan rate of 0.6 m/s.

3. RESULTS AND DISCUSSIONS

3. 1. Chemical Composition Characterization

Optical emission spectroscopy was done to characterize the percentage of elements contained in the samples. Table 1 presents the chemical composition of 6061 aluminum alloys which are characterized using OES (optical emission spectroscopy).

Tabel 1. Chemical composition of comercial 6061 aluminum alloys (wt.%)

Si	**Fe**	**Cu**	**Mn**	**Mg**	**Zn**	**Ti**
0.643	0.497	0.227	0.106	0.871	0.039	0.01
Cr	**Ni**	**Pb**	**Sn**	**V**	**Cd**	**Al**
0.085	0,01	0.002	0.002	0.06	0.01	Bal

The dominants of alloying elements are Mg with 0.871 wt.% value and Si with 0.643 wt.%. Other alloying elements such as Fe, Cu, and Mn are detected in this alloy.

3. 2. Hardness Test

The hardness test was utilized to investigate the effect of number pass on hardness properties of the Al 6061 alloy. Figure 2 presents the hardness of the ECAP (equal channel angular pressing) processed of the alloy under different variations of passes.

The ECAP process increases the hardness number of Al 6061 alloy, and it is also noted that further hardness number improvement is proportional to the number of passes increased. It can be concluded that the improvement in hardness number is caused by grain refinement concerning the standard of the Hall-Petch relationship predicts that the yield strength would increase as grain size decreases [16].

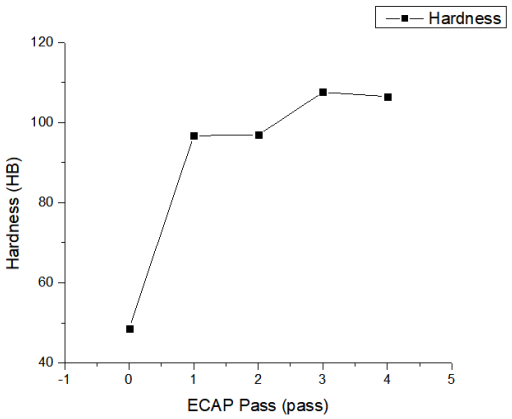

Figure 2. Hardness characteristics of the Al 6061 alloy under different processing conditions

Besides that, the strengthening mechanism such as fragmentation and homogeneous distribution of precipitates and the high number of dislocation density also could improve hardness number. Figure 2 depicts the hardness characteristics of the examined alloys under various processing settings. The hardness of the annealed Al 6061 alloy was 48.6 HB and increased to 107.58 HB in 3 passes number of ECAP. The ECAP processed alloy improves grain refinement and the number of dislocation networks at grain boundaries and within grains significantly.

Furthermore, the presence of smaller strengthening phase particles within the matrix of the ECAP processed alloy creates barriers to unrestricted dislocation migration inside the matrix. Slip or dislocation movement occurs across these grain boundaries, and it can also aid in the cross slip of screw dislocations obstructed by precipitates or dislocation locks during plastic deformation [17]. Dislocation changes direction as it passes from one grain to the next because the grain borders of polycrystalline grains have different crystallographic orientations. Dislocation entanglement occurs because of such variations in dislocation direction, preventing dislocation mobility. The increases hardness of materials by strain hardening due to mutual restriction of dislocation glide on the intersecting system [18].

Figure 3 reveals that optical microscope results showing the grain structure after ECAP processing. The shear strain affects their dislocation density and realignment to produce new cells and grains. The effect of cryogenic treatment caused a higher density of dislocation in the grain and cell interiors. The increasing ECAP number of passes leads to a significant grain size reduction to the sub-micrometer scale of 1-2μm. It can be seen in the sample with four passes in Figure 2€ had a smaller grain size than

the sample with a smaller number of passes in the ECAP process. The microstructure of the ECAP processed sample consists of elongated and rounded grain shapes surrounded by dislocation walls. The effect of ECAP pass number in cryogenic treatment could increase dislocation density inside cells and grain. In other words, the sample with four passes of ECAP has more dislocation density than the sample with a smaller number of passes and annealed sample. The dislocation movements are also affected by low-temperature pressing. The Al 6061 with four passes of ECAP had much free dislocation of grain because of dislocation deposition in cell and grain boundaries. Slip bands are formed as the result of the high strain caused during ECAP processing. Their grain sizes also fall dramatically; for a 0-way pass, the grain size is around 10 µm, while for four-way passes, the grain size is approximately 2.5 µm. There was also a high distribution of precipitates that segregated along grain boundaries. The fragmentation of these precipitates during ECAP processing could explain the rise in precipitates. Furthermore, the shattered precipitates were sheared into multiple pieces, which prevented growth [19]. At the interface between the particles and the matrix, there is no sign of deformation. According to the literature, significant dislocation density and lattice misorientation can develop during particle deformation, resulting in inhomogeneous deformation and grain size discrepancies in the particle's immediate surroundings [20].

3. 3. Open Circuit Potential Measurement

Two electrochemical techniques, such as OCP and Tafel polarization, are used to investigate the corrosion behavior of Al 6061 after ECAP is processed. Figure 4 represents the open circuit potential that studied the passive film's characteristic on the surface of Al 6061. All ECAP-deformed Al 6061 alloys have a higher free corrosion potential than annealed Al 6061. This phenomenon explained that the increasing ECAP number of passes could improve the oxide film on the surface, decreasing electrochemical reactions. It can be seen from Figure 4 that there is some fluctuation in the potential time curve in all samples, which reflects dissolution and repassivation events, which are connected to the activity of different impurities contained in the samples.

Open circuit potential is an important variable to understand the corrosion resistance of materials. The higher value of free corrosion potential indicated the difficulty of material to corrode [21]. According to Table 2, the free corrosion potential value of Al 6061 with four passes has the highest value of all samples. This result indicates that Al 6061 with four passes of ECAP was the noblest of all samples.

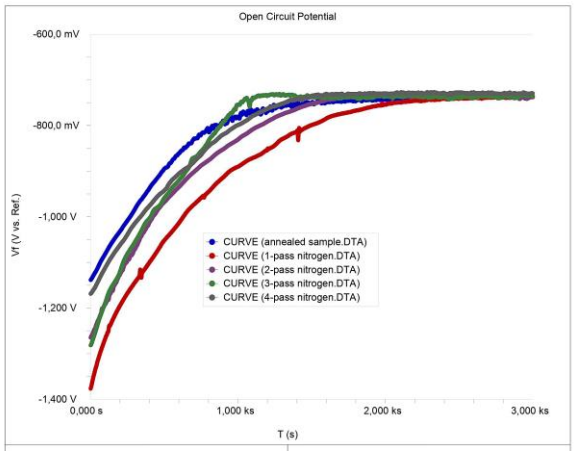

Figure 4. Potential time curve of annealed and ECAP processed Al 6061 with the variation of passes in 3.5% NaCl solution

Table 2. Free corrosion potential for 1 hour of Al 6061 alloy

Sample	Vmin (mV)	Vmax (V)	Eoc (mV vs SCE)
As-annealed	-733.4	-1140	-733.4
1-pass nitrogen	-733.5	-1380	-733.5
2-passes nitrogen	-728.9	-1269	-728.9
3-passes nitrogen	-727.7	-1284	-727.7
4-passes nitrogen	-725.4	1170	-725.4

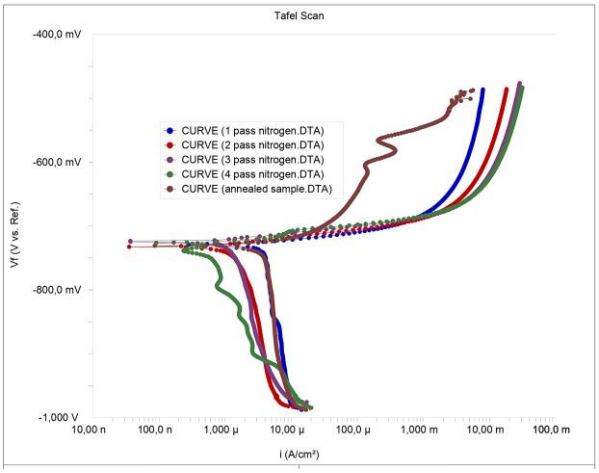

Figure 5. Tafel polarization curve of as-annealed and ECAP processed Al 6061 in 3.5% NaCl solution

Table 3. Electrochemical parameters obtained from Tafel polarization of annealed and ECAP processed Al 6061 alloys

Sample	Ecorr (mV)	Icorr (µA/cm^2)	Corr rate (mmpy)
As-annealed	-730.9	4.05	133.3e-3
1-pass nitrogen	-729.4	3.60	118.6e-3
2-passes nitrogen	-732.6	1.52	50.17e-3
3-passes nitrogen	-725.6	1.38	45.43e-3
4-passes nitrogen	-726.4	0.005	16.04e-3

3. 4. Tafel Polarization

Tafel polarization curves of the annealed and ECAP processed alloy are shown in Figure 5. The alloy was immersed in 3.5% NaCl solution for 1 hour to obtain their stable OCP values.

It can be observed from Fig. 5 that the cathodic current density slope shifted left with the increased ECAP number of passes. Table 3 also shows that the corrosion potential (Vcorr) of the annealed alloy decreased from -730.9 mV to -726.4 mV after four passes. The corrosion rate also decreased with the increased ECAP number of passes from 133.3e-3 mmpy of annealed alloy to 16.04e-3 mmpy after four passes. The effect of grain refinement is caused by the increase in the ECAP number of passes, which affects a more uniform corrosion attack and lower corrosion rate [22]. The Tafel slope in the anodic curve of Al 6061 decreased with the higher number of passes in the ECAP process. This phenomenon explains that the ECAP number of passes has a noticeable effect on the anodic reaction.

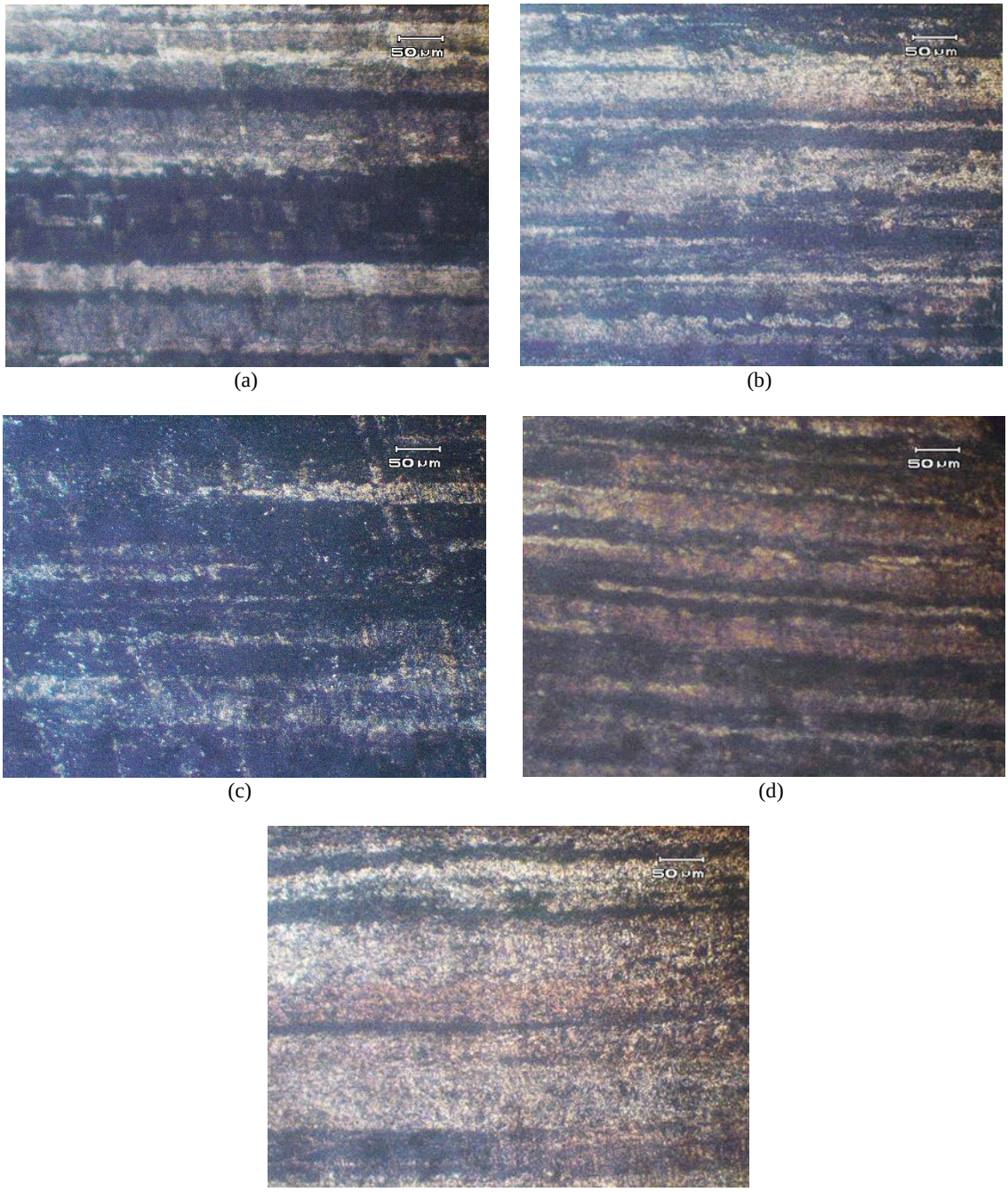

(a) (b) (c) (d) (e)

Figure 3. The optical microscope results of Al 6061 alloys with the variation of (a). As-annealed, (b). 1-pass ECAP, (c) 2-pass ECAP, (d) 3-pass ECAP and (e). 4-pass ECAP

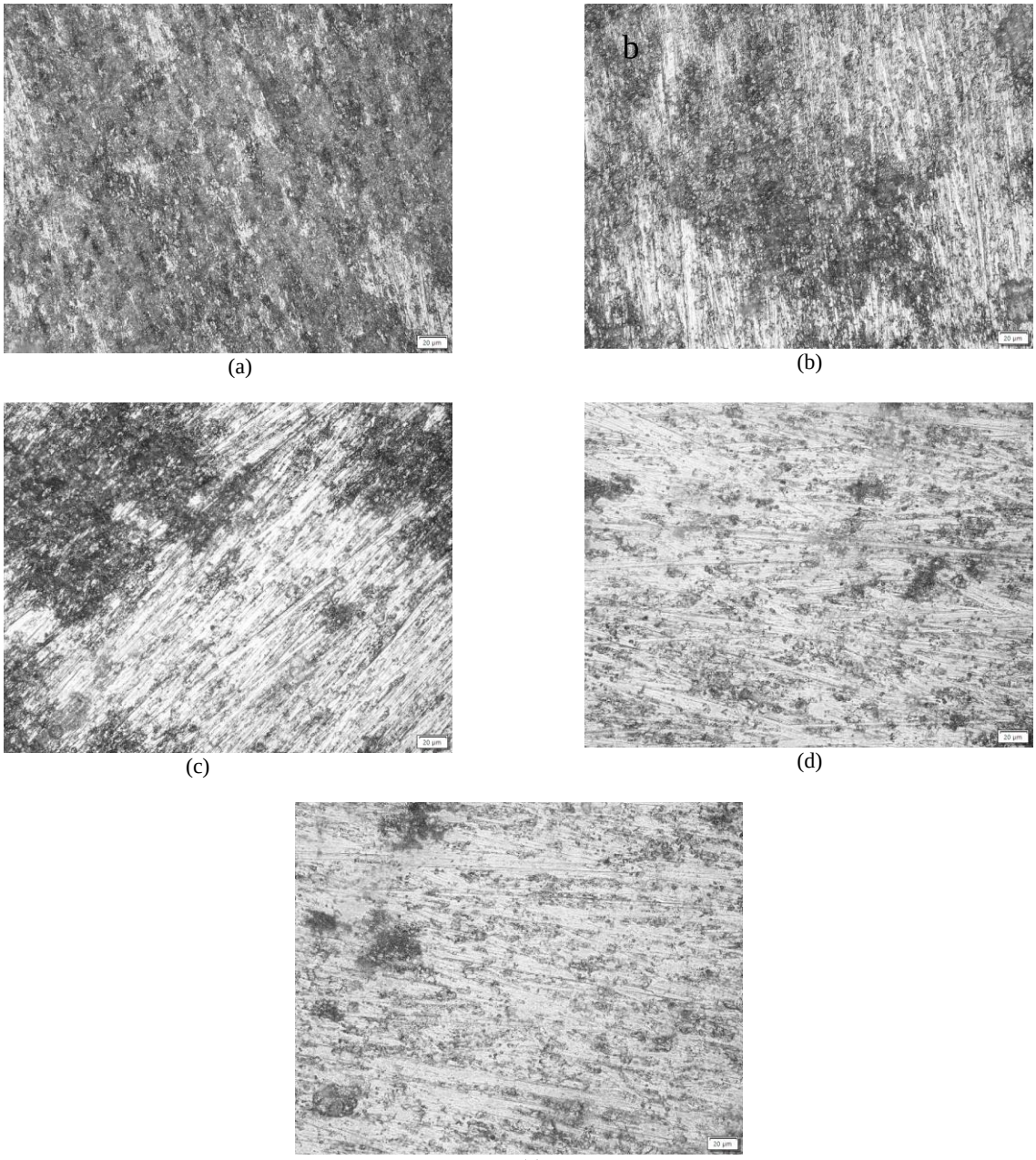

Figure 4. The optical microscope results of Al 6061 alloys with the variation of (a). As-annealed, (b). 1-pass ECAP, (c) 2-pass ECAP, (d) 3-pass ECAP and (e). 4-pass ECAP after corrosion test in 3.5% NaCl

Figure 4 shows the optical microscope of corroded alloy in 3.5% NaCl solution. It can be observed that the high amount of corrosion attacks on the surface of the as-annealed alloy after the Tafel polarization test in 3.5% NaCl solution. The ECAP-processed of Al 6061 alloys exhibit lower localized corrosion than the as-annealed Al 6061. The ECAP processed samples of Al 6061 alloys after the Tafel polarization test illustrates less localized corrosion on the surface of alloy with three and four passes in Figs. 4(d) and 4(e). This phenomenon is caused by the improvement of grain refinement and secondary phases distribution, which lower the corrosion rate of Al 6061 alloy. Furthermore, an alloy with a higher Ecorr value indicates more passivated oxide film, which caused a lower corrosion rate because of the slow dissolution rate of fine grain structure [23]. This fact also supported the corrosion morphology of the alloy in Figs. 4(a), 4(b), and 4(c) are more corroded than the others because of their coarse grain.

4. CONCLUSIONS

In the current study, the effect of ECAP processing on the hardness, microstructure, and corrosion behavior of Al 6061 was successfully done. The hardness of the sample before aging

was 48.6 HB and increased to 107.58 HB in three passes number of ECAP. The effect number of passes was in line with grain refinement, which affects the hardness. The Al 6061 annealed and ECAP processed microstructure revealed the elongated and rounded shapes of grain bounded by dislocation walls. Besides that, the increased ECAP number of passes led to a significant grain size reduction from 10 μm in the Al 6061 annealed to 2.5 μm after four passes of the ECAP process. The corrosion behavior of the Al 6061 deformed by ECAP had nobler free corrosion potential than the annealed Al 6061. The corrosion rate also decreased with the increased ECAP number of passes from 133.3e-3 mmpy of Al 6061 annealed to 16.04e-3 mmpy after four passes.

ACKNOWLEDGEMENT

The author would like to thank the Indonesian Institute of Sciences' Research Center of Metallurgy and Materials, which funded this research in DIPA 2013.

REFERENCES

[1] T. Dokšanović, I. Džeba, and D. Markulak, "Applications of aluminium alloys in civil engineering," *Teh. Vjesn. - Tech. Gaz.*, vol. 24, no. 5, pp. 1609–1618, 2017. Doi: 10.17559/tv-20151213105944

[2] X. H. Zeng, P. Xue, L. H. Wu, D. R. Ni, B. L. Xiao, and Z. Y. Ma, "Achieving an ultra-high strength in a low alloyed Al alloy via a special structural design," *Mater. Sci. Eng. A*, vol. 755, no. March, pp. 28–36, 2019. Doi: 10.1016/j.msea.2019.03.126

[3] V. Shrivastava, G. K. Gupta, and I. B. Singh, "Heat treatment effect on the microstructure and corrosion behavior of Al-6061 alloy with influence of α-nanoalumina reinforcement in 3.5% NaCl solution," *J. Alloys Compd.*, vol. 775, pp. 628–638, 2019. Doi: 10.1016/j.jallcom.2018.10.111

[4] M. A. Agwa, M. N. Ali, and A. E. Al-Shorbagy, "Optimum processing parameters for equal channel angular pressing," *Mech. Mater.*, vol. 100, pp. 1–11, 2016. Doi: 10.1016/j.mechmat.2016.06.003

[5] A. I. Alateyah, T. A. Aljohani, M. O. Alawad, H. A. El-Hafez, A. N. Almutairi, E. S. Alharbi, R. Alhamada, B.W. El-Garaihy, and W. H. El-Garaihy, "Improved corrosion behavior of AZ31 alloy through ECAP processing," *Metals (Basel)*, vol. 11, no. 2, pp. 1–19, 2021. Doi: 10.3390/met11020363

[6] P. Sonia, J. K. Jain, and K. K. Saxena, "Influence of severe metal forming processes on microstructure and mechanical properties of Mg alloys," *Adv. Mater. Process. Technol.*, pp. 1–24, 2020. Doi: 10.1080/2374068X.2020.1802554

[7] G. M. Naik, S. Narendranath, and S. S. S. Kumar, "Effect of ECAP die angles on microstructure mechanical properties and corrosion behavior of AZ80 Mg alloy," *J. Mater. Eng. Perform.*, vol. 28, no. 5, pp. 2610–2619, 2019. Doi: 10.1007/s11665-019-04080-5

[8] E. Avcu, "The influences of ECAP on the dry sliding wear behaviour of AA7075 aluminium alloy," *Tribol. Int.*, vol. 110, pp. 173–184, 2017. Doi: 10.1016/j.triboint.2017.02.023

[9] M. Cabibbo, E. Santecchia, P. Mengucci, T. Bellezze, and A. Viceré, "The role of cryogenic dipping prior to ECAP in the microstructure, secondary-phase precipitation, mechanical properties and corrosion resistance of AA6012 (Al-Mg-Si-Pb)," *Mater. Sci. Eng. A*, vol. 716, pp. 107–119, 2018. Doi: 10.1016/j.msea.2018.01.037

[10] Z. Zhao, G. Wang, Y. Zhang, J. Gao, and H. Hou, "Microstructure evolution and mechanical properties of Ti-6Al-4V alloy prepared by multipass equal channel angular pressing," *J. Mater. Eng. Perform.*, vol. 29, no. 2, pp. 905–913, 2020. Doi: 10.1007/s11665-020-04673-5

[11] E. Mabruri, I. N. G. P. Astawa, and E. P. Utomo, "Studi equal channel angular pressing (ECAP) suhu nitrogen cair pada paduan Al-Mg-Si (Al 6061)," *Maj. Metal.*, vol. 29, no. 3, pp. 215–222, 2014.

[12] B. Wang, X. Li, J. Liu, and H. Jiang, "Comparison of atmospheric corrosion behavior of Al-Mn and Al-Zn-Mg-Cu alloys in a tropical coastal environment," *Mater. Corros.*, vol. 69, no. 7, pp. 888–897, 2018. Doi: 10.1002/maco.201709920

[13] D. Song, C. Li, N. Liang, F. Yang, J. Jiang, J. Sun, G. Wu, A. Ma, and X. Ma, "Simultaneously improving corrosion resistance and mechanical properties of a magnesium alloy via equal-channel angular pressing and post water annealing," *Mater. Des.*, vol. 166, p. 107621, 2019. Doi: 10.1016/j.matdes.2019.107621

[14] J. Zuo, L. Hou, X. Shu, W. Peng, A. Yin,

and J. Zhang, “Effect of deformation on precipitation and the microstructure evolution during multistep thermomechanical processing of Al-Zn-Mg-Cu Alloy,” *Metals (Basel)*, vol. 10, no. 11, pp. 1–16, 2020. Doi: 10.3390/met10111409

[15] V. Puspasari, M. A. Prasetyo, J. Velix, M. S. Anwar, S. Herbirowo, and E. Mabruri, “Pengaruh annealing terhadap kekerasan dan struktur mikro baja tahan karat AISI 410-3MO-3Ni,” *Maj. Metal.*, vol. 35, no. 2, pp. 75–82, 2020.

[16] H. Huang, H. Liu, L. Wang, K. Yan, Y. Li, J. Jiang, A. Ma, F. Xue, J. Bai, “Revealing the effect of minor Ca and Sr additions on microstructure evolution and mechanical properties of Zn-0.6 Mg alloy during multi-pass equal channel angular pressing,” *J. Alloys Compd.*, vol. 844, p. 155923, 2020. Doi: 10.1016/j.jallcom.2020.155923

[17] M. K. Pathak, A. Joshi, K. K. S. Mer, and R. Jayaganthan, “Mechanical properties and microstructural evolution of bulk UFG Al 2014 alloy processed through cryorolling and warm rolling,” *Acta Metall. Sin. (English Lett.)*, vol. 32, no. 7, pp. 845–856, 2019. Doi: 10.1007/s40195-018-0849-7

[18] S. Fritsch and M. F. X. Wagner, “On the effect of natural aging prior to low temperature ECAP of a high-strength aluminum alloy,” *Metals (Basel).*, vol. 8, no. 1, 2018. Doi: 10.3390/met8010063

[19] Z. S. Zahari, D. N. A. Sh’Ri, M. A. H. A. Hassan, and W. S. W. Harun, “Effect of ECAP die angle to the microstructure and mechanical properties of bulk nanostructured Al-6061,” *IOP Conf. Ser. Mater. Sci. Eng.*, vol. 469, no. 1, 2019. Doi: 10.1088/1757-899X/469/1/012054

[20] M. Orłowska, E. Ura-Bińczyk, L. Olejnik, and M. Lewandowska, “The effect of grain size and grain boundary misorientation on the corrosion resistance of commercially pure aluminium,” *Corros. Sci.*, vol. 148, pp. 57–70, 2019. Doi: 10.1016/j.corsci.2018.11.035

[21] E. Mabruri, H. M. Sigit, M. A. Prasetyo, A. Nikitasari, and A. De Fretes, “Pitting corrosion resistance of CA6NM and 410 martensitic stainless steels in various environments,” in *IOP Conference Series: Materials Science and Engineering 858*, pp. 012049, 2020. Doi: 10.1088/1757-899X/858/1/012049

[22] M. I. Abd El Aal and M. M. Sadawy, “Influence of ECAP as grain refinement technique on microstructure evolution, mechanical properties and corrosion behavior of pure aluminum,” *Trans. Nonferrous Met. Soc. China (English Ed.)*, vol. 25, no. 12, pp. 3865–3876, 2015. Doi: 10.1016/S1003-6326(15)64034-1

[23] S. Arthanari, J. C. Jang, and K. S. Shin, “Corrosion performance of high pressure die-cast Al-Si-Mg-Zn alloys in 3.5 wt% NaCl solution,” *J. Alloys Compd.*, vol. 783, pp. 494–502, 2019. Doi: 10.1016/j.jallcom.2018.12.313

Metalurgi (2021) 2: 77 - 86

METALURGI
Majalah Ilmu dan Teknologi
p-ISSN 0126-3188 | e-ISSN 2443-3926
www.ejurnalmaterialmetalurgi.com

INCREASING OF METAL RECOVERY IN LEACHING PROCESS OF SPENT CATALYST AT LOW TEMPERATURE: THE ADDITION OF HYDROGEN PEROXIDE AND SODIUM CHLORIDE

Kevin Cleary Wanta[a,*], Edward Yonathan Natapraja[a], Ratna Frida Susanti[a], Gelar Panji Gemilar[b], Widi Astuti[c], Himawan Tri Bayu Murti Petrus[d]

[a]Department of Chemical Engineering, Parahyangan Catholic University
Jalan Ciumbuleuit No. 94 Bandung, Indonesia 40141
[b]PT Petrokimia Gresik
Jalan Jenderal Ahmad Yani, Gresik, Indonesia 61119
[c]Research Unit for Mineral Technology, Indonesian Institute of Sciences (LIPI)
Jalan Ir. Sutami Km. 15, Tanjung Bintang, Lampung Selatan, Indonesia 35361
[d]Department of Chemical Engineering, Gadjah Mada University
Jalan Grafika No. 2 Kampus UGM, Yogyakarta, Indonesia, 55281
*E-mail: kcwanta@unpar.ac.id

Masuk tanggal : 07-07-2021, revisi tanggal : 31-08-2021, diterima untuk diterbitkan tanggal 09-09-2021

Abstrak

Salah satu faktor yang memengaruhi proses *leaching* dari suatu sumber mineral adalah karakteristik mineral dari bahan baku tersebut. Tidak semua fasa mineral dapat ter*leaching* secara langsung dan sempurna. Dengan demikian, beberapa mineral memerlukan perlakuan khusus sehingga proses *leaching* dapat berlangsung dengan maksimal. Studi ini akan terfokus pada mempelajari pengaruh penambahan senyawa aditif, yaitu hidrogen peroksida dan natrium klorida, dalam proses *leaching spent catalyst* dengan menggunakan larutan asam sulfat. Proses *leaching* dilakukan pada konsentrasi larutan asam sulfat 1 M selama 240 menit pada suhu ruang. Konsentrasi hidrogen peroksida divariasikan pada 0–9%v/v sedangkan konsentrasi natrium klorida divariasikan pada 0–0,8 mol/L. Hasil percobaan menunjukkan bahwa kedua senyawa aditif tersebut mampu meningkatkan perolehan nikel secara signifikan. Perolehan nikel tertinggi sebesar 95,08% tercapai saat penggunaan hidrogen peroksida sebesar 9%v/v. Perolehan nikel ini lebih tinggi 3,5 kali dibandingkan dengan tanpa penambahan hidrogen peroksida. Sementara itu, konsentrasi natrium klorida sebesar 0,8 mol/L mampu memberikan perolehan nikel tertinggi sebesar 50,38% atau meningkat sebesar 1,9 kali bila dibandingkan dengan tanpa penambahan natrium klorida.

Kata Kunci: *Leaching, spent catalyst*, hidrogen peroksida, natrium klorida, nikel

Abstract

One of the factors that affect the leaching process of a mineral source is the mineral characteristics of the raw materials. Not all mineral phases can be leached completely and directly. Thus, some minerals require special treatment so that the leaching process can take place optimally. The purpose of this research is to investigate the effect of adding additive compounds, such as hydrogen peroxide and sodium chloride, to the leaching process of spent catalyst using a sulfuric acid solution. The leaching process was carried out at room temperature for 240 minutes with a concentration of 1 M sulfuric acid solution. The highest nickel recovery of 95.08% was obtained when hydrogen peroxide was used at a concentration of 9%v/v. The experimental results showed that the two additive compounds were able to increase nickel recovery significantly. The highest nickel recovery of 95.08% was achieved when hydrogen peroxide was used at 9%v/v. The nickel recovery is 3.5 times higher than without the addition of hydrogen peroxide. Meanwhile, a sodium chloride concentration of 0.8 mol/L was able to provide the highest nickel recovery of 50.38 %, or a 1.9 times increase over the control.

Keywords: *Leaching, spent catalyst, hydrogen peroxide, sodium chloride, nickel*

DOI : http://dx.doi.org/10.14203/metalurgi.v36i2.591

Metalurgi is Sinta 2 Journal (https://sinta.ristekbrin.go.id/journals/detail?id=3708) accredited by Ministry of Research & Technology, Republic Indonesia

1. INTRODUCTION

The hydrometallurgical process, particularly the atmospheric pressure acid leaching (APAL) process, is a common method for metal recovery. The APAL process extracts and dissolves valuable metal ions into solvents from various mineral sources under atmospheric conditions. [1]-[2]. Some advantages of this process include the ability to obtain the product in purer conditions than the pyrometallurgical method, being more economical, requiring less energy, and being environmentally friendly [2]-[4].

In general, the main principle of the APAL process is to react solvent with metal compounds to produce metal ions that are easily soluble in aqueous solutions. During the leaching process, the diffusion step and the chemical reaction step control the rate of the leaching process. To improve the performance of the metal ion leaching process, various fundamental factors such as temperature, particle size, agitation, solvent type, solvent concentration, pulp density, and time are influenced [5]-[7].

However, mineral characteristics, the phase and form of minerals contained in the mineral resources, greatly affect the performance of the leaching process. Not all metal elements or compounds in the raw materials can be dissolved in the solvent directly and completely. In other words, it is needed an extra effort to leach the metal from the raw materials. For example, nickel will be easier to leach if the nickel contained in mineral sources is in Ni(II) ions or nickel-based compounds that can be changed into Ni(II) ions. Nickel metal (Ni°) has properties that are slightly soluble in acids, such as sulfuric acid or hydrochloric acid, and insoluble in water [8]-[9]. Meanwhile, Ni(II) (Ni^{2+}) ions are water-soluble, especially in the form of a nickel-based compounds such as nickel sulfate, nickel chloride, nickel nitrate, or nickel acetate [8]-[9].

The solubility of nickel or nickel-based compounds needs more attention when the leaching process is carried out on raw materials with a large enough nickel-metal (Ni^o) component, like a spent catalyst. Spent catalysts usually still have metal components in the form of pure metal elements. In the spent catalyst Ni/γ-Al_2O_3, the nickel metal (Ni°) is still much in the catalyst [10]. Because pure metal cannot be completely dissolved in an aqueous or acid solution, not all nickel can be leached. Thus, in addition to optimizing the fundamental factors, other efforts are required to maximize the nickel leaching process from this spent catalyst.

This study will focus on efforts to maximize nickel recovery in the leaching process using spent catalysts. The basic idea of this study is to convert the "insoluble" component of nickel-metal (Ni°) into Ni(II) ions. As a result, these Ni(II) ions can react with other anions (from the solvent), such as SO_4^{2-} ions, and form water-soluble salts. This idea is reinforced by observing the Pourbaix diagram of nickel, as shown in Fig. 1.

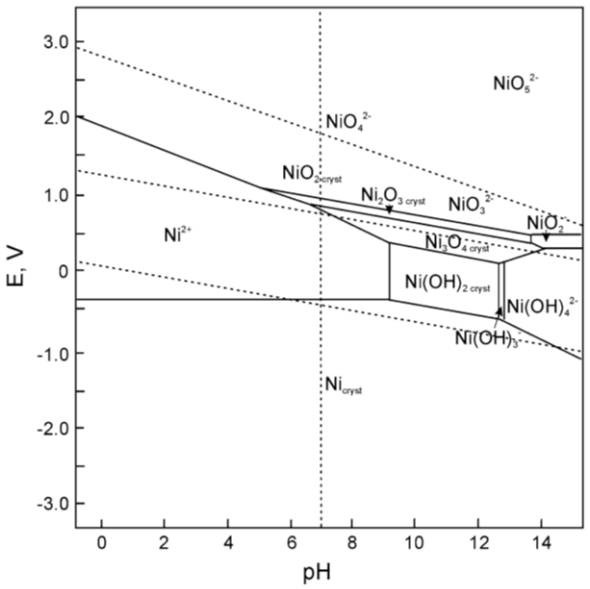

Figure 1. Pourbaix diagram of nickel in water [11]

In that Pourbaix diagram, Ni° (Ni_{cryst}, nickel-metal) is stable at all pH values as long as the voltage potential (E) is below –0.5 V. If the voltage potential (E) is increased, Ni° can be converted into Ni(II) (Ni^{2+}) ions. It is possible to make an effort by adding additive compounds such as hydrogen peroxide (H_2O_2) or sodium chloride (NaCl).

In the metal leaching process, hydrogen peroxide is a compound that can act as an oxidizing or reducing agent [12]. However, in an acidic medium, hydrogen peroxide acts more as an oxidizing agent [12]-[13]. Thus, hydrogen peroxide can oxidize lower valence metal elements/ions to higher valence metal (ions/ compounds). In the case of nickel metal (Ni°) conversion from spent catalyst in sulfuric acid (H_2SO_4) solution, hydrogen peroxide will oxidize Ni° to Ni(II) ions or in the form of nickel oxide (NiO) compounds. This condition is desirable in this study because this oxidation process will produce nickel ions which can be dissolved in aqueous solution directly or indirectly through NiO compounds. Then, the Ni(II) ions will react with another anion (SO_4^{2-}) or the NiO compounds will react with H_2SO_4 to form $NiSO_4$ salt which is easily soluble in water. The reaction mechanism follows the following reaction equation [14]-[15]:

Oxidation reactions

$Ni_{(s)} = Ni^{2+}_{(aq)} + 2e^-$ E = 0,25V (1)

$Ni_{(s)} + H_2O_{2(aq)} = NiO_{(s)} + H_2O_{(l)}$ (2)

Dissolution reactions

$Ni^{2+}_{(aq)} + H_2SO_{4(aq)} = NiSO_{4(aq)} + 2H^+_{(aq)}$ (3)

$NiO_{(s)} + H_2SO_{4(aq)} = NiSO_{4(aq)} + H_2O_{(l)}$ (4)

Overall reaction

$Ni_{(s)} + H_2O_{2(aq)} + H_2SO_{4(aq)} = NiSO_{4(aq)} + 2H_2O_{(l)}$ (5)

In the absence of hydrogen peroxide, Ni° will not be leached into an aqueous solution. Therefore, the use of hydrogen peroxide has excellent potential to increase nickel recovery in the leaching process in an acidic medium [16]-[18].

Another additive that is applied to improve the performance of the leaching process is chloride salts, such as sodium chloride (NaCl). The addition of chloride salts to the sulfate leaching medium is mostly done for the chalcopyrite leaching process [19]. Some chloride-based compounds such as ferric chloride ($FeCl_3$), cupric chloride ($CuCl_2$), sodium chloride (NaCl) are good oxidizing agents [20]. The addition of chloride salts, such as NaCl into the leaching system can increase the complex formed in the solution [4], [20]-[22]. Besides, the NaCl (chloride salts) addition is also expected to increase the voltage potential. Thus, chloride salts may be able to convert elements/compounds in the passive area (pure metal) into ions that are easily soluble in an aqueous solution. This concept will be applied in the nickel leaching process from the spent catalyst. Based on the Pourbaix diagram of nickel in Figure 1, the nickel-metal (Ni^o) phase is in the passive zone which is insoluble in an aqueous solution. The addition of salt in the system is expected to convert Ni° into Ni(II) ions. Sodium chloride compounds also increase the formation of complex compounds so that the nickel recovery process will be better [4], [20]-[22]. In addition, the addition of salt, such as NaCl, into sulfuric acid can increase the electrolyte level of the solution [23]. It is possible that during the extraction process, the value of the voltage potential (E) will also increase so that the possibility that Ni° turns into Ni(II) ions becomes larger (based on Fig. 1).

This study is designed on a spent catalyst leaching process using the sulfuric acid solution at room temperature. The effect of adding additives, such as H_2O_2 and NaCl, on nickel and aluminum recovery is investigated. The leaching process at room temperature requires a very long processing time if the desired metal recovery is high. These low operating conditions have the advantage of lower energy use. As a result, the findings of this study are expected to have a positive impact, allowing metals to be obtained with high recovery and in a short period of time.

2. MATERIALS AND METHODS

2.1 Materials

Spent catalysts used in this study were the catalysts that had been saturated from the reforming process at PT Petrokimia Gresik. A solution of sulfuric acid (H_2SO_4) was used as a solvent at a concentration of 1 M. Other materials such as hydrogen peroxide (H_2O_2) and sodium chloride (NaCl) were also used as additives.

2.2 Procedure

The leaching process took place using a series of equipment, as shown in Fig. 2.

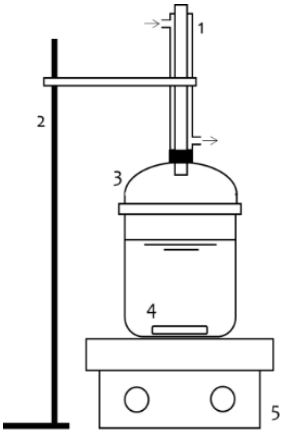

1. Condensor
2. Stand, boss, and clamp
3. Leaching vessel
4. Magnetic stirrer
5. Hotplate

Figure 2. Leaching equipment

After the equipment was assembled, 300 ml of 1 M H_2SO_4 solution was poured into the leaching vessel. A solution of NaCl or H_2O_2 at a certain concentration was mixed with that H_2SO_4 solution. The concentration of H_2O_2 solution was varied in the range of 0-9%v/v while the concentration of NaCl was varied in the range of 0-0.8 mol/L. Then, the temperature of this mixture was adjusted at 30 ^oC and stirred at 200 rpm. After the desired operating conditions are achieved, 60 grams of spent catalyst, with a size of -200 mesh, was entered into the leaching vessel. This step indicated that the leaching had been started and counted as t = 0. A sampling of 10 ml was carried out periodically at 30, 90, and 240 minutes. This sample was first separated between the solid phase and the liquid phase. The liquid phase formed was then analyzed for the content of Ni(II) ions using AAS (atomic absorption spectrometry) and Al(III) ions using a UV–Vis spectrophotometer.

2.3 Data Analysis

The percentage recovery of metal ions was calculated using the following equation.

$$\%\text{Recovery} = \frac{C_t}{C_o} \text{ x } 100\% \quad (6)$$

where C_t is the concentration of dissolved metal (Ni^{2+} or Al^{3+}) ions at t; C_o is the maximum concentration of metal (Ni^{2+} or Al^{3+}) ions in spent catalysts.

3. RESULTS AND DISCUSSIONS

3.1 The Characteristics of Spent Catalyst

As the raw material, the spent catalysts used in this study were characterized first. The material characterization carried out consisted of the constituent composition and the mineral phase contained in the catalyst. The composition of the catalyst is known by analyzing the sample using XRF (x-ray fluorescence). The analysis result is presented in Table 1.

Table 1. The composition of raw materials

Element	Composition (wt.%)
Al	38.22
Ni	37.66
Ca	22.61
P	0.44
Fe	0.43
K	0.23
Si	0.22

Table 1 shows that the constituent elements of this spent catalyst are dominated by aluminum (Al) and nickel (Ni). These analysis results are in line with the analysis results for the mineral phase contained in the catalysts. The mineral phase was analyzed using XRD (x-ray diffraction) and the analysis results are presented in Fig. 3.

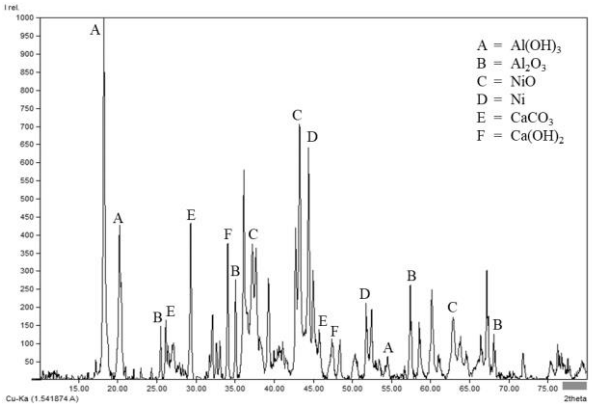

Figure 3. XRD pattern for raw materials

The analysis result using XRD in Fig. 3 shows that the catalyst used comprises a mineral phase $Al(OH)_3$, Al_2O_3, NiO, Ni, $CaCO_3$, dan $Ca(OH)_2$.

For the nickel leaching process, two nickel phases can be utilized, i.e. NiO and Ni° (nickel-metal) phases. It is easy to obtain nickel from the NiO phase because the reaction between NiO and the solvent (H_2SO_4) can be carried out directly by following the reaction equation (4). However, for the leaching process from the Ni° phase, nickel can not be leached directly. In Fig. 3, nickel-metal (Ni°) has a reasonably high intensity, especially at 44.3° and 51.8°. Nickel under this phase will be the focus of this study. Ni° is expected to be reduced from the spent catalyst by leaching with the addition of H_2O_2 or NaCl. The addition of both additives can oxidize Ni° to become Ni(II) ions and then, those ions dissolve in an aqueous solution.

3.2 The Effect of Hydrogen Peroxide (H_2O_2) Addition on the Leaching Process of Spent Catalyst

In this section, the parameter studied is the concentration of hydrogen peroxide compounds. The variations used for this parameter are 0; 1.5; and 9%v/v. The experimental results are presented in Fig. 4.

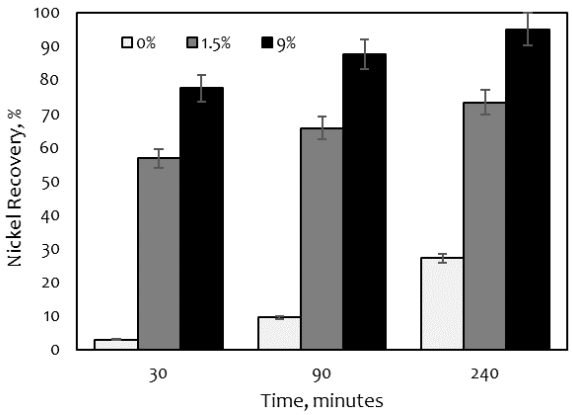

Figure 4. The effect of hydrogen peroxide addition on nickel recovery

A certain concentration of hydrogen peroxide added to the system has a significant effect on the nickel recovery process. The experimental results in Fig. 4 demonstrate this. This is evidenced by the experimental results in Fig. 4. According to the experimental results, the higher the hydrogen peroxide concentration, the higher the nickel recovered.

Based on Fig. 4, the highest nickel percentage was achieved at 95.08% using hydrogen peroxide at 9%v/v and a leaching time of 240 minutes. The results obtained are reasonable and in line with the existing theory. Long operating duration increases the probability of a molecule interacting with the others. This condition will optimize the leaching process

mechanism and can recover more nickel. However, when the leaching time was 30 minutes, the use of hydrogen peroxide increased significantly when compared to the difference in nickel recovery. When compared to the percentage of nickel recovery without the addition of hydrogen peroxide, the addition of hydrogen peroxide at 30 minutes can increase nickel recovery by 19.5 times for a concentration of 1.5 %v/v and 26.6 times for a concentration of 9 %v/v.

The results of this experiment indicate that using hydrogen peroxide in the nickel leaching process is an intriguing and promising endeavor. This process was carried out at room temperature, where this operating condition is classified as low temperature. In general, leaching at low temperatures results in a low percentage of recovery, or it takes a very long time if a high percentage of recovery is desired. The experiments conducted in this study, on the other hand, demonstrated that hydrogen peroxide was capable of providing high recovery in a relatively short time and at low temperatures.

As explained in the introduction section, hydrogen peroxide acts as an oxidizing agent and will oxidize Ni° (insoluble) to Ni(II) ions (soluble). This phenomenon causes the percentage of nickel recovery will increase after the addition of hydrogen peroxide. Fig. 5 shows that the intensity of the Ni phase decreases significantly when the residue sample is treated with hydrogen peroxide. This is visible at 44.3°. The results of this XRD analysis support the findings of previous studies, demonstrating that the leaching process with the addition of H_2O_2 has been successfully optimized because Ni° has been converted into Ni(II) ions and dissolves in acid. As a result, the nickel recovery percentage increased very significantly.

Unlike the nickel leaching process, the addition of hydrogen peroxide in this study does not provide a significant difference to the aluminum recovery process. This can be seen in Fig. 6. The leaching process at all concentrations of hydrogen peroxide only gave an average percentage of aluminum recovery of 42.5±4%. When it views from the mineral phase present in the spent catalyst (Fig. 3), aluminum is not in a pure metal phase but the Al_2O_3 and $Al(OH)_3$ phases which can directly react with sulfuric acid, then form Al(III) ions. These Al(III) ions will dissolve in an acidic medium and form $Al_2(SO_4)_3$ salt. The reaction equations that occur are [24]-[25]:

$$Al_2O_{3(s)} + 3H_2SO_{4(aq)} = Al_2(SO_4)_{3(aq)} + 3H_2O_{(l)} \quad (7)$$

$$Al(OH)_{3(s)} + 3H_2SO_{4(aq)} = Al_2(SO_4)_{3(aq)} + 3H_2O_{(l)} \quad (8)$$

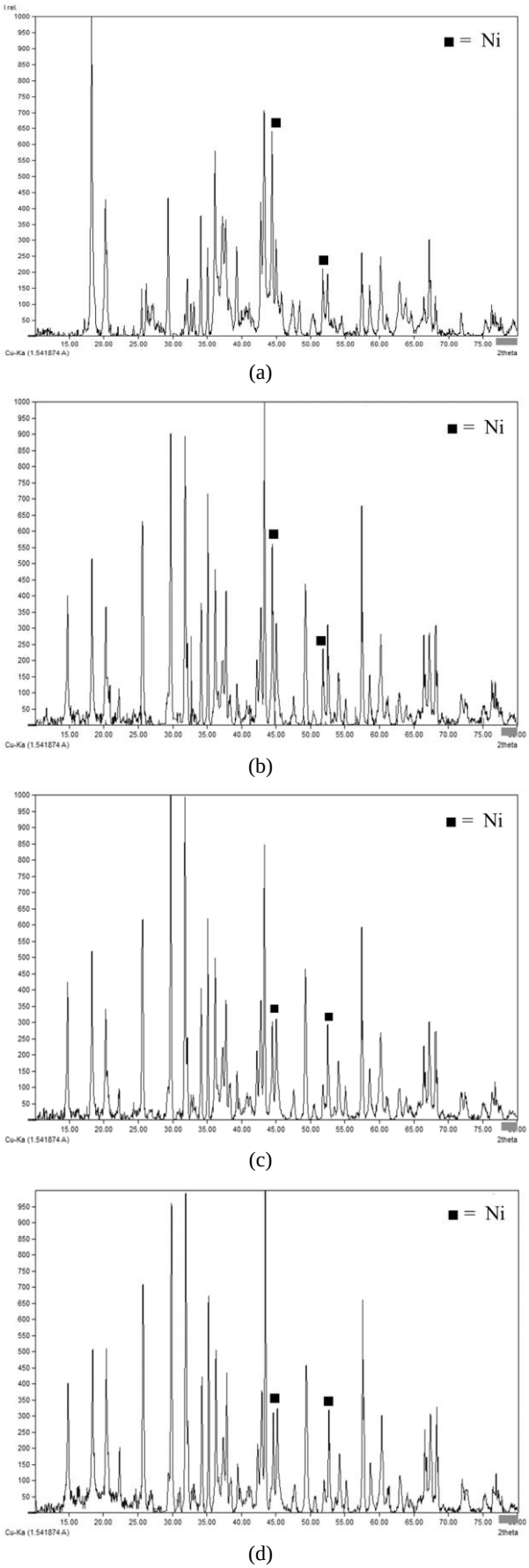

Figure 5. XRD pattern (a) raw materials and residue from leaching process (b) without the addition of H_2O_2, (c) with the addition H_2O_2 by 1.5%v/v, and (d) 9%v/v

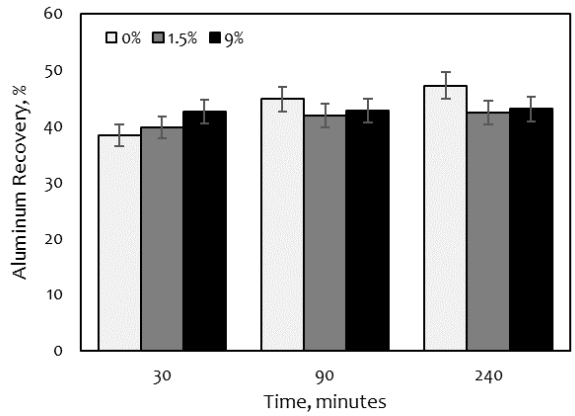

Figure 6. The effect of hydrogen peroxide addition on aluminum recovery

In other words, for the leaching process of this spent catalyst, the use of hydrogen peroxide has more effect on the nickel recovery.

3.3 The Effect of Sodium Chloride (NaCl) Addition on the Leaching Process of Spent Catalyst

Another parameter studied in this study is the addition of salt, i.e. sodium chloride (NaCl) during the leaching process. The salt concentration was varied at 0, 0.1, and 0.8 mol/L. For this study, there is no addition of hydrogen peroxide into the system. The effect of this variation can be observed from the percentage of nickel recovery, as shown in Fig. 7.

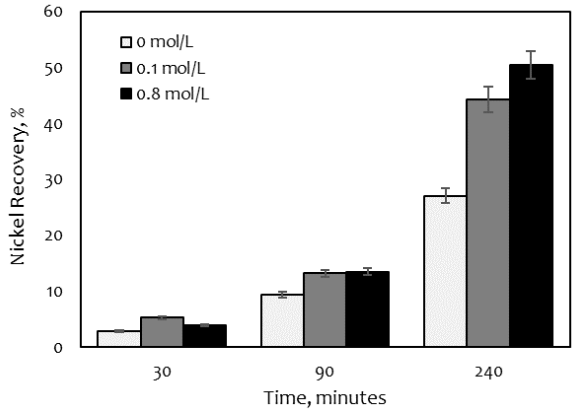

Figure 7. The effect of sodium chloride addition on nickel recovery

Figure 7 shows that the addition of sodium chloride during the leaching process has a positive impact on nickel recovery as the leaching process takes longer. This condition is very obvious, especially at the 240 minutes leaching time. For 240 minutes, sodium chloride was able to increase the percentage of nickel recovery from 27.07% to 44.25% (for the addition of 0.1 mol/L NaCl) and 50.38% (for the addition of 0.8 mol/L NaCl). The phenomenon resulting from this study is a promising effort to maximize the nickel leaching process. The effect of sodium chloride as an additive is not as significant as hydrogen peroxide. However, the addition of sodium chloride was able to increase nickel recovery by about two times even though the leaching process was carried out at a low temperature, 30 °C where the leaching rate at this temperature was prolonged.

The use of sodium chloride can convert the nickel phase from Ni° to Ni(II) ions because theoretically, there is an increase in the voltage potential value. This result is further proven from the results of analyzing the mineral phase of the residue from the leaching process. The results of the analysis are presented in Fig. 8. Based on Fig. 8, the nickel-metal (Ni°) phase decreased significantly after the addition of sodium chloride. This can be observed from the XRD pattern and peak intensity of the Ni° phase, especially at 44.3° and 51.8°. The decrease in peak intensity and increase in nickel recovery further strengthens the study results where the addition of sodium chloride can increase the rate of nickel leaching process from spent catalyst.

Furthermore, when Fig. 7 is compared to Fig. 4, there is a difference in the tendency of the addition of hydrogen peroxide and sodium chloride. A comparison of the two figures shows that the addition of sodium chloride is not as aggressive as hydrogen peroxide. Increasing the time of 30 and 90 minutes in sodium chloride did not result in a significant increase in nickel recovery. This is in contrast to the addition of hydrogen peroxide, where the difference in time significantly increases nickel recovery. This phenomenon indicates that the oxidation process of Ni° to Ni(II) ions will be more spontaneous when hydrogen peroxide is added.

An analysis of aluminum recovery was also performed for this parameter, and the results are shown in Fig. 9. In general, no significant changes occurred in aluminum recovery. This condition is similar to the study of the addition of hydrogen peroxide. However, Fig. 9 has a consistent trend in each leaching time. The addition of 0.1 mol/L sodium chloride gives slightly better leaching results. In this condition, the recovered aluminum is in the range of 45.66-48.68%. This study shows that, like hydrogen peroxide, the addition of sodium chloride has an effect on the nickel leaching process when compared to aluminum.

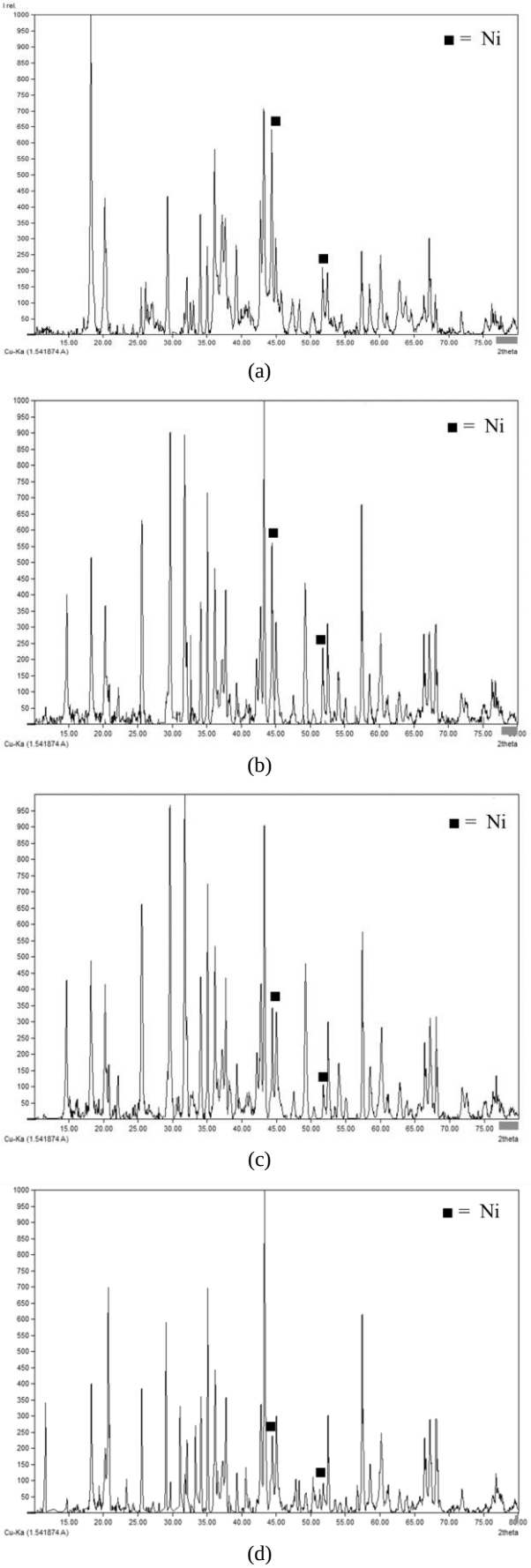

Figure 8. XRD pattern (a) raw materials and residue from leaching process (b) without the addition of NaCl, (c) with the addition NaCl by 0.1 mol/L, and (d) 0.8 mol/L

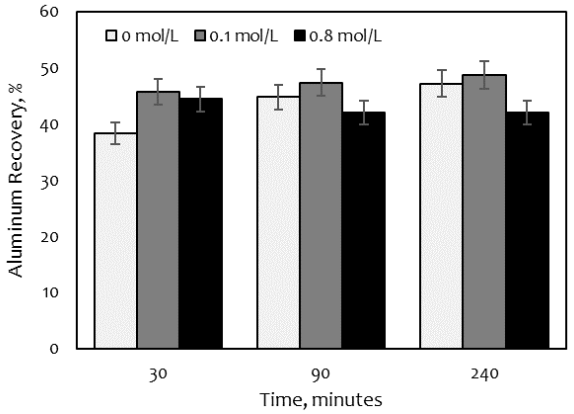

Figure 9. The effect of sodium chloride addition on aluminum recovery

Overall, the results of this experiment are supported by the results obtained from several previous studies [16]-[18], [20]-[22]. Those studies confirmed that hydrogen peroxide and sodium chloride are the good additive agent for the metal recovery, especially nickel in the low temperature extraction process. Both additives have a positive effect to leaching process becaust the nickel metal (Ni^o) phase contained in the spent catalysts can be extrated into the acid solution.

4. CONCLUSIONS

The addition of additives such as hydrogen peroxide and sodium chloride has a positive effect on the nickel leaching process from the spent catalyst. These two additive compounds are capable of converting nickel metal (Ni°) into Ni(II) ions which are easily soluble in an aqueous solution. As a result, the use of these additive compounds can increase nickel recovery. In general, the higher the concentration of additive compounds, the higher the nickel recovery. In this study, the use of hydrogen peroxide concentration of 9%v/v was able to leach nickel by 95.08% or an increase of 3.5 times when compared to without the addition of hydrogen peroxide. Meanwhile, the use of sodium chloride of 0.8 mol/L was able to leach nickel by 50.38% or an increase of 1.9 times. However, the use of these two additive compounds did not tend to affect the aluminum recovery.

ACKNOWLEDGEMENT

The author would like to express gratitude to PT. Petrokimia Gresik and LIPI's Science Services for Research Laboratorium for their assistance.

REFERENCES

[1] K. C. Wanta, W. Astuti, I. Perdana, and H. T. B. M. Petrus, "Kinetic study in

atmospheric pressure organic acid leaching: Shrinking core model versus lump model," *Minerals*, vol. 10, no. 7, pp. 1-10, 2020. Doi: 10.3390/min10070613

[2] K. Korkmaz, "Comparative study of high pressure and atmospheric acid leaching for the extraction of nickel and cobalt from refractory nickel laterite ores," Middle East Technical University, Ankara, Turkey, Thesis, May, 2014.

[3] K. C. Wanta, F. H. Tanujaya, R. F. Susanti, H. T. B. M. Petrus, I. Perdana, and W. Astuti, "Studi kinetika proses atmospheric pressure acid leaching bijih laterit limonit menggunakan larutan asam nitrat konsentrasi rendah," *J. Rekayasa Proses*, vol. 12, no. 2, p. 19, 2018. Doi: 10.22146/jrekpros.35644

[4] R. G. McDonald and B. I. Whittington, "Atmospheric acid leaching of nickel laterites review. Part I. Sulphuric acid technologies," *Hydrometallurgy*, vol. 91, no. 1-4, pp. 35-55, 2008. Doi: 10.1016/j.hydromet.2007.11.009

[5] W. Astuti, T. Hirajima, K. Sasaki, and N. Okibe, "Comparison of effectiveness of citric acid and other acids in leaching of low-grade Indonesian saprolitic ores," *Miner. Eng.*, vol. 85, pp. 1-16, 2016. Doi: 10.1016/j.mineng.2015.10.001

[6] X. Fan, W. Xing, H. Dong, J. Zhao, Y. Wu, B. Li, W. Tong, X. Wu "Factors research on the influence of leaching rate of nickel and cobalt from waste superalloys with sulfuric acid," *Int. J. Nonferrous Metall.*, vol. 02, no. 02, pp. 63-67, 2013. Doi: 0.4236/ijnm.2013. 22008

[7] H. B. T. M. Petrus, K. C. Wanta, H. Setiawan, I. Perdana, and W. Astuti, "Effect of pulp density and particle size on indirect bioleaching of Pomalaa nickel laterite using metabolic citric acid," *IOP Conf. Ser. Mater. Sci. Eng.*, vol. 285, no. 1, 2018. Doi: 10.1088/1757-899X/285/1/ 012004

[8] IARC Working Group, "Nickel and nickel compounds", in *IARC Monographs on the Evaluation of Carcinogenic Risks to Humans*, vol. 49, Lyon, France: International Agency for Research on Cancer, WHO, pp. 263–266, 1990.

[9] E. Nielsen, P. B. Larsen, *Nickel, inorganic and soluble salts. Evaluation of health hazards and proposal of a health based quality criterion for drinking water.* Copenhagen, Denmark: The Danish Environmental Protection Agency, 2013.

[10] K. C. Wanta, F. D. Putra, R. F. Susanti, G. P. Gemilar, W. Astuti, S. Virdhian, and H. T. B. M. Petrus, "Pengaruh derajat keasaman (pH) dalam proses presipitasi hidroksida selektif ion logam dari larutan ekstrak spent catalyst," *J. Rekayasa Proses*, vol. 13, no. 2, p. 94, 2019. Doi: 10.22146/jrekpros.44007

[11] F. Ciesielczyk, P. Bartczak, K. Wieszczycka, K. Siwińska-Stefańska, M. Nowacka, and T. Jesionowski, "Adsorption of Ni(II) from model solutions using co-precipitated inorganic oxides," *Adsorption*, vol. 19, no. 2-4, pp. 423-434, 2013. Doi: 10.1007/s10450-012-9464-5

[12] A. O. Adebayo, K. O. Ipinmoroti, and O. O. Ajayi, "Dissolution of chalcopyrite with hydrogen peroxide in sulphuric acid," *Pak. J. Sci. Ind. Res.*, vol. 49, no. 2, pp. 65-71, 2006.

[13] A. Szymczycha-Madeja, "Kinetics of Mo, Ni, V and Al leaching from a spent hydrodesulphurization catalyst in a solution containing oxalic acid and hydrogen peroxide," *J. Hazard. Mater.*, vol. 186, no. 2-3, pp. 2157-2161, 2011. Doi: 10.1016/j.jhazmat.2010.11.120

[14] H. Li, S. Li, J. Peng, C. Srinivasakannan, L. Zhang, and S. Yin, "Ultrasound augmented leaching of nickel sulfate in sulfuric acid and hydrogen peroxide media," *Ultrason. Sonochem.*, vol. 40, pp. 1021-1030, 2018. Doi: 10.1016/j.ultsonch.2017.08.031

[15] M. A. Rabah, F. E. Farghaly, and M. A. Abd-El Motaleb, "Recovery of nickel, cobalt and some salts from spent Ni-MH batteries," *Waste Manag.*, vol. 28, no. 7, pp. 1159-1167, 2008. Doi: 10.1016/j.wasman.2007.06.007

[16] M. A. Rabah, "Recovery of aluminium, nickel-copper alloys and salts from spent fluorescent lamps," *Waste Manag.*, vol. 24, no. 2, pp. 119-126, 2004. Doi: 10.1016/j.wasman.2003.07.001

[17] N. S. Randhawa, K. Gharami, and M. Kumar, "Leaching kinetics of spent nickel–cadmium battery in sulphuric acid," *Hydrometallurgy*, vol. 165, pp. 191-198, 2016. Doi: 10.1016/j.hydromet.2015.09. 011

[18] E. Rudnik and M. Nikiel, "Hydrometallurgical recovery of cadmium and nickel from spent Ni-Cd batteries," *Hydrometallurgy*, vol. 89, no.

1-2, pp. 61-71, 2007. Doi: 10.1016/j.hydromet.2007.05.006
[19] M. F. C. Carneiro and V. A. Leão, "The role of sodium chloride on surface properties of chalcopyrite leached with ferric sulphate," *Hydrometallurgy*, vol. 87, no. 3-4, pp. 73-82, 2007. Doi: 10.1016/j.hydromet.2007.01.005
[20] K. H. Park, D. Mohapatra, K. Hong-In, and G. Xueyi, "Dissolution behavior of a complex Cu-Ni-Co-Fe matte in $CuCl_2$-NaCl-HCl leaching medium," *Sep. Purif. Technol.*, vol. 56, no. 3, pp. 303-310, 2007. Doi: 10.1016/j.seppur.2007.02.013
[21] M. Skrobian, T. Havlik, and M. Ukasik, "Effect of NaCl concentration and particle size on chalcopyrite leaching in cupric chloride solution," *Hydrometallurgy*, vol. 77, no. 1-2, pp. 109-114, 2005. Doi: 10.1016/j.hydromet.2004.10.015
[22] R. Winand, "Chloride hydrometallurgy," *Hydrometallurgy*, vol. 27, pp. 285-316, 1991. Doi: 10.1016/0304-386X(91) 90055-Q
[23] M. Mungkin, "Studi pengaruh bahan aditif NaCl dan Na-EDTA pada elektrolit baterai berbahan filtrasi air jeruk nipis," vol. 3, no. 1, pp. 2-7, 2018.
[24] L. S. Li, Y. S. Wu, Y. Y. Liu, and Y. C. Zhai, "Extraction of alumina from coal fly ash with sulfuric acid leaching method," *Guocheng Gongcheng Xuebao/The Chinese J. Process Eng.*, vol. 11, no. 2, pp. 254-258, 2011.
[25] A. Zhao, T. A. Zhang, G. Lv, and W. Tian, "Kinetics of the leaching process of an australian gibbsitic bauxite by hydrochloric acid," *Adv. Mater. Sci. Eng.*, vol. 2016, pp. 1-7, 2016. Doi: 10.1155/2016/5813542

Metalurgi (2021) 2: 87 - 92

LIPI

METALURGI
Majalah Ilmu dan Teknologi
p-ISSN 0126-3188 | e-ISSN 2443-3926
www.ejurnalmaterialmetalurgi.com

THE EFFECT OF VARIATIONS IN ELECTROLYTE TEMPERATURE AND CURRENT ON THE SYNTHESIS OF MANGANESE DIOXIDE FROM MANGANESE SULFATE PRECURSORS BY ELECTROLYSIS METHOD

Rizta Febian Adi Endani[a,*], Lia Andriyah[b], Soesaptri Oediyani[a], Latifa Hanum Lalasari[b], Tri Arini[b], Nadia Chrisayu Natasha[b], Fariza Eka Yunita[b], Ariyo Suharyanto[b]

[a]Metallurgical Engineering, Sultan Ageng Tirtayasa University
Jalan Jendral Sudirman Km.3, Cilegon, Indonesia 42434
[b] Research Center for Metallurgy and Materials
Building 470, PUSPIPTEK Serpong Area, South Tangerang, Indonesia 15343
*E-mail: febianrizta@gmail.com

Masuk tanggal : 28-07-2021, revisi tanggal : 02-09-2021, diterima untuk diterbitkan tanggal 09-09-2021

Abstrak

Perkembangan ilmu dan teknologi dewasa ini dalam bidang elektronik, khususnya penyimpanan energi meningkatkan permintaan dalam penggunaan baterai sekunder litium. Pengembangan baterai litium difokuskan pada kapasitas penyimpanan energi dengan menggunakan mangan dioksida (MnO_2) sebagai bahan katoda baterai litium. Mangan dioksida dipilih sebagai bahan katoda baterai litium karena memiliki kapasitas penyimpanan yang tinggi yaitu sekitar 615 mAh/g dibandingkan dengan material lain seperti grafit yang memiliki kapasitas penyimpanan 372 mAh/g. Sintesis MnO_2 dilakukan dengan metode elektrolisis dari prekursor mangan sulfat ($MnSO_4$) yang diperoleh dari proses pelindian bijih mangan Kabupaten Trenggalek. Proses elektrolisis dilakukan selama 5 jam dengan menggunakan variasi temperatur elektrolit 30, 40, 50 dan 60ºC serta variasi arus 2, 3, 4 dan 5 A untuk mengetahui pengaruh temperatur elektrolit dan arus terhadap perolehan massa, polimorfi struktur dan morfologi MnO_2 yang terbentuk. Perolehan massa tertinggi diperoleh pada penggunaan temperatur elektrolit 60 ºC dan arus 5 A yaitu sebesar 11,4 gram. Hasil karakterisasi MnO_2 dengan menggunakan XRF (*x-ray fluorescence*) *Thermo type* ARL 9900 menunjukkan kadar mangan dioksida sebesar 85,472% dan hasil analisa dengan menggunakan XRD (*x-ray diffraction*) Shimadzu *type* 7000 diperoleh polimorfi struktur senyawa MnO_2 yang terbentuk adalah polimorfi α-MnO_2. Citra SEM (*scanning electron microscope*) menunjukkan bahwa partikel MnO_2 memiliki bentuk bulat berduri dan cenderung beraglomerasi dengan nilai diameter partikel berkisar antara 50-70 nm.

Kata Kunci: Elektrolisis, MnO_2, $MnSO_4$, temperatur elektrolit, arus

Abstract

The advancement of science and technology in the field of electronics, particularly in the field of energy storage, is increasing the demand for the use of lithium secondary batteries. The use of manganese dioxide (MnO_2) as a lithium battery cathode material is focusing the development of lithium batteries on energy storage capacity. Manganese dioxide was chosen as the cathode material for lithium batteries because it has a high storage capacity of about 615 mAh/g compared to other materials such as graphite which has a storage capacity of 372 mAh/g. MnO_2 was synthesized by the electrolysis method from manganese sulfate ($MnSO_4$) precursor which was obtained from the Trenggalek manganese ore leaching process. The electrolysis process was carried out for 5 hours using variations in electrolyte temperature of 30, 40, 50, and 60 ºC as well as variations in a current of 2, 3, 4, and 5 A to determine the effect of electrolyte temperature and current on mass gain, structural polymorphy, and morphology of MnO_2 formed. The highest mass gain was obtained at the use of an electrolyte temperature of 60 ºC and a current of 5 A, which was 11.4 grams. The characterization of MnO_2 using XRF (x-ray fluorescence) Thermo type ARL 9900 revealed manganese dioxide levels of 85.472%, and the analysis using XRD (x-ray diffraction) Shimadzu type 7000 revealed that the polymorphy structure of the MnO_2 compound formed was α-MnO_2 polymorphy. The MnO_2 particles have a spiny round shape and tend to agglomerate, as shown by the SEM (scanning electron microscope) image, with particle diameter values ranging from 50 to 170 nm.

Keywords: *Electrolysis, MnO_2, $MnSO_4$, electrolyte temperature, current*

DOI : http://dx.doi.org/10.14203/metalurgi.v36i2.594

Metalurgi is Sinta 2 Journal (https://sinta.ristekbrin.go.id/journals/detail?id=3708) accredited by Ministry of Research & Technology, Republic Indonesia

1. INTRODUCTION

Batteries have been the most widely developed electrical energy storage technology as science and technology have progressed, particularly in the field of electronics in energy storage. Lithium battery is a secondary battery that is widely developed today. Lithium batteries have advantages including high storage capacity, no memory effect, and can be recharged [1]. The development of lithium batteries is focused on increasing battery storage capacity and battery charging speed. One of the materials that are widely used as a lithium battery cathode is manganese dioxide (MnO_2). Based on data from the Geological Agency, Ministry of Energy and Mineral Resources, it is stated that manganese resources in Indonesia are about 60,893,820 tons and total manganese reserves are 87,236,536 tons [2]. With the manganese potential in Indonesia, the processing and utilization of manganese ore can be distinguished based on the manganese content in the ore. Manganese ore processing based on grade can be divided into two, pyrometallurgical and hydrometallurgical. Manganese ore with levels above 45% or commonly referred to as metallurgical grade is processed pyrometallurgical into ferromanganese metal as a ferroalloy for the manufacture of iron and steel. Meanwhile, manganese ores with levels below 45% are hydrometallurgically treated and used for the production of non-metallurgical grades which are suitable for use in the dry battery industry as battery electrodes [3].

Manganese dioxide was chosen as the cathode material for lithium batteries because it has a high storage capacity of about 615 mAh/g [4]. Manganese dioxide is an oxide of manganese that can be crystalline or amorphous. The crystalline structure has a polymorphic crystal structure, such as β-MnO_2, α-MnO_2, γ-MnO_2 or δ-MnO_2. The polymorphic structure of MnO_2 can possess a widely varying structural composition, and hence electrochemical activity [5]. Each of these crystalline structures has a tunnel structure with different sizes. β-MnO_2 (pyrolusite), α-MnO_2 (ramsdellite), γ-MnO_2 (nsutite) and δ-MnO_2 (vernadite) have tunnel structures (1x1), (2x2), (1x1)(1x2), and (1x∞) successively [6]. Among the various polymorphies of MnO_2, such as β-MnO_2, α-MnO_2, δ- MnO_2, and γ-MnO_2, the polymorphic structure α-MnO_2 is much more active both chemically and electrochemically [7]. The polymorphic structure α-MnO_2 is the most suitable for battery applications and can be made chemically and electrochemically [8].

2. MATERIALS AND METHODS

2 liters of $MnSO_4$ were filtered for impurities before being poured into a 2000 ml beaker. 5 ml of $MnSO_4$ solution was taken and diluted up to 100 times in a volumetric flask before being analyzed for elemental content using ICP-OES (inductively coupled plasma-optical emission spectrometry). The anode was then wrapped in a screen mesh cloth and two graphite electrodes (16 x 5 x 0.3 cm^3) were prepared. $MnSO_4$ solution was electrolyzed for 5 hours with electrolyte temperature variations of 30, 40, 50, and 60 °C and current variations of 2, 3, 4, and 5 A.

The MnO_2 obtained was then dried in an oven for 2 hours and at a temperature of 110 °C. Furthermore, the MnO_2 formed was weighed using a digital balance and analyzed using XRF (x-ray fluorescence) Thermo type ARL 9900 to determine the levels of compounds contained in the MnO_2 sample. XRD (x-ray diffraction) Shimadzu type 7000 analysis was also carried out to determine the polymorphy formed and SEM analysis to determine the polymorphy of MnO_2 formed.

Manganese ore is obtained from Trenggalek. At first, manganese ore was analyzed using XRF to determine the elements contained in the ore, and the results of XRF testing are shown in Table 1. Manganese ore was then leached using the sulfuric acid solution at a stirring speed of 400 rpm, the acid concentration of 12% H_2SO_4, temperature 75 °C for 180 minutes to produce $MnSO_4$ precursor solution which will be used as raw material for MnO_2 synthesis.

Table 1. XRF analysis of manganese ore from Trenggalek[9]

Oxide Compounds	Wt.%
MnO_2	46.03
SiO_2	48.73
Fe_2O_3	3.77
CaO	1.10
BaO	0.46
MgO	0.00
P_2O_5	0.56

3. RESULTS AND DISCUSSIONS

ICP-OES (inductively coupled plasma-optical emission spectrometry) was used to determine the manganese content of the $MnSO_4$ precursor solution during the initial characterization. Table 2 shows the results of the ICP-OES analysis of the $MnSO_4$ solution, which shows that the manganese content in the precursor is around 387.185 ppm.

Table 2. ICP-OES analysis for $MnSO_4$ solution

Element	ppm
Aluminum (Al)	0.505078
Gold (Au)	0.012406
Boron (B)	0.085176
Calcium (Ca)	4.18425
Iron (Fe)	0.194278
Potassium (K)	0.324122
Lithium (Li)	0.0204
Magnesium (Mg)	1.05311
Manganese (Mn)	387.185
Sodium (Na)	0.964326

3.1 Electrolysis Process

Electrolysis is a decomposition reaction in an electrolyte by an electric current. When an electric current is passed through an electrolyte solution in an electrolytic cell, a chemical reaction occurs. [10].

The color change that occurs in the $MnSO_4$ precursor during the electrolysis process is directly visible. The solution was pink before the electrolysis process was carried out, as shown in Fig.1(a), and after the electrolysis process was completed for 5 hours, the solution changed color to dark brown, as shown in Fig.1(b), where a very significant change in the color of the solution was obtained at an electrolyte temperature of 60 °C and a current of 5 A.

(a)

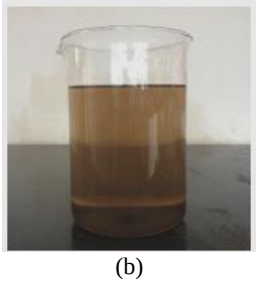

(b)

Figure 1. (a) Precursor solution before electrolysis process; (b) Precursor solution after electrolysis process

The $MnSO_4$ solution will decompose into Mn^{2+} and SO_4^{2-} ions during the electrolysis process. Mn^{2+} ions will flow to the anode, causing the reaction described in Eq. (1) to occur [11].

$$Mn^{2+} + 2H_2O \rightleftharpoons MnO_2 + 4H^+ + 2e^-$$
$$MnO_2 + Mn^{2+} + 2H_2O \rightleftharpoons 2MnOOH + 2H^+$$
$$MnOOH \rightleftharpoons MnO_2 + H^+ + e^- \quad (1)$$

Eq. 2 depicts the reaction that occurs at the cathode.

$$2H^+ + 2e^- \rightleftharpoons H_2 \quad (2)$$

While Eq. 3 shows the total electrolysis reaction,

$$MnSO_4 + 2H_2O \rightleftharpoons MnO_2 + H_2SO_4 + H_2 \quad (3)$$

3.2 Electrolysis with Temperature Variation of the Electrolyte

The electrolysis procedure was carried out with electrolyte temperatures ranging from 30 to 40, 50, and 60 °C. According to the findings of the study, the lowest mass gain of MnO_2 was obtained at 30 °C, which was 2.98 grams, and the highest mass gain of MnO_2 was obtained at 60 °C, which was 11.4 grams.

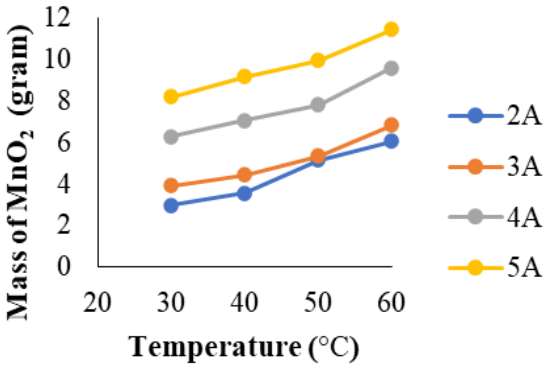

Figure 2. Effect of electrolyte temperature variations on mass gain of MnO_2

The greater the mass of MnO_2 obtained, the higher the temperature of the electrolyte used. Because the mass gain of MnO_2 obtained was greater and the electrolyte temperature tended to be more constant at 60 °C, the optimum condition of the electrolysis process was achieved.

3.3 Electrolysis with Current Variation

The current variations used were 2, 3, 4, and 5 A. According to the findings of the study, the lowest mass gain of MnO_2 was obtained at 2 A current, which was 2.98 grams, and the highest MnO_2 mass was obtained at 5 A current, which was 11.4 grams.

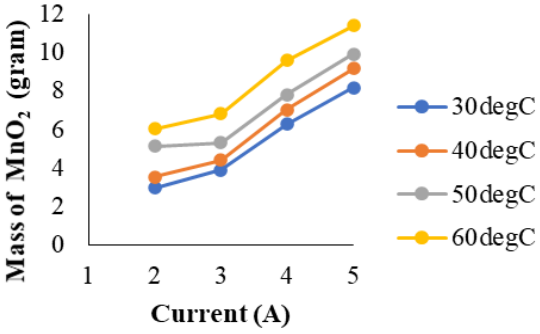

Figure 3. Effect of current variation on mass gain MnO_2

The reaction rate of the electrolysis process can be affected by current. The higher the current user, the more MnO_2 is formed.

3.4 MnO_2 XRF Analysis

The levels of MnO_2 formed after the electrolysis process were determined using XRF (x-ray fluorescence) analysis. Table 3 shows the XRF characterization results, which show MnO_2 levels of 85.472 wt.%.

Table 3. XRF analysis for MnO_2

Compound	Wt.%
K_2O	0.066
MoO_3	0.019
TiO_2	0.044
MnO_2	85.472
Fe_2O_3	2.128
SiO_2	8.377
V_2O_5	0.05
P_2O_5	0
CaO	0.084
Cr_2O_3	0.174
NiO	0
SO_3	3.574
Cl	0
Sc_2O_3	0.009

The increase in MnO_2 levels after the electrolysis process was initially 46.03 wt.% and increased to 85.472 wt.%. This indicates that the electrolysis process used can increase the levels of MnO_2 formed. The higher purity of MnO_2 obtained will improve MnO_2's electrical performance as a lithium battery cathode even more.

3.5 XRD Analysis on MnO_2

The polymorphy of the crystal structure formed in MnO_2 compounds was also determined using XRD (x-ray diffraction). XRD analysis was performed on three samples, the lowest current of 2 A at a temperature of 60 °C, the highest current of 5 A at a temperature of 30 °C, and the highest current of 5 A at a temperature of 60 °C. Using the OriginPro 2021 software, the polymorphs in MnO_2 compounds were identified by comparing the results of the sample x-ray diffraction test with data from the ICDD (international center for diffraction data) standard. Figure 4 shows comparative images of x-ray diffraction for each currency. The comparison image of the experimental MnO_2 sample's x-ray diffraction pattern has similarities with the X-ray diffraction pattern based on ICDD standard No. 00-044-0141, which is a diffraction pattern of α-MnO_2 polymorphy with a tetragonal crystal system. The XRD test was performed with an angle of 2θ between 15° and 90°. Typical peaks of α-MnO_2 were found at 2θ (°) = 26, 29, 37, 42, and 56 in sample 2A; 60 °C, and impurity peaks were found at 2θ (°) = 24, 27, 32, and 55. Typical peaks of α-MnO_2 were found at 2θ (°) = 18, 26, 29, 36, 37, 46, 47, 49, 52, 56, 57, 60, and 73 in sample 5 A; 30 °C, with impurity peaks found at 2θ (°) = 16, 25, 27, 28, 35, 43, and 55. Typical peaks of α-MnO_2 were found at 2θ (°) = 18, 26, 29, 37, 42, 50, and 57 in sample 5A; 60 °C, and impurity peaks were found at 2θ (°) = 27, 35, 38, and 55.

The sample contains approximately 82.7% α-MnO_2 compounds and 17.3% graphite, according to XRD analysis. The presence of other compounds in the MnO_2 sample caused the formation of this impurity peak, with graphite containing the most impurity.

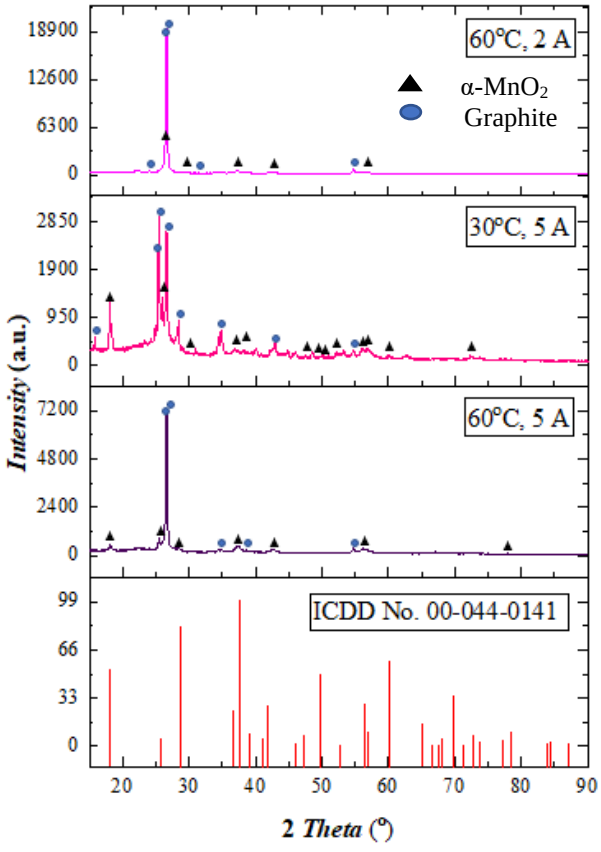

Figure 4. X-ray diffraction pattern for electrolyzed MnO_2 based on ICDD No. 00-044-0141

The brittle nature of the graphite electrode can cause graphite impurities because graphite is easily eroded and mixed with MnO_2. Based on the three XRD images obtained, it is possible to conclude that MnO_2 compounds with α-MnO_2 structural polymorphy are obtained at each temperature and current used. Polymorphy with a

α-MnO_2 structure is best suited for use as a battery cathode material [12]. Because it has a crystal structure large enough to accommodate and decompose oxygen molecules, the structure of α-MnO_2 has the best electrocatalytic ability [6].

3.6 SEM Analysis on MnO_2

SEM (scanning electron microscope) analysis was also performed to determine the morphology of the MnO_2 formed. At a temperature of 60 °C and a current of 5 A, SEM analysis was performed on the sample with the highest mass gain of MnO_2.

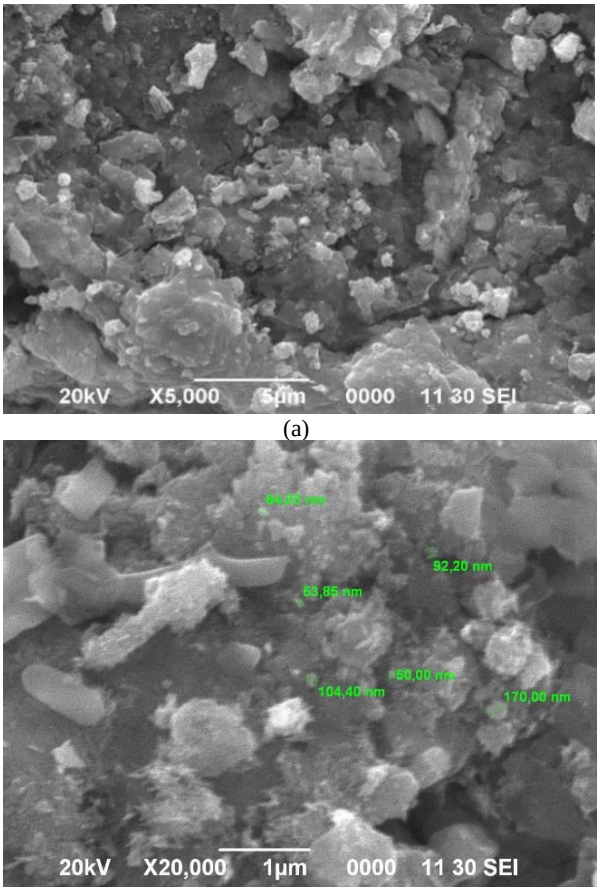

Figure 5. (a) Morphology of MnO_2 using SEM at 60 °C and 5A current, (b) Magnification of (a) which MnO_2 diameter particle size

Figure 5 shows that the particle diameters of the MnO_2 particles produced at a current of 5 A range from 50 to 170 nm at a magnification of 20,000x. The acquisition of a much smaller diameter of the MnO_2 particle increases the surface area of the particle, allowing the MnO_2 particle's electrical storage performance to improve.

4. CONCLUSIONS

The highest mass gain was obtained at the use of an electrolyte temperature of 60 °C and a current of 5 A, which was 11.4 grams. The higher temperature of the electrolyte, the mass gain of MnO_2 will increase, as well as the higher the current used, the mass gain of MnO_2 will be increase. The brittle nature of the graphite electrode can cause graphite to be easily eroded and mixed with MnO_2. The MnO_2 compound has a spiny round shape and tends to agglomerate with particle diameter values ranging from 50-170 nm.

ACKNOWLEDGEMENT

The authors would like to thank the staff and researchers at the Metallurgical and Materials Research Center LIPI (RCMM-LIPI) who have helped a lot in this research and this research was supported by the RCMM-LIPI.

REFERENCES

[1] A. Biswal, B. C. Tripathy, K. Sanjay, T. Subbaiah, and M. Minakshi, "Electrolytic manganese dioxide (EMD): A perspective on worldwide production, reserves and its role in electrochemistry," *RSC Adv.*, vol. 5, no. 72, pp. 58255-58283, 2015. Doi: 10.1039/c5ra05892a

[2] Pusat Sumber Daya Geologi, "Pemutakhiran data dan neraca sumber daya mineral status 2015," pp. 1-25, 2015. http://psdg.geologi.esdm.go.id/Neraca/2015/ (diunduh pada tanggal 13 November 2020 pukul 20.21 WIB)

[3] B. R. A. Safitri, "Analisis kandungan mineral logam mangan (Mn) di kawasan pertambangan desa bangkang," *Jurnal Ilmiah IKIP Mataram*, vol. 2, no. 1, pp. 122-132, 2010.

[4] X. Huang, D. Lv, Q. Zhang, H. Chang, J. Gan, and Y. Yang, "Highly crystalline macroporous β-MnO2: Hydrothermal synthesis and application in lithium battery," *Electrochim. Acta*, vol. 55, no. 17, pp. 4915-4920, 2010. Doi: 10.1016/j.electacta.2010.03.090

[5] M. Devenney, S. W. Donne, and S. Gorer, "Application of combinatorial methodologies to the synthesis and characterization of electrolytic manganese dioxide," *J. Appl. Electrochem.*, vol. 34, no. 6, pp. 643-651, 2004. Doi: 10.1023/B:JACH.0000021915.73788.4c

[6] N. Saridewi, S. Arif, and A. Alif, "Sintesis nanomaterial mangan oksida dengan metode bebas pelarut," *J. Kim. Val.*, vol. 1, no. November, pp. 117-123, 2015. Doi: 10.15408/jkv.v0i0.3147

[7] V. P. Viscarini and N. U. R. Rokhima,

"Sintesa partikel MnO_2 dengan teknik elektrokimia dalam sel membran," *Biomass Chem Eng*, vol. 49, no. 23-6, pp. 1-15, 2015.

[8] G. K. Putri, "Sintesis MnO_2 dengan metode elektrokimia sebagai elektrokatalis pada metal air battery," *Diss. Institut Teknologi Sepuluh Nopember.*, vol. 9, no. 5. 2017.

[9] L. Andriyah dan E. Sulistiyono, "Proses pemurnian mangan sulfat dengan pengendapan selektif menggunakan karbon aktif dan larutan NaOH," Technical Report, 2014.

[10] E. Marlina, S. Wahyudi, and L. Yulianti, "Produksi brown's gas hasil elektrolisis H_2O dengan katalis $NaHCO_3$," *Jurnal Rekayasa Mesin*, vol. 4, no. 1, pp. 53-58, 2013.

[11] L. M. Kwon, J. W. Kim, U. U. Chi and J. J. Shin "A study on the preparation of electrolytic manganese dioxide," *Journal of the Korean Chemical Society*, vol. 17, no. 4, pp. 306-313, 1973.

[12] K. Song, J. Jung, Y. U. Heo, Y. C. Lee, K. Cho, and Y. M. Kang, "α-MnO_2 nanowire catalysts with ultra-high capacity and extremely low overpotential in lithium-air batteries through tailored surface arrangement," *Phys. Chem. Chem. Phys.*, vol. 15, no. 46, pp. 20075-20079, 2013. Doi: 10.1039/c3cp53754d

INDEKS PENULIS

INDEKS KATA